A Neural Model of Call-Counting in Anurans

Author:
Dave Houtman

Supervisor:
Andre Longtin

Thesis submitted to the
Faculty of Graduate and Postdoctoral Studies
in partial fulfillment of the requirements
for the M.Sc. degree in Physics

Department of Physics

Faculty of Science

University of Ottawa /
Ottawa-Carleton Institute for Physics

M.Sc. Thesis

June 2012

Abstract

Temporal features in the vocalizations of animals and insects play an important role in a diverse range of species-specific activities such as mate selection, territoriality, and hunting. The neural mechanisms underlying the response to such stimuli remain largely unknown. Two species of anuran amphibian provide a starting point for the investigation of the neurological response to species-specific advertisement calls. Neurons in the anuran midbrain of *Rana pipiens* and *Hyla regilla* exhibit an atypical response when presented with a fixed number of advertisement calls. The general response to these calls is mostly inhibitory; only when the correct number of calls is presented at the correct repetition rate will this inhibition be overcome and the neurons reach a spiking threshold. In addition to rate-dependent call-counting, these neurons are sensitive to missed calls: a pause of sufficient duration—the equivalent of two missed calls—effectively resets a neuron to its initial condition. These neurons thus provide a model system for investigating the neural mechanisms underlying call-counting and interval specificity in audition.

We present a minimal computational model in which competition between finely-tuned excitatory and inhibitory synaptic currents, combined with a small propagation delay between the two, broadly explains the three key features observed: rate dependence, call counting, and resetting. While limitations in the available data prevent the determination of a single set of parameters, a detailed analysis indicates that these parameters should fall within a certain range of values. Furthermore, while network effects are counter-indicated by the data, the model suggests that recruitment of neurons plays a necessary role in facilitating the excitatory response of counting neurons—although this hypothesis remains untested. Despite these limitations, the model sheds light on the mechanisms underlying the biophysics of counting, and thus provides insight into the neuroethology of amphibians in general.

Contents

Abstract..... *i*

Statement of Contribution..... *1*

List of Figures..... *2*

List of Tables..... *4*

List of Symbols..... *5*

Glossary..... *7*

Chapter 1: Background

1.1 Introduction..... 12

1.2 Biological Motivation..... 12

1.3 Structure of this Thesis..... 17

1.4 Numerical Competence..... 18

1.5 Previous Numerical Models..... 23

1.6 Interval Selectivity..... 28

1.7 Neurophysical Background..... 31

1.8 Summary..... 35

Chapter 2: The Experimental Evidence for Frequency-Dependent Call-Counting in Anurans

2.1 Introduction..... 36

2.2 Methodology..... 36

2.3 The Optimum PRR of Call-Counting Neurons..... 39

2.4 Counting..... 40

2.5 Reset on Missed Calls..... 42

2.6 Supporting Data..... 47

2.7 Summary..... 50

Chapter 3: A Plausible Model

3.1 Introduction..... 51

3.2 The N-(N-1) Data..... 51

3.3 One- and Two-Parameter Alpha Functions..... 54

3.4 An Intuitive Model based on Alpha Function-like Conductances..... 55

3.5 Implications of the Model for the Single-Call Response Data..... 61

3.6 Propagation Jitter and its Complications..... 66

3.7 Summary..... 68

Chapter 4: The Single-Call Response Model

4.1 Introduction..... 69

4.2 A Mathematical Description of the Single-Call Response Model..... 70

4.3 Assumptions, Approximations, and Inherent Limitations of the Model..... 71

4.4 An Analytical Estimation of the Parametric Values Derived From the Available Data..... 77

4.5 Computational Methodology and Modeling..... 84

4.6 Reduction of Parameters..... 87

4.7 The Best Fit Parameter Set..... 88

4.8 Summary..... 92

Chapter 5: Response of the Model to Additional Calls

5.1 Introduction..... 94

5.2 Plasticity..... 94

5.3 Response of the Model to Multiple Calls..... 100

5.4 Response of the Model to Missed Calls..... 102

5.5 Frequency Dependence..... 105

5.6 The N-(N-1) Data Revisited..... 107

5.7 Summary..... 109

Conclusion..... 111

Appendix A: Alpha Functions

A.1 One- and Two-parameter Alpha Functions..... 117

A.2 Alpha Functions via the Euler Method..... 120

A.3 The Non-Dimensionalization of Time in the One-parameter Alpha Function..... 122

A.4 The Sum of N Alpha Functions..... 124

A.5 The Continuity of $g_n(t)$ and $g'_n(t)$..... 126

References..... 129

Statement of Contribution

Author: Dave Houtman

Title: A Neural Model of Call-Counting in Anurans

Statement: The research that comprises this thesis was performed by the author under the supervision of Dr. Andre Longtin in partial fulfillment of the requirements for a Masters of Science degree as mandated by the University of Ottawa. The work contained herein has its origins in observations first made by Dr. Gary Rose and his colleagues at the University of Utah which was subsequently published in *Nature Neuroscience* (2002) [1]. This thesis contains original theoretical research based largely upon experimental data provided by Gary Rose, along with information published in the *Journal of Neuroscience* (2007) [2], which is frequently cited throughout this document. We are grateful to Dr. Rose and his colleagues for both their original data and for the many insights offered in the aforementioned articles, as well as for the assistance of Gary Rose himself.

The original contribution of this work lies in the neural model which was constructed to explain counting in anurans, along with concomitant effects seen in the experimental data. The model—the first in this field derived entirely from the data—is capable of broadly recreating the observed features in their entirety. Due to experimental limitations, the model is deficient in some of its details; nonetheless it provides important insights into the mechanisms underpinning the behaviour of counting neurons in lower species. In addition to advancing the subject, these insights suggest directions for further experimentation which would confirm particular features of the model itself.

List of Figures

#	Section	Description
1-1	1.2	The general features of a neuron.
1-2	1.2	Sample output due to eight input calls delivered at 80 Hz. Adapted from *Edwards et al.* (2007).
1-3	1.5	The Numerosity Detection System of Dehaene and Changeux (1993).
1-4	1.5	Results of the Numerosity Detection System of Dehaene and Changeux (1993).
1-5	1.5	The Spike Selection Unit (SSU) of Abarbanel and Talathi (2006).
1-6	1.5	A Binary Shift Register functionally equivalent to the neural circuit of Figure 1-4.
1-7	1.6	The Time Delay Circuit (TDC) of Abarbanel and Talathi (2006).
1-8	1.6	The Interval Recognition Unit (IRU) of Abarbanel and Talathi (2006).
1-9	1.7	The circuit diagram for a model neuron having only an ion pump and a leak current.
1-10	1.7	The equivalence circuit for a generic model neuron having multiple current sources and sinks.
2-1	2.2	Drawing of a frequency-sensitive call-counting neuron of the anuran *torus semicircularis*. Courtesy of Dr. Gary Rose.
2-2	2.3	The voltage-dependence of frequency-sensitive counting neurons on input call frequency (PRR). Adapted from *Edwards et al.* (2007).
2-3	2.4	The dependence of a frequency-sensitive counting neuron on input call count delivered at optimum PRR. Adapted from *Edwards et al.* (2007).
2-4	2.5	Pairing of calls produces subthreshold response. Adapted from *Edwards et al.* (2007).
2-5	2.5	High-frequency attenuation of spike production with increased call frequency. Adapted from *Edwards et al.* (2007).
2-6	2.5	The dependence of a frequency-sensitive counting neuron on missed calls. Adapted from *Edwards et al.* (2007).
2-7	2.6	The average response of call-counting neurons to 1-4 input calls at a PRR of 80 Hz.
3-1	3.2	The N-(N-1) data.

3-2	3.4	d^2V/dt^2 versus time according to equation 3-9.
3-3	3.4	A simplified model of excitatory and inhibitory currents.
3-4	3.4	Inhibitory current follows excitatory current.
3-5	3.4	No crossovers—and hence no extrema—are possible when $V(t)$ is decreased to near the inhibitory reversal potential V_i.
3-6	3.4	The effect on $V(t)$ produced by shifting the excitatory current relative to the inhibitory current.
3-7	3.5	Response to a single-call recorded from call-counting neurons, from data set A, courtesy of Gary Rose.
3-8	3.5	Three sample outputs from Figure 3-7 showing a possible inverse correlation between the width of the initial EPSP and recovery time.
3-9	3.5	Three sample outputs from Figure 3-7 showing the possible effect of delayed excitation.
4-1	4.3	The average of a number of trials from a set of data whose variation is critically dependent upon some noisy parameter α creates an artefact which does not exist in the original data set.
4-2	4.4	The determination of g_L from the plot of $ln[(V_R - V(t)) / (V_R - Vo)]$ versus $-g_L t$.
4-3	4.4	The determination of A_e from equation 4.14.
4-4	4.4	The determination of A_i from equation 4.16.
4-5	4.7	The best-fit parameter set, using the single-call data, but with call 1-d removed.
4-6	4.7	The model and the experimental data, using 2 two-parameter alpha functions.
4-7	4.7	The effect of changing various parameters on the fit of the model to the single-call response data.
4-8	4.8	The effect of changing the value of τ_{ir} on the output of the model.
5-1	5.3	A five-counter generated by facilitating the excitation.
5-2	5.4	The effect of missed pulses/calls on the voltage response of a call-counting neuron with a call frequency of 79 Hz.
5-3	5.4	The effect of missed pulses/calls on the voltage response of a call-counting neuron, this time with a call frequency of 40 Hz.
5-4	5.5	The response to multiple calls using a barely-subthreshold parameter set.
A-1	Appendix A	Sample one- and two-parameter alpha-functions.

List of Tables

#	Section	Description
2-1	2.5	Summary of Information displayed in data set A.
4-1	4.4	Summary of the variables used in the model.
4-2	4.7	Summary of best-fit Parameter set values.
5-1	5.1	Summary of values used in Figures 5-1, 5-2, and 5-3.

List of Symbols

α_x	The alpha function parameter which characterizes the overall shape of the curve; the inverse of τ_x, i.e $\alpha_x = 1/\tau_x$, where x may be excitatory *(e)* or inhibitory *(i).*
α_{xd}, α_{xr}	The decay (d) and rise (r) values of a two-function alpha parameter; x is generally assumed to be inhibitory in this particular usage.
A_x	The amplitude of an alpha function; $x=e$ (excitation) or i (inhibition).
β_n	A function equal to $(1- e^{-n\alpha\Delta t})^{-1}$, a quantity which occurs frequently when alpha functions are triggered at regular intervals.
C	The membrane capacitance, taken as *1 uF* throughout this thesis.
D	The depression parameter, which decreases when calls occur closer together.
dt	The size of the time increment used in iterations with the Euler method.
$\delta(t-t_o)$	Equal to 1 when a spike occurs at time t_o and 0 otherwise; the integral of a Dirac delta function.
F	The facilitation parameter, which increases when calls occur closer together.
Δ_F	The amount by which the facilitation parameter increases on each call.
F_o	The initial value of facilitation prior to the first call.
g_L	The leak conductance, the inverse of the leak resistance, presumed to be constant throughout the neuron and over the time course of study.
$g_x(t)$	The synaptic conductance, often in the form of an alpha function, where x may be either e (excitatory) or i (inhibitory).
I_b	A fixed bias current, which could be intrinsic to a neuron, as for example from a current pump embedded in the cell membrane, or applied externally, as from an injected current source.
I_x	Synaptic currents; x may be excitatory *(e)* or inhibitory *(i).*
S	A spike due to incoming calls or pulses.
$\{t_1, t_{2...}t_n\}$	The set of times of incoming calls; t_1 is the time of the first call, etc.
t_i	The arrival time of a call or pulse.
τ_x	The time constant of an alpha function; the time required for a 1-parameter alpha function to reach its maximum value.
τ_F	The time constant of the facilitation parameter.

τ_{xr}, τ_{xd}	The rise and decay time constants for a two-parameter alpha function; x may be excitatory *(e)* or inhibitory *(i)*.
Δt	The delay time between the onset of the excitatory current and the onset of the inhibitory current.
φ_n	Functional shorthand for $\beta_1 e^{-\alpha \Delta t} - n\beta_n e^{-n\alpha \Delta t}$, a term which occurs frequently when alpha functions are triggered at uniform intervals.
V_L	The membrane leak reversal potential, assumed to be ~78 mV.
V_m	The value of the voltage at a minimum or maximum in a plot of *V(t)*.
V_R	The resting voltage of a neuron, it is equal to the sum of all leak currents and bias currents present when synaptic inputs and gating channels are inactive.
V_x	A generalized reversal potential; x may be excitatory *(e)* or inhibitory *(i)*.
x	Subscript used to indicate either excitatory *(e)* or inhibitory *(i)* effects, whether applied to amplitudes (A_x), conductances ($g_x(t)$), currents (I_x), or time constants (τ_x, α_x).

Glossary

Advertisement call	The species-specific call made by an *anuran* (usually, but not always, the male of the species) to attract a mate.
Afferent	Existing inward from an object, or preceding it, as for example in the case where one neuron is closer to a source of stimuli than another, or (metaphorically) is 'upstream' from it.
Alpha function	A mathematical function in the form $f(x)=Axe^{-ax}$, where A and a are constants that characterize the amplitude and rise time of the function respectively. Alternately, the form $f(x)=Axe^{-x/\tau}$ is frequently used.
AMPA	A fast-acting glutamate-type neurotransmitter.
Anuran	A family of the class *Amphibia* that includes frogs and toads.
Battery term	A term in the form (V_x-V) in the equation governing the *synaptic* current. Derived from the analogous situation in which a battery is situated in a circuit in such a way that its polarity is in opposition to an applied voltage.
BEF (Best Excitatory Frequency)	The primary or 'carrier' frequency underlying a pulse that triggers the optimal response from a call-counting neuron, typically 800 Hz in this study.
Bioacoustics	The branch of science dealing with the production of sound in species and the effect it has on them.
Call	One particular type of vocalization made by an animal.
Conductance	The inverse of resistance; high conductance is positively correlated with high current flow.
Current clamp	A particular kind of *patch clamp* technique, in which current, either positive or negative, is injected into a neuron to counter naturally-occurring current changes, and the resulting voltage response is measured.
Dendrite	The structure of a neuron which helps transmit electrical signals towards its soma, or cell body; the neuron's 'input cabling'.
Depression	A form of synaptic *plasticity* in which synaptic conductances decrease as the incoming spike rate increases; *ant. Facilitation.*
Depolarization	A lessening of the potential difference between the inside and outside of a cell; the intracellular fluid becomes less negative

	than the extracellular fluid, which is taken to be at ground; *ant: Hyperpolarization*.
DOG (Difference-of-Gaussians)	A mathematical operation in which an object is convolved with slightly different Gaussians and then subtracted from one another, resulting in a band-pass operation frequently used e.g. to sharpen images.
DU (Detection Unit)	One of the three components comprising the model of Abarbanel and Talathi, it essentially functions as a coincidence detector in the final stage of the *IRU*.
EPSP (Excitatory Post-Synaptic Potential)	A *depolarizing* response due to the influx of positive charge or, alternately, the efflux of negative charge at a neuron's synapses.
Excitation	*Depolarization* of the charge across a membrane due to an influx of positive charge or an efflux of negative charge; so called because the neuron's voltage moves towards its spiking threshold and so is more likely to spike; *ant*: *Inhibition*.
Extrema	The set of all minima or maxima of a function $f(x)$ over a range $a<x<b$; the points at which $df/dx=0$.
Facilitation	A form of synaptic *plasticity* in which synaptic conductances *increase* as the incoming spike rate increases; *ant. Depression*.
Fechner's Law	An observation, due originally to Ernst Weber, relating the magnitude of a stimulus to its perceived intensity. Gustav Fechner attempted to put Weber's observations on solid theoretical grounds, with the result that collectively these observations are referred to variously as Weber's Law, Fechner's Law, or the Weber-Fechner Law. In the context of this thesis, the term refers to the observation that it is more difficult to distinguish between two large collections of objects than two collections of a small number of objects, even when the numerical distance is the same for each pair of collections.
Frequency tuning analysis	A procedure in which a range of frequencies is presented to an organism and the response measured at a single neuron. The output indicates the range of frequencies over which the neuron is tuned.
GABA receptor	A fast response receptor embedded in the postsynaptic cell wall which triggers an inhibitory (hyperpolarizing) response. One variant of the GABA channel (known as $GABA_A$) is relatively fast to activate and deactivate.
Hodgkin-Huxley model/neurons	A model first proposed by Alan Hodgkin and Andrew Huxley in 1952 describing the flow of Na^+ and K^+ ions across the membrane of a neuron; such neurons are frequently referred to as 'Hodgkin-Huxley' neurons.

Hyperpolarization	An increase in the potential difference between the inside and outside of a neuron, with the intracellular fluid becoming more negative than the extracellular fluid, which is taken to be at ground; *ant:* Depolarization.
Inferior colliculus	A nucleus of the mammalian midbrain which serves to process incoming signals from a variety of sources connected to the auditory pathway.
Inhibition	*Hyperpolarization* of the charge across a membrane, so-called because the neuron's voltage moves away from its spiking threshold and so is less likely to spike; *ant*: *Excitation*.
Interval number threshold	The minimum number of calls required to trigger spiking in a call-counting neuron, i.e. the call-count threshold beyond which spiking is inevitable.
IPI (Interpulse Interval)	The time interval between calls or pulses; the inverse of PRR.
IPSP (Inhibitory Post-Synaptic Potential)	A *hyperpolarizing* response due to the influx of negative charge, or the efflux of positive charge. Such changes may be due to charge pumps, voltage-sensitive ion gates, or from the effect of other neurons synapsing on the neuron whose voltage is under study.
IRU (ISI Recognition Unit)	The sum of the three components (the *SSU*, *TDC*, and *DU*, defined elsewhere in this glossary) in the model of Abarbanel and Talathi.
ISI (Interspike Interval)	The time interval between incoming spikes; the inverse of *PRR*.
Lateral inhibition	Suppression of the output of neighbouring neurons in the model of Dehaene and Changeux.
N-counter	A call-counting neuron that triggers on or after the N^{th} call.
N-(N-1) data	The data obtained by subtracting the averaged output that results from N-1 input calls from the averaged output of N calls.
NDMA receptor	A receptor embedded in the postsynaptic cell membrane which triggers an excitatory (depolarizing) response. NMDA channels are relatively slow to activate and deactivate.
Neuroethology	The branch of behavioural science that attempts to link the reaction of a species to stimuli with the underlying neural mechanisms responsible.
Numerosity	The approximate number of things. The term avoids the confusion inherent in the word 'number', which may be used to refer to either an exact value, an amount relative to some other amount, or an approximate total. 'Numerosity' is—

	perhaps deliberately—a somewhat fuzzy term.
Numerosity Detection System	A counting model proposed by Dehaene and Changeux, consisting of an Input Retina, a Topographical Map, and a Numerosity Detector.
Patch clamp	A technique in which the tip of a very fine glass pipette is applied to a cell wall, allowing measurements of current, voltage, or conductance to be made under a variety of experimental conditions.
Perceptron	A single layer network capable of some form of learning according to an algorithm devised by Marvin Minsky and Seymour Papert in 1969.
Plasticity	Changes in synaptic strength which depend upon the history of the synapse; these changes may be activity- or use-dependent, and may persist over short or long time scales.
Postsynaptic	The side of a synapse which receives information (neurotransmitters, messengers, etc.). A neuron is postsynaptic to its *afferents*.
Potentiation	To increase the conductance of a *synapse* with increased use; *syn. Facilitation*
Presynaptic	The side of a *synapse* which transmits information (neurotransmitters, messengers, etc.).
Propagation delay	A delay, typically of a few milliseconds, between a *call* or *pulse* and the onset of its effects in a neuron.
Propagation jitter	Variability in the arrival time of a call or pulse from its norm, owing to noise in the processes responsible for the propagation of the signal.
PRR (Pulse Repetition Rate)	The calling rate i.e. the number of calls per second, usually delivered at its *BEF*.
Pulse	A single input call operating at its *BEF*; frequently, the term is used as a shorthand for the spike delivered by the putative *afferent* to a call-counting neuron. In actual fact, there is a delay between the actual call and the pulse it produces, although this detail has been mostly omitted in many of the arguments made in this document.
Rebound spike	A spike which results when an *inhibitory* effect is removed.
Recruitment	The amplification of *facilitation/depression* due to the participation of an increasingly larger population of *afferents* to a neuron, in response to repeated calls.
Reversal potential	The voltage (V_x) for a specific ionic species x at which the *battery term* reverses its value, from positive to negative, or negative to positive.

Single-call response	The response of a neuron to a single incoming call.
SSU (Spike Selection Unit)	The first of three components in the model of Abarbanel and Talathi, its purpose is to output the N^{th} incoming spike at the N^{th} stage of the SSU.
STP (Short term potentiation)	*Facilitation* of synaptic current with increasing use over a relatively short period of perhaps a few milliseconds.
Subitization	The ability to visually estimate the number of items at a glance, without counting; a feature present in many creatures.
Synapse	The connection between neurons which allows for the transmission of information, either electrically or chemically.
TDC (Time Delay Circuit)	The second of three components in the model of Abarbanel and Talathi, responsible for delaying a pulse so that it falls within a predetermined time window.
Tempotron	A neural algorithm for selecting a specific pattern of spikes from amongst a broader collection of input spikes.
Tone burst	A brief burst of (often) white noise designed to elicit a response from a neuron.
Torus semicircularis	The *anuran* homologue of the *inferior colliculus*.
Voltage clamp	A particular kind of *patch clamp* technique, in which the voltage of a neuron is held constant, and the current response measured.
Whole-cell recordings	A *patch clamp* technique in which the area of the cell wall attached to the pipette is ruptured and excised, so that the inside of the cell and the pipette are effectively one; electrophysiological readings made inside the pipette therefore reflect the behaviour of the neuron itself.

Chapter 1: Background

1.1 Introduction

The raw vocalizations of animals and insects—the various chirps, crows, squawks, trills, bays, croaks, grunts and roars used to signal danger and distress—are but one element in the communication between species. Other auditory components, such as the interval between calls, their number, duration, repetition rate, response delay, and the fidelity of their reproduction, are believed to play an important role in a variety of processes necessary for mating, predation, and survival. The study of these effects along with their production is known as *bioacoustics*.*

Nature provides abundant examples. Birdsong is believed to be essential for species identification, mate selection, and the determination of genetic fitness [3][4]. Lions appear to be able to judge the size of a neighboring pride of unseen intruders based on the number of distinct roars they hear; if their own number is greater, they will attack, and if not—since mistakes are costly—they will retreat [5]. Bats use echolocation to map their surroundings and forage for insects. And recently, tiger moths have been found to jam bat sonar by generating their own ultrasonic chirps [6].

In each of the cases cited above, a species-specific neurological response is essential if a particular vocalization is to have any effect in promoting a creature's survival. Despite intense study, the neural correlates of such signalling—the process by which one or more neurons register and respond to a specific pattern of auditory stimuli—remain largely unknown.

1.2 Biological Motivation

Recent research by Dr. Gary Rose and his colleagues at the University of Utah has identified neurons in the midbrain of two species of *anuran* amphibian (i.e. frogs and toads) that respond to highly-specialized, species-specific advertisement (or mating) *calls*.

* Terms defined in the glossary are italicized on their first usage in the body of this document.

Significantly, these neurons are located in the anuran *torus semicircularis*, the homologue of the mammalian *inferior colliculus,* a region in which auditory input signals received from the lower brainstem via the hearing apparatus are processed before being transmitted to higher regions of the amphibian brain. The fact that this location is used by a number of species for auditory processing provides corroborating evidence that the specialized neurons of the *torus semicircularis* do indeed constitute the putative neural correlates of a call-response centre in the anuran brain.

Neurons in all regions of the brain—whether of fishes, lions, crickets, frogs or humans—behave much the same. In every case, a resting potential of approximately -65 *mV* is maintained inside the cell, measured relative to the extracellular fluid, which is taken as 'ground'. A further voltage drop from the resting potential is referred to as *hyperpolarization*; a voltage increase, *depolarization*. Such changes result from the actions of various active and passive functional units embedded in the cell's membrane. The former group includes pumps, which control the flow of Na^+, K^+, Cl^- and Ca^{+2} ions across the membrane, and channels, which are triggered to open or close when certain set voltages are reached. And since cell walls are inherently porous, there is always a certain amount of passive leakage. The voltage difference that results from this molecular machinery is just the Nernst potential due to the concentration of the various ions present at any time on either side of the membrane.

It is the voltage-triggered channels which impart nonlinear behaviour on the operation of neurons, and this allows spiking to occur (see Figure 1-1 below). Above a minimum threshold voltage of perhaps -40 *mV*, Na^+ channels will open allowing extracellular Na^+ ions to flood the cell, depolarizing it to above 0 *mV* (and usually higher). But this in turn immediately triggers K^+ channels to open, and the resulting outward flow of positive charge causes the cell to hyperpolarize again, even undershooting briefly to -80 *mV* before the system re-equilibrates to its resting state, due to the pumps and the leakage current. This behaviour is collectively known as the action potential (although we shall continue to refer to it rather more informally as 'spiking'). Transient changes in polarization of a longer duration due to synaptic input from other neurons may be characterized as an *IPSP* (*Inhibitory Post-Synaptic Potential*) if hyperpolarizing occurs or an *EPSP* (*Excitatory Post-Synaptic Potential*) if a depolarization is observed.

Each neuron receives electrical impulses from, and transmits impulses to, other neurons across short gaps called *synapses*. The number of synapses impinging on any one neuron may number in the hundreds or thousands, and the electrochemical behaviour at

each synapse is itself a complicated process which is affected by the type of neurotransmitter present at the synapse, as well as drugs, ionic concentrations, antagonists of various sorts, and the history—both short term and long—of the synapse itself. The direction in which information flows dictates the terminology applied at the synapse; a neuron receiving a signal across a synapse is on the *postsynaptic* side, while one conveying information is *presynaptic*. Thus a single neuron may be both postsynaptic to a set of incoming signals, and simultaneously presynaptic to the signals it passes on to the neurons 'downstream'.

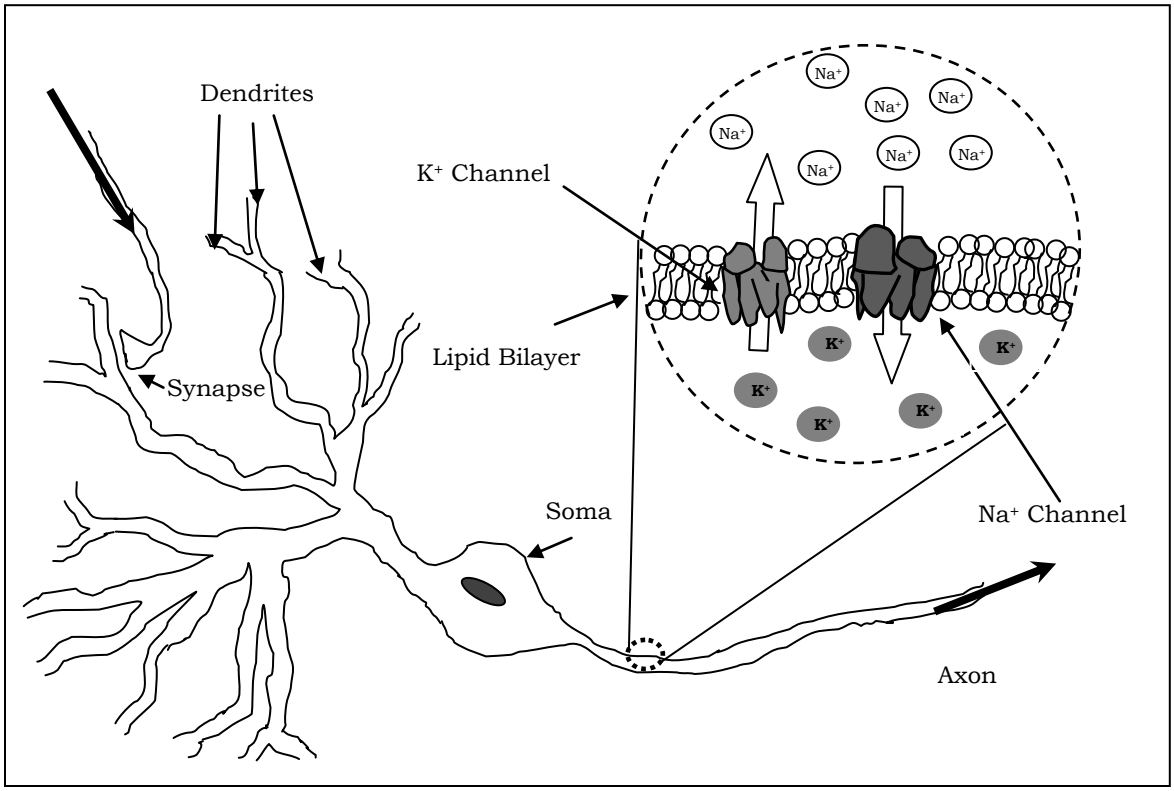

Figure 1-1. The general features of a neuron (bottom left), with the two solid arrows indicating the direction of signal propagation. The relevant ion channels are shown in the inset (top right). The hollow arrows indicate the direction of positive ion flow during an action potential, when the channels embedded in the lipid membrane (in gray) open and the ions, first Na^+ and then K+, flow along their concentration gradients.

Experimentally, both the voltage and current across the cell membrane of neurons have been studied by inserting fine wires into the axon—the branch of the neuron carrying outgoing information—of an organism under study. (Squids, by virtue of the large diameter of their axons, have historically been used.) More recently, *patch clamps* have replaced wires as the method of choice for the experimental investigation of neuronal behaviour, since this allows for a far wider choice of organisms to be studied, and in far greater detail as well. (Indeed, the technique has been refined to the point where

individual pores may be observed in action; even the channels in the walls of mitochondria have been studied using patch clamps [7].) In this method, a fine pipette is placed in contact with a cell's lipid bilayer and a small amount of suction applied. Recording devices in the pipette may be used to measure the flow of current across the cell wall, or the cell wall under the pipette may be ruptured, allowing the contents of the pipette to measure properties inside the cell itself—a method referred to as '*whole-cell recording*.'

Exactly such a technique was used to record the output from Gary Rose's call-counting neurons. Spiking was triggered only when a particular temporal call signature was transmitted to call-counting neurons (discussed in more detail below). In a paper published by Christofer J. Edwards, Christopher J. Leary and Gary J. Rose in *J. Neuroscience* (2007) [2] (and henceforth referred to simply as *Edwards et al.*), whole-cell recordings of neurons in the anurans *Rana pipiens* and *Hyla regilla* were shown to be sensitive to the frequency, number, and interval between input calls. The typical response of each of these neurons to a single call is a hyperpolarizing IPSP. Furthermore, under most circumstances, repeated calls, whether randomized or uniformly spaced, merely generate additional IPSPs. As the call rate increases, these neurons begin to generate subthreshold oscillations in which, following each call, the membrane depolarizes somewhat, but not sufficiently enough to generate spiking. Only when the input call frequency, or *PRR* (*Pulse Repetition Rate*), reaches a specific desired value, typically in the range of 20 to 80 Hz, is the inhibition overcome and some *excitatory* current begins to dominate. With sufficient excitation, the neuron reaches its spiking threshold, usually after a preset number of calls.

Following a brief recovery period, the call-counting behaviour of the neuron is generally reproducible given identical stimuli, although noise appears to play a significant role in altering the response of the neuron to individual calls and hence, on occasion, the call count needed to elicit spiking. Furthermore, a minimum threshold of calls—typically 2 to 8, but usually a fixed number for each individual neuron—is required for spiking to occur. Interestingly, a missed pulse partially 'resets' the neuron, typically resulting in an IPSP on the next call or two following the missed signal.

Figure 1-2 shows a typical response. When presented with a number of calls at the correct frequency (80 Hz in the sample shown) the input calls (shown in blue) trigger spiking in the recorded output of the neuron (in black). The effect is only seen when both the call frequency and the call number (eight, in the example shown) are correct.

For simplicity, neurons which require a minimum of N calls at their optimum call frequency to elicit spiking will henceforth be referred to as an '*N-counter*'; thus the sample below is an 8-counter.

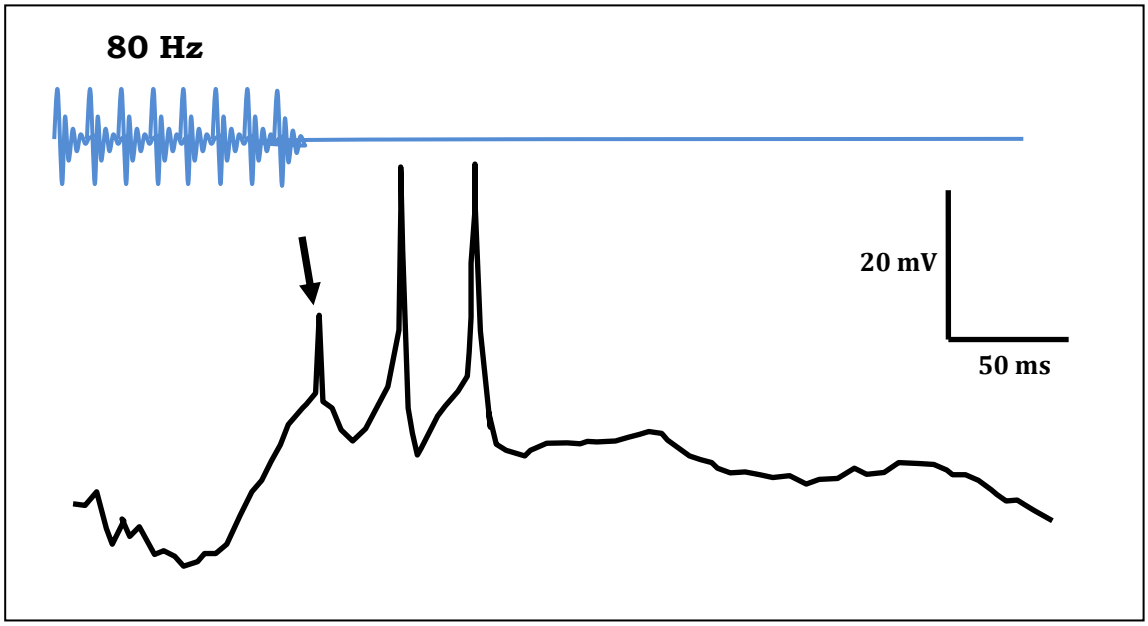

Figure 1-2. Sample output (in black, at bottom) due to eight input calls delivered at 80 Hz. (top, in blue). The arrow indicates the onset of the first spike due to the eighth call. Spikes are attenuated somewhat due to averaging over a number of samples. In reality, a time delay is present between the start of calls and the onset of a response, and this has been removed here for clarity. Adapted from *Edwards et al., J. Neuroscience (2007).*

In this regard, one key feature of interspecies communication is of particular interest. Many species appear to have an innate ability to 'count' stimuli, a feature broadly referred to as '*numerosity*', i.e. the ability to estimate the relative number of things. Furthermore, when numerosity involves events of a temporal nature (since numerosity can also be assessed visually or by tactility), a second important feature is often present, that of the time interval between the elements being enumerated. For example, the trills in a songbird's call will not elicit the desired response if delivered too hastily, even if their number and sequence are correct: songbird courtship is not simply about saying the right things; it is about good timing as well. Both numerical competence and interval-selectivity will be elaborated upon in greater detail later in this chapter.

1.3 Thesis Structure and Research Approach

A fuller discussion of the paper by *Edwards et al.* is left to Chapter 2; here we present the results of this research in broad terms only, the purpose being to emphasize the significance of these findings in helping to understand the importance of counting and interval selectivity in particular, as well as to establish a conceptual framework for both the experimental results and the theoretical model that follows.

Chapter 2 looks at the experimental evidence in more detail, and examines the available information, not just that found in the aforementioned *J. Neuroscience* article by *Edwards et al*, but in related sources as well. Furthermore, two pieces of raw data have been provided by Gary Rose, and while restricted in the amount of information they provide, they nonetheless supply useful clues as to how to proceed.

Chapter 3 considers this data and, based on different threads of evidence, postulates a simple model. A crucial insight comes from examining the voltage difference between two signals, one the averaged result of N input calls, the second the averaged result of N-1 calls. The difference of the two signals indicates that while the overall effect of N calls appears complicated, the underlying cause may have a simple explanation. This observation leads us to a simple descriptive model involving only a single excitatory current, a single inhibitory current, and a propagation delay that qualitatively explains the variability in the output seen in data set A.

Chapter 4 expands on these qualitative arguments and attempts to put the model on firm theoretical grounds, drawing conclusions from the supporting experimental evidence, including both data sets A and B. While it is not possible to derive exact values for many of the parameters postulated owing to both the limited amount of data and the limitations imposed by the theory itself, we were nonetheless able to estimate rough values for some of variables based on general features seen in the data, using the model itself as a guide. For some parameters, it is not even possible to estimate an approximate range of values; in such cases the only available approach is to use a combination of accepted values, deduction, and guidance from the model. In the last resort, a brute force approach was applied, in which millions of combinations of possible parametric values were used in an attempt to match the model to the experimental data.

Chapters 3 and 4 are based on the response of call-counting neurons to a single input call; in Chapter 5 the model is broadened to include the response to multiple calls using values estimated in the previous chapter (to the extent that these values can be ascertained). In order to explain the increase in excitation seen after multiple calls, it is necessary to introduce an additional feature into the model, that of *facilitation*, and this requires the inclusion of three additional parameters. This final element allows us to estimate the efficacy of the model in its ability to explain the three principal features of the Rose neurons: counting, input call rate (PRR) and the effect of missed calls.

This thesis concludes with a summary of the evidence presented, its limitations and implications, as well as suggestions for improvement and further experimentation.

1.4 Numerical Competence

As stated above, the ability to estimate the quantity or incidence of things in the environment—its numerosity, or what one author refers to as 'the number sense'*—is a core feature in the survival of many species. Four specific examples help elucidate this subject, and bring to light a major complication present in its investigation:

(1) When presented with two trays of food and the opportunity to select from only one of these trays, chimpanzees will almost inevitably select the tray with the larger amount of food, even when the contents of each tray are divided into two piles. Specifically, if the first tray contains one pile of four pieces of chocolate chips and another of three, and the second tray contains piles of five pieces and one piece, then when given the chance, the chimp will select the pile with the larger total number, rather than the tray with the largest individual pile [8]. This implies that, rather than simply sizing up each separate pile from amongst the four available, chimpanzees are able to estimate the overall numerosities of each tray.

(2) In an experiment performed by Hank Davis and Sheree Anne Bradford [9], rats were trained to select from amongst several tunnels projecting perpendicularly off of a

* The quote is from Dantzig T., *Number: the Language of Science 4th Ed.*, Pi Press, New York, N.Y. (2005). Stanislaw Dehaene uses this term, which is on page 1 of Dantig's book, in the title of his book: *The Number Sense: How the Mind Creates Mathematics*, Oxford University Press, Oxford, U.K. (1997) from which many of the examples in this section are drawn. Additional examples have been taken from Brian Butterworth's book, *What Counts: How Every Brain is Hardwired for Math*, The Free Press, New York, N.Y. (1999).

main chamber. In each trial every tunnel contained food, but only one had a door at its entrance that could be opened. Within any one set of trials, the total number of tunnels was held constant and their absolute position randomized. Although the location of the one accessible tunnel was randomized, its 'address' relative to the other tunnels was held constant. This was designed to eliminate the possibility that the rats were measuring either the distance or time to the desired tunnel; they had to 'count' their way up to the correct tunnel. This feat was performed accurately over several trials, with differing numbers of tunnels and configurations, and with several different test subjects. The response time dropped with each trial as the animals became more familiarized with the experimental setup and procedures, suggesting that the animals were able to 'count' up to the accessible tunnel.

(3) In a recent paper by Han Gross *et al.* [10], honeybees were taught to navigate to a sugar solution using a training sample consisting of a pattern of two or three randomly-spaced dots as a visual cue. The testing was controlled to eliminate low-order cues such as dot size and colour. When the pattern was changed from blue dots to yellow lemons, then, provided the number of symbols in the navigation pattern was the same as the training sample, a statistically significant percentage of bees still successfully navigated to the sugar, indicating that they had acquired the ability to distinguish the numerosity of the symbols they encountered.

(4) In an elegant experiment by Russell Church and Warren Meck [11], rats were trained to press one of two levers depending on the number of tones or light flashes they were presented with. If they either saw two light pulses *or* heard two tones, they were trained to press the left lever; if four pulses *or* flashes were presented, then the right lever. Curiously, when presented with two tones *and* two light flashes simultaneously, the rats pressed the right lever, indicating that they detected four distinct stimuli, rather than two pairs of stimuli (i.e. the left lever response). The evidence suggests that rather than provoking a simple, Pavlovian 'conditioned' response, the rats were responding to the total number of individual events; they were thus able to 'count' the total stimuli despite the different modalities being presented.

These examples serve to illustrate that the ability to enumerate the occurrences of things or events is apparently innate in many species and appears to play a varied but useful role in nature. But close inspection reveals something else: that the concept of numerosity and 'the number sense' is somewhat ill-defined. It can be used variously to

refer to the relative size or magnitude of things in one case (the chimpanzees in example 1), the number of increments in another (the rats in the chamber, example 2), and an exact number in a third case (as in example 3, with the honeybees). As the experiment with the level-pressing rats demonstrates (example 4), numerosity is not limited by modality—it may be visual, audible, and perhaps even tactile—and yet a sense of 'number' is apparent: the rats would appear to have an innate sense of '1-ness', '2-ness', etc.

The imprecision inherent in terms like 'number', 'count' and 'calculation' is a reflection of the fact that, when we use these terms, we are in fact referring to a range of activities which, while they may overlap, are distinct operations in their own right. Just such an observation was made by Stanislaw Dehaene, a specialist in the field of numerosity and the brain, who wrote (in 2003) that "…[numerical accumulation] relies on a highly composite set of processes, many of which are probably not specific to the number domain…[evidence] suggests that the neural basis of calculation must be heterogeneous." [12]*

The problems inherent in defining and classifying numerical competence have a long history, one that reaches back into the history of mathematics itself. In a review article written in 1988, two researchers in animal numerical competence, Hank Davis and Rachelle Pérusse, lamented the 'terminological chaos' that bedevilled their field at the time [13]. Davis and Pérusse in turn cite a still-earlier researcher, Stanley Stevens, who wrote (in 1951) that "there is a need for some new and univocal terms for [the] various meanings [for terms like 'number' and 'numerals']"[14]. (In a prophetic moment, Stevens adds parenthetically that "…the inertia of usage being what it is, the need [for more precise terminology] will most likely persist.") Stevens in turn cites the likes of Bertrand Russell, Hermann Weyl, and David Hilbert in pointing out that even amongst philosophers of mathematics, these terms are frequently ill-defined and misused. So the problem indeed has a rich history.

Davis and Pérusse suggest a framework for classifying numerical competence which is worth reviewing, since it goes some way toward unravelling the various semantic threads

---

* Dehaene's original quote uses the term 'mental arithmetic' where I have inserted the words 'numerical accumulation'. Apparently, Dehaene does not see any substantial difference between 'arithmetic', 'numerical accumulation' or 'counting'—they are all part of the same process—although I would argue that addition and counting are two separate processes. Again, this only serves to underline the definitional challenges that mine this field of study.

that comprise the subject. Their four categories indicate the related, but distinct, operations involved in estimating the numerosity of a quantity—'counting', in various senses of the word:

1. Relative numerosity judgements—When presented with a choice between two piles of food, an animal will invariably go for the larger pile. But this should not be used to infer that they actually tallied the morsels available. The ranking of things according to relative magnitude, while having nothing to do with discrete enumeration, is nonetheless an integral part of numerical competence.

2. *Subitization*— When viewing five items or fewer, humans, and many other species as well, are able to perform rapid, accurate enumeration—a process known as subitization. As the number of items viewed increases beyond five, accuracy falls, and the process of counting 'at a glance' fails us.* The process of rapid, accurate counting of numerosities less than four to six items has been demonstrated in a variety of species, such as raccoons[15], parrots [16], and chimps [17].

3. Estimation—As with subitization, the ability to 'size up' a collection of objects is inherent, but with decreased accuracy as the number of objects or events increases. This ability has been demonstrated, for example, in pigeons that have been trained to differentiate between 45 and 50 pecks [18].

4. Counting— Davis and Pérusse define counting in somewhat rigid terms as having both cardinality and ordinality, and insist that "one must have a series of number tags available which occur in ordered form." Counting is then defined in terms of one-to-one relationships, order, and abstraction.

Despite this attempt at classification, problems persist. Consider just the last item on the list, which is the most problematic. This strict definition of the term 'counting' seems to introduce its own difficulties. Should an intuitive definition of the term require "number tags" ('1', '2', '3'...) for each item? Surely adding one pebble to a pile of others

---

* There are rare exceptions. Oliver Sacks reports the case of twin autistic *savants* with the extraordinary ability to instantly 'count' the contents of a box of 111 matches accidently dropped on the floor (and just as quickly factor that number into primes.) The process appeared to be entirely unconscious: the twins 'saw' the number 111, clearly indicating that subitization need not be limited to numerosities of five or less. Details may be found in *The Man Who Mistook His Wife for a Hat* (Harper and Row, 1987, pg. 199). Sacks' story appears to have made its way to Hollywood: an almost identical scene involving toothpicks appears in the movie *Rain Man*. Dehaene discounts such stories, as no proper studies have been done; see *The Number Sense* (ibid), pgs. 70-71.

does not require that each pebble has a name according to its order, when only the highest cardinal value is important? (Echoing Stevens, Davis and Pérusse preface their introduction to this subject with the words "…the attribution of counting to nonhuman subjects is extremely awkward…," and add that "Counting is unquestionably the most overused term in the numerical competence literature.")

Perhaps more importantly, numbers by themselves have no physical representation; we readily talk about the number '2' without asking the question, '2 of what?'—and the experiment with rats (example 4) demonstrates that this degree of abstraction is not limited to humans. Since 'counting' in its strictest sense involves the addition of one to a number—an operation performed on two entities each of which have no physical representation—the act of counting must, at some level, involve symbolic manipulation. Furthermore, inherent in a count of numbers is the notion of an operation being repeatedly performed on successive values. So the act of counting is not an isolated operation; it must overlap with those of arithmetic, calculation, memory, and symbolic manipulation—all equally ill-defined. The same may be said to a lesser degree of the other three items in Davis and Pérusse's list.

Thus, the process by which an organism enumerates the stimuli in its environment is not simply a single distinct feat, but rather is due to a variety of interrelated and overlapping activities all of which, at a level far removed from the intricate functioning of neurons and synapses, gyri and cortices, we simply label as 'counting.'*

To remove the potential for 'terminological chaos', I shall adopt a more mundane and (hopefully) intuitive definition of counting for the purpose of this thesis. 'To count' is

---

* There is an additional dimension to this subject that seems to have been entirely overlooked by researchers (as far as I can tell), which concerns the *motivation for* and *permanency of* numerical competence. In almost all of the experiments conducted by various numerosity researchers—Stevens, Davis, Dantzig, Dehaene, Butterworth, etc.—there is an implicit assumption that whenever counting has been tested for and found, it must therefore be innate in the brains of the creatures being studied; in essence, the experiments have revealed a *pre-programmed* capability. But such experiments usually involve highly artificial environments, in which olfactory and visual cues have been mostly eliminated, and the motivation 'to count' is entirely contrived—situations never found in nature. Except in those cases where numerosity offers immediate survival value (specifically mating, self-preservation and territoriality)—the lions mentioned in the introduction are one example, and Gary Rose's call-counting frogs are another—counting in its various forms may *not* afford enough survival value to warrant being hard-wired into the brains of most creatures (particularly those of the lower orders), especially when olfaction and vision offer simpler cues at lower evolutionary cost. It is just possible that many of the creatures studied do *not* possess the innate counting abilities attributed to them by their researchers, but rather construct something resembling "numerosity on the fly", as required, when all other naturally occurring stimuli have been removed, and when motivated to do so by rewards or electric shocks. Far from being an extraordinary, innate ability revealed by experiment, some forms of numerical competence may be truly extraordinary precisely because they can be *transiently* provoked in the neural networks of these creatures—who would otherwise have little use for numerical capabilities in the wild; only human expectation makes this appear to be a permanent, even essential, feature of the organism. And scientists, being devotedly numerical creatures themselves, may be rather more inclined to overlook this point.

simply to increment the current number of discrete items or events being held in some form by one when an additional item or event is added. The result of N such events should then be represented by a relatively distinct analog value; the preceding analog values do not require 'tagging' with ordinal numbers, merely a suitably unique response to the N^{th} event. In the context of this thesis, that analog value is a voltage sufficient to generate spiking from a counting neuron.

In other words, for the purpose of this thesis, counting is synonymous with successive iteration, rather than estimation, enumeration, addition or measurement.

1.5 Counting Models

Notwithstanding the concerns expressed above, a few authors have attempted to explain counting using a variety of neurological models. Two such models will be briefly discussed here, and these should suffice to give a sense of the research thus far. The second of these models is in fact a component in a larger circuit designed to recognize the intervals between spikes, the subject of the following section. Thus, only the counting component of that model will be discussed in this section, and the complete circuit will be described in the section that follows.

The first model is due to Dehaene and Changeux [19]. Their *Numerosity Detection System* (from 1993) is comprised of three separate modules, shown below in Figure 1-2. The first stage functions as a 'retina' for the system, although the authors report that with a small modification it was able to handle audible signals, and should be able to handle signals of mixed modality. In the simulations performed, up to five input 'point' stimuli of varying intensities were applied to a row of 50 clusters, shown in Figure 1-2 below (top left). Each cluster (represented by an open circle in the diagram) corresponds to thousands of neurons possessing similar response properties. Interconnections between clusters ensure that each input point image is smeared out between adjacent clusters into a broad, roughly bell-shaped distribution. Hence two adjacent point sources can potentially give rise to overlapping distributions of clusters.

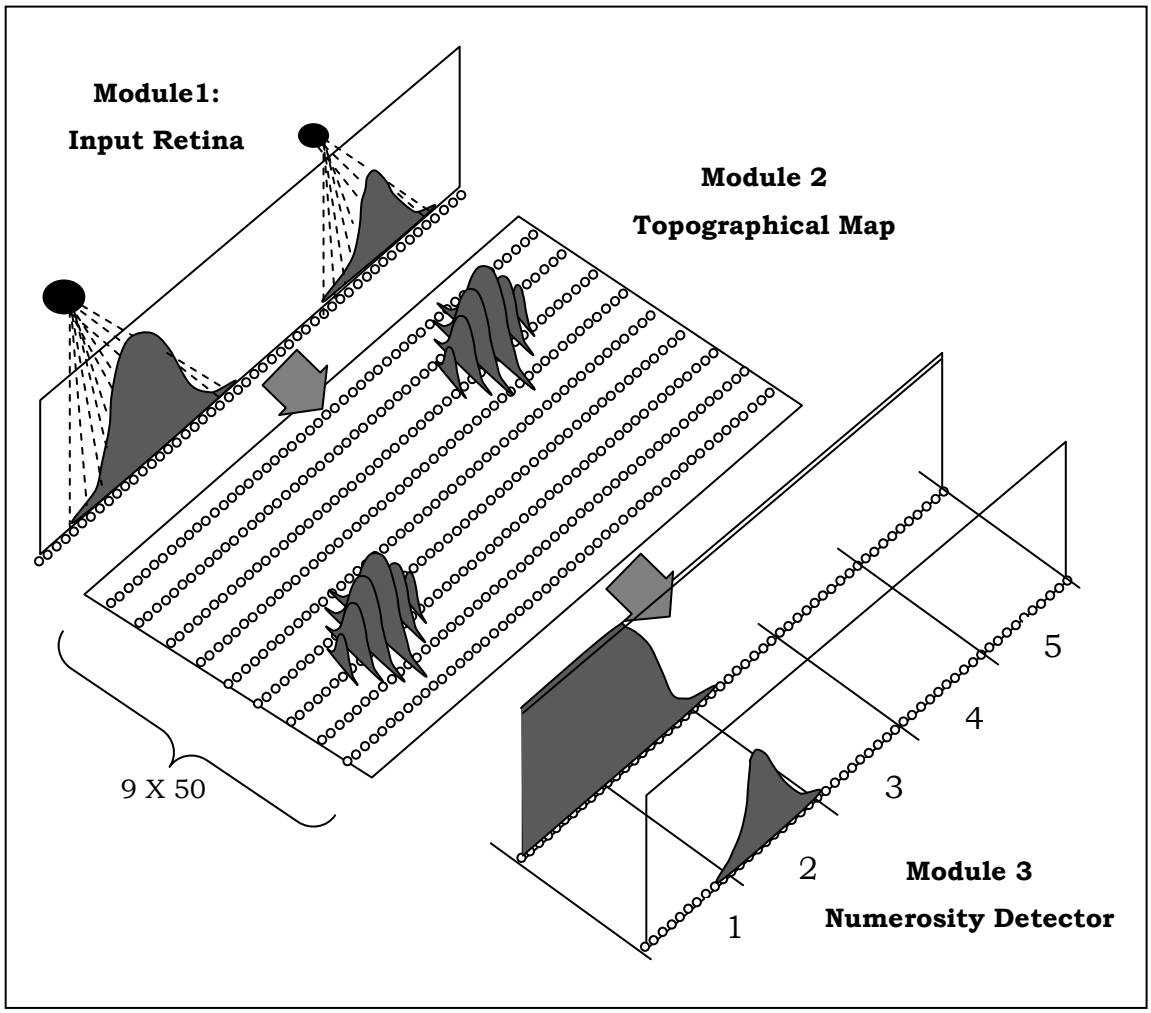

Figure 1-3: The Numerosity Detection System (NDS) of Dehaene and Changeux. Adapted from Dehaene and Changeux (1993). See text for details.

The second module consists of a topographical map that encodes object locations. For each locus of clusters at the input stage, a *difference-of-Gaussians* (*DOG*) filtering scheme ensures that adjacent clusters are localized by *lateral inhibition* so that activation sites are less likely to overlap. Additionally, the network is constructed in such a way that broader input distributions will be represented at locations 'deeper' into the topographical map, further ensuring that adjacent input points are non-overlapping, regardless of their initial intensity. The filtering also ensures that each locus of clusters on the topographical map is of equal intensity. Thus the second stage serves to separate and normalize the information presented at the input stage.

The third component is the numerosity detector itself, which, at this point, merely sums up the total intensity of the clusters on the topographical surface; the greater the number of active loci, the more contiguous clusters will be triggered in the final stage. At this

point, the location of the last excited cluster reflects the total quantity of points at the input stage; the module acts as a 'numerical thermometer' of sorts. An additional stage serves only to localize these clusters through lateral inhibition to give a discrete representation of the input value; clusters corresponding to those with excited neighbours in the previous stage are inhibited in the final stage, so only those corresponding to the highest cardinal number (with no excited neighbours) will be activated (shown in the bottom right corner of Figure 1-3).

The model exhibits a response consistent with many of the features found in cognitive and behavioural studies of numerosity. In particular, *Fechner's law*—the observation that it is more difficult to distinguish between two large collections of objects than two collections of a small number of objects, even when the numerical distance is the same for each pair of collections—seems to be well represented in the data from trials conducted on the model, reproduced below in Figure 1-4.

To summarize these results, the model of Dehaene and Changeux seems to have captured many of the features associated with counting and numerosity. While certain features of the model seem somewhat jury-rigged—for example, the need to position loci by location on the topographical map in order to minimize overlap—the model is not implausible. Whether or not it has any actual neural correlates is a separate question entirely.

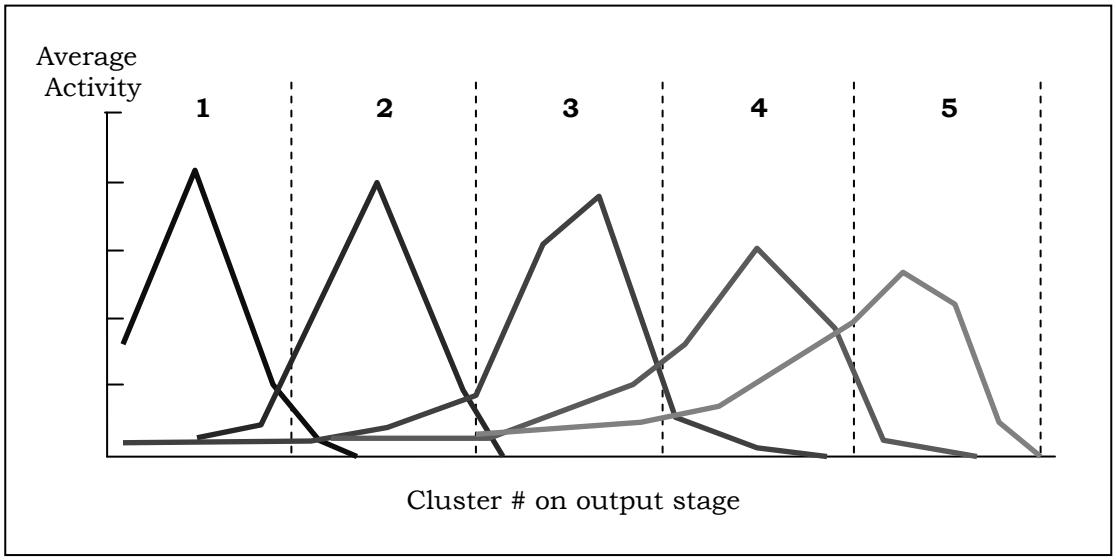

Figure 1-4. Results of the Numerosity Detector System of Dehaene and Changeux shown in Figure 1-3 and described in the text. The response to each of 500 randomized input sets consisting of 1 to 5 point stimuli shows decreased accuracy as the number of inputs (indicated at the top of each column) increase, as Fechner's Law would suggest. From Dehaene and Changeux (1993).

The second model is due to Abarbanel and Talathi [20][21]. In a recent papers, they describe a model consisting of three components, of which only the first, the *Spike Selection Unit* (*SSU*, shown in Figure 1-5 below) concerns us here; as mentioned, the remaining two components are dealt with in the next section. In both this and Figures 1-7 and 1-8, dotted circles represent *Hodgkin-Huxley* neurons, hatched circles represent bistable neurons, arrows indicate excitatory inputs, and solid filled dots represent inhibitory inputs.

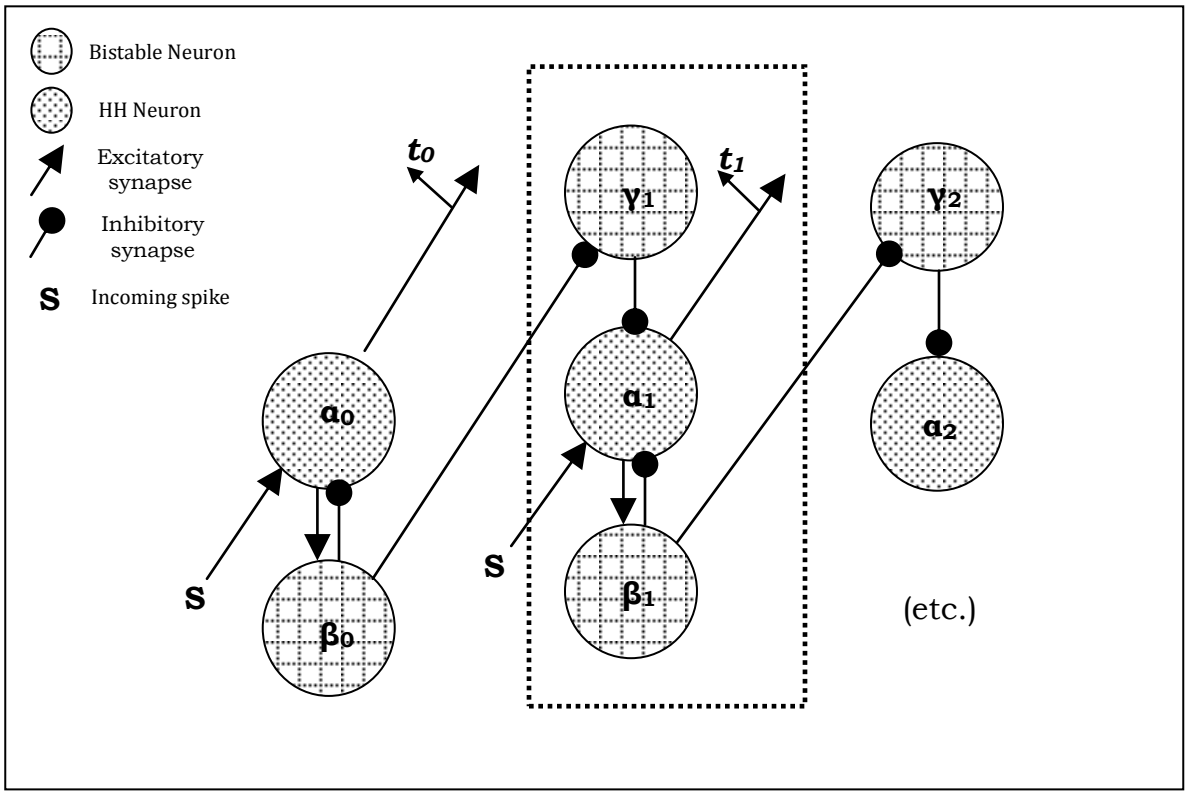

Figure 1-5: The Spike Selection Unit (SSU) of Talathi and Abarbanel (2006). Neurons labelled γ_n and β_n are bistable. In the absence of input, γ_n oscillates and β_n is at rest. a_n is a Hodgkin-Huxley neuron, which awaits (at each stage) the input of a spike (S) to activate its β_n neuron into oscillation, but only provided it is not inhibited by its presynaptic γ_n neuron. Whenever a γ_n neuron is inhibited (by a β_{n-1} neuron) and a spike then occurs at a_n, β_n freely oscillates, thus inhibiting γ_{n+1}.

Despite the apparent complexity of the SSU, its operation is straightforward. At each stage, γ_n is a bistable neuron which is initially activated, oscillating at 20 Hz. This has the effect of inhibiting its postsynaptic Hodgkin-Huxley neuron (labelled a_n in the middle of each stage). When the initial spike (S) occurs, only the first neuron, a_o, is activated by the spike, which it transmits at t_o; all other a_n's are suppressed by their γ_ns. When triggered by S, a_o activates its postsynaptic neuron, labelled β_0, which goes into

oscillation. In doing so, it performs two actions. First, it inhibits its presynaptic Hodgkin-Huxley neuron a_o, preventing it from being activated by any further spikes. Second, it suppresses the postsynaptic neuron to which it is connected (labelled γ_1), thereby inhibiting its oscillation, freeing *its* postsynaptic a_1 neuron for activation. When the next spike arrives, only the a_1 neuron is capable of receiving it, and the cycle repeats. In effect, as each a_n receives a spike, it both transmits that spike to a specific output location (at time t_n as indicated) shutting down its own stage so that no more input can be received, while simultaneously activating the next stage via the inhibition of γ_{n+1} by β_n.

Hence the SSU truly functions as a spike selection unit; the N^{th} spike of a set $\{t_o, t_1, t_2 \ldots t_N\}$ will be output only at the N^{th} output stage, with each stage activating in strict succession. But by the same token, the SSU can also be used as a counter in which, for example, activation of the fifth output stage is used to trigger some process related to the fifth input call in a series. Curiously, Abarbanel and Talathi seem unaware of this possibility; the word 'count' does not appear in their papers describing the circuit, and their primary concern is with its use in interval selectivity, the subject of the following section.

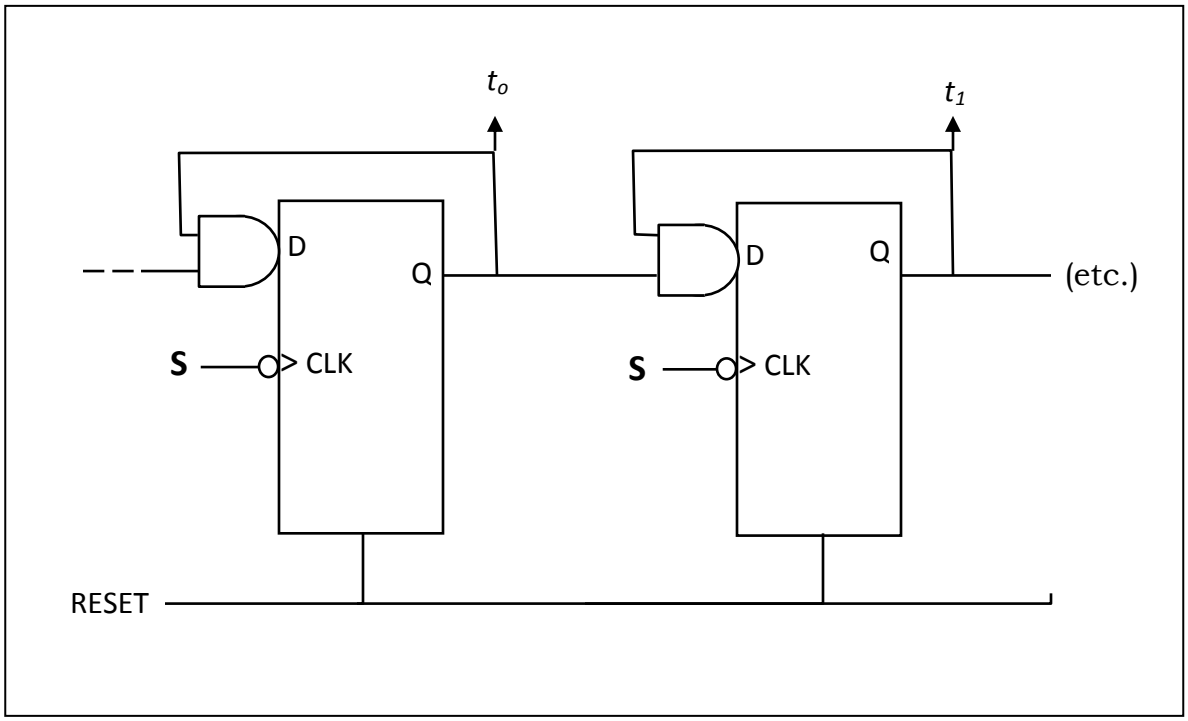

Figure 1-6. A binary shift register (SN74LS323) functionally equivalent to the neural circuit shown in Figure 1-5, from the TTL Data Book, with simplifications; much of the control logic circuitry has been removed for clarity. (Adapted from the TTL Data Book, 2nd Ed. page 7-444).

[It's worth noting that the SSU in Figure 1-5 operates in a manner remarkably similar to that of a standard TTL shift register, a sample of which is shown above in Figure 1-6. Note that the dotted box in Figure 1-5 corresponds roughly to the operation of one of the flip-flops in Figure 1-6. The only significant difference is that Talathi and Abarbanel's model shuts off each stage as it falls into disuse; the flip-flops in Figure 1-6 remain stuck at +5 Volts as they are triggered.]

The two models discussed above suffer somewhat from having a 'constructed' feel to them; there is a sense that only human engineering, rather than evolution, could design anything so specific. (But one needs to be careful here: evolution was similarly criticized by creationists on the grounds that the eye was too sophisticated a device to have been constructed entirely by chance alone.) Additionally, there is something rather 'digital' about the design of these two models (especially the second, as the TTL circuit demonstrates), where one suspects that a simpler 'analog' design might just suffice. Finally, it should be noted that both of the above models are entirely theoretical exercises; no attempt has been made to correlate experimental evidence with either of these models. Aside from the implicit suggestion that 'since it works, it may therefore reflect the true behaviour of the neural correlate,' there is no biological data to verify the actual existence of such circuits.

1.6 Interval Selectivity

The pauses between vocalizations, their duration and regularity, often play a role almost as important as the sounds that bracket them. Indeed, since calls alone are not sufficient to produce spikes in the neurons of many species, it is perhaps more accurate to say that the intervals between calls are the most important feature in intraspecies communication since that is where the information about the stimulus is actually stored.

Bats offer a primary example: the delay between a chirp and its echo forms *the* basis of echolocation. Evidence suggests that a site in the *inferior colliculus* of bats contains the requisite neural circuitry needed for this operation [22][23]. But other species rely on intervals as well, and have highly specialized circuitry designed to filter intervals of specific duration [24].

The model of Abarbanel and Talathi, introduced above, was designed to recognize *interspike intervals* (*ISIs*). In addition to the SSU shown in Figure 1-5, two other components are required to detect specific interval sequences: a *Time Delay Circuit* (*TDC*, shown in Figure 1-7 below) and a *detection unit* (*DU*, not shown but described below). Collectively, these three components—the SSU, TDC, and DU—comprise an *ISI Recognition Unit* (*IRU*, shown in Figure 1-8).

The TDC delay circuit shown in Figure 1-7 functions as follow. In the absence of an input spike, neuron B oscillates at 20 Hz and suppresses neuron C, which is limited to producing subthreshold oscillations. When a spike occurs at time t_o (transmitted via the SSU), neuron A (which would otherwise be at rest) is excited and inhibits B, which in turn allows C to produce a *rebound spike* some time $\tau(R)$ later (where R is a tunable parameter that characterizes inhibitory synaptic strength). Depending on the value of R, neuron C may fire spontaneously ($\tau(R)=0$), not at all ($\tau(R)=\infty$), or at some value in between.

Up to this point, the circuit functions much like the individual modules of the SSU itself: a presynaptic pulse at time t_o primes neuron C for the arrival of the next spike following at $t_1 = t_o + T_o$ (routed via the SSU). Where the two circuits differ is at neuron C, where two spikes will be transmitted to the detection unit (DU) by C *only* provided they fall within a certain time window, δt.

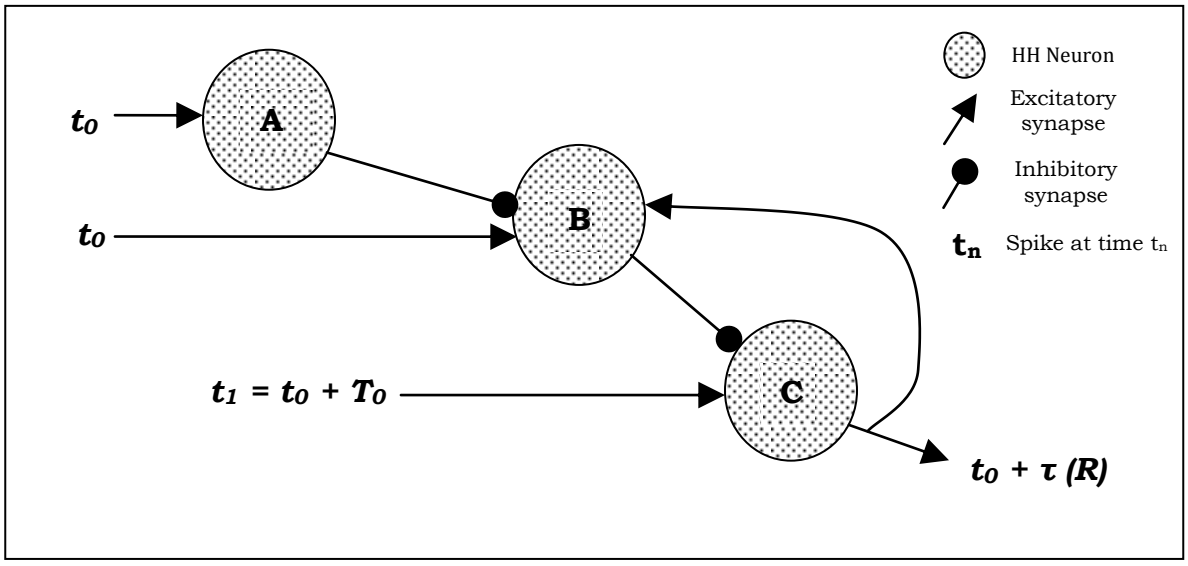

Figure 1-7: the Time Delay Circuit (TDC) of Abarbanel and Talathi. Neuron B initially oscillates and inhibits C. When a spike is received at time t_o, A is set in oscillation, which inhibits B, causing C to trigger a rebound spike at time $\tau(R)$ later, and simultaneously allowing C to receive a pulse at time t_1. If t_1 occurs in the time window $\delta t > |\tau(R) - T_o|$ then two pulses will be sent to the next stage (the DU), otherwise only one will be passed on.

Consider the situation in which the second spike (at t_1) arrives after the rebound spike, at $t_o + \tau\,(R)$. At this point, the rebound spike has already 'restarted' B via the excitatory return pathway. This in turn inhibits C again so that no other spikes can be transmitted on to the detection unit; the pulse at time t_1 is effectively blocked. So if $T_o > \tau(R)$ then the DU receives only a single spike at time $t_o + \tau_o(R)$. Similarly, if $T_o < \tau(R)$, then the spike due to t_1 arrives *before* the rebound spike, exciting B, shutting down C again, and removing the possibility of the rebound spike; again the DU only receives one spike at time $t_o + T_o$. The circuit is constructed such that only when the two pulses—at t_1 and $t_o + \tau_o(R)$ —arrive in a window of time $\delta t > |\,\tau(R) - T_o\,|$ are they transmitted to the DU. Thus, the purpose of the TDC is effectively to delay the spike arriving at t_o by a value equal to the interspike interval time T_o so that it coincides with the pulse arriving at t_1. The sole purpose of the DU (not shown) is simply to detect when two pulses arrive within δt of each other and fire if this signal is detected: the DU is just a coincidence detector. A learning rule supplied by Abarbanel and Talathi adjusts R using δt so that $\tau_o(R) \approx T_o$. A diagram of a single interval detection unit of a complete IRU is shown below in Figure 1-8.

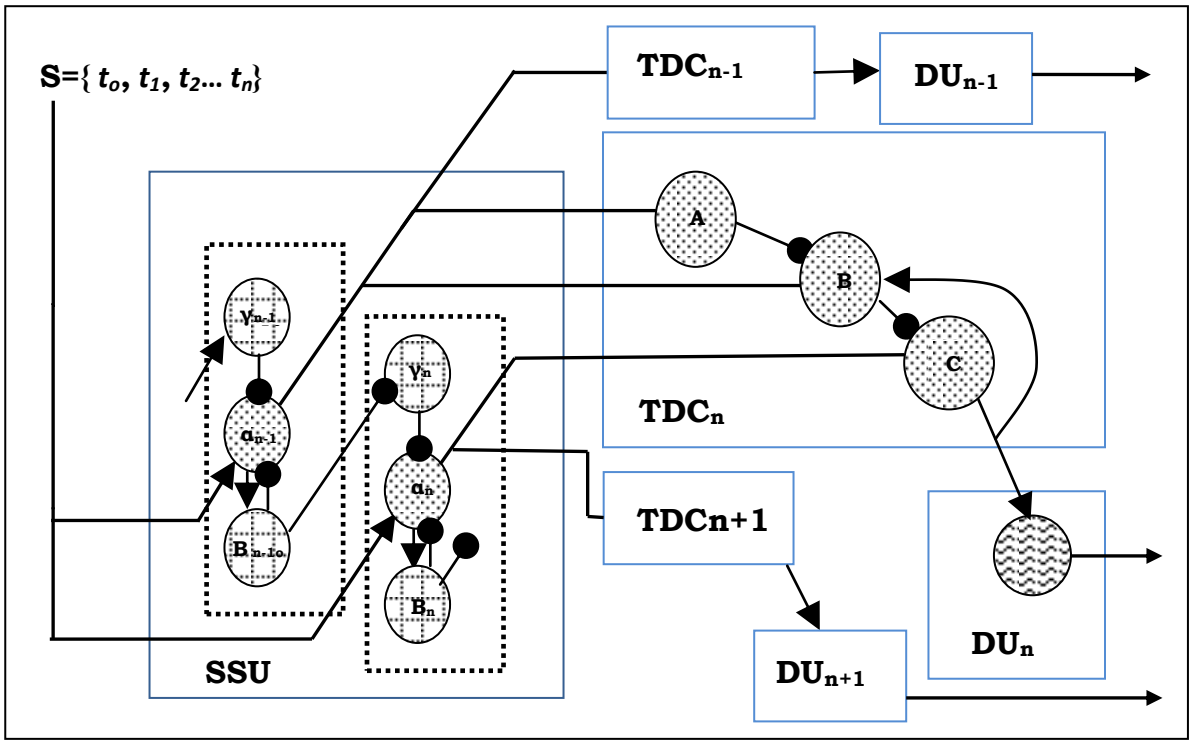

Figure 1-8. The Interval Recognition Unit (IRU) of Abarbanel and Talathi (2006). Each spike in the set S{ t_o, t_1, t_2... t_n} is transmitted simultaneously to each section of the SSU. The n^{th} spike is transmitted by the n^{th} section to the n^{th} TDC, which delays the spike by an amount of time corresponding to the expected delay until the next spike—the time delay is established through a training algorithm. If this delay falls within a particular time window δt, DU fires, indicating that an appropriate time interval between the n^{th} and $n+1^{th}$ pulse has been detected.

Before concluding this section, it is necessary to briefly address a second model exclusively designed to register and respond to a pattern of spikes and intervals. Dubbed the *tempotron* [25] (in analogy with Minsky and Pappert's *perceptron* [26]), it is not so much a circuit as an algorithm for selecting a specific pattern of spikes from amongst a broader collection of input spikes. In the tempotron, synaptic inputs to a neuron are weighted according to an iterative learning algorithm which increments synaptic input whenever an output spike is generated by a 'desired' input spike (in the sequence of spikes to be learned), and decrements the synaptic weight when an output spike is generated inappropriately by the neuron.

The tempotron is thus capable of learning to respond to a specific set of inputs at regular intervals, and so might be used to explain the behaviour of the neurons observed by Gary Rose and his colleagues. However, while possible, the specificity of the responses to input calls seen in the Rose neurons suggest that the tempotron does not offer an appropriate explanation for the behaviour of the call-counting neurons under study as reported in *Edward et al.* In particular, the distinct pattern of initial inhibition followed by the progressive depolarization to excitation and spiking, combined with the curious resetting properties of these neurons on missed pulses, cannot be adequately explained by the tempotron. The evidence suggests that the tempotron is probably not the right tool to use in explaining the unique behaviour found in the counting neurons of the anuran *torus semicircularis*.

1.7 Neurophysical Background

In a seminal paper published in 1952 [27], Alan Hodgkin and Andrew Huxley showed that the flow of ions across the neural membrane, combined with the hypothetical response of voltage-triggered channels in the membrane wall, were sufficient to describe the mechanism by which spikes were triggered, and (ultimately) by which they propagate. (The connection between neuroscience and electricity goes back much further still, to 1791 and Galvani who, curiously for this author, was also studying frogs.)

This present work is not immediately concerned with the Hodgkin-Huxley model, which deals with the flow of Na^+ and K^+ ions and the role they play in spike generation (as was briefly addessed in Section 1.2). Our concern here is with the inhibitory and excitatory synaptic currents that lead to voltages which will eventually generate spiking, along with

the conditions that must be met for this to occur. However the fundamental, underlying theory remains the same. A simple law governs the voltage behaviour of neurons which, while functionally of Newtonian simplicity, quickly leads to an equation of such mathematical intransigence that one is immediately forced to consider how best to simplify the model even further—and all this even before noise has been incorporated. The equation which models the electrophysiology of the membrane at any time is just Kirchoff's current law. The equation is simply

$$C\frac{dV}{dt} = -\sum I_{out} - \sum I_{in}\ , \tag{1.1}$$

where V is the voltage inside the neuron relative to the intercellular fluid; C is the capacitance of the membrane; and I_{in} and I_{out} are the currents in to and out of the cell respectively. Specific current sources, such as leak currents, synaptic currents, ion channel currents and experimentally applied external currents—whether flowing inward or outward— may be introduced into equation 1.1 as required. In each case the response of the neuron is the same: the voltage change per unit time is proportional to the difference between outflowing and inflowing currents, a simple fact which will be exploited more fully to help develop our model in Chapter 3.

For the simple case in which a fixed bias current I_b is externally applied or, alternately, the case in which the membrane contains a current pump which supplies a constant flow of charge, equation 1.1 simply becomes

$$C\frac{dV}{dt} = -I_b \tag{1.2}$$

with the standard result that

$$V = \frac{-I_b}{C}t + V_0. \tag{1.3}$$

Current flow is measured as positive if positive ions flow *outward* thereby hyperpolarizing the neuron, and negative if they travel *inward*, depolarizing it [28]. An injection of positive ions thus constitutes a negative current flow (and so $I_b < 0$) in equation 1.2, and dV/dt increases with time. Thus the definition of current flow is consistent with our expectations.

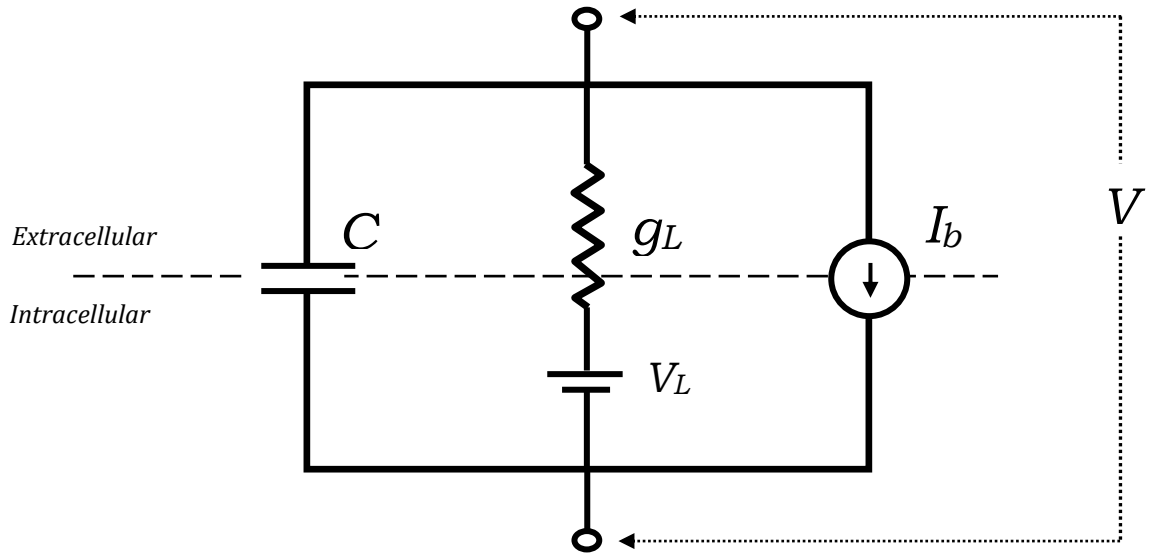

Figure 1-9. The circuit diagram for a model neuron having only an ion pump and a leak current.

Frequently, the current I_x is taken to have an ohmic response of the form

$$I_x = g_x(V - V_x), \tag{1.4}$$

where V_x is a fixed voltage set according to the nature of the current source, and g_x is the *conductance*, the inverse of the membrane resistance.

If an ohmic leak current is added to the circuit (shown in Figure 1-9), then equation 1.1 can be written

$$-C\frac{dV}{dt} = I_b + g_L(V - V_L), \tag{1.5}$$

with the result that

$$V = V_0 e^{\left(\frac{-g_L}{C}\right)t} + (V_L - \frac{I_b}{g_L}). \tag{1.6}$$

We note for future reference that in a neuron with only a bias current and a leak current present, the eventual resting voltage (as $t \to \infty$ in equation 1.6) will be

$$V_{t\to\infty} \equiv V_R = \left(V_L - \frac{I_b}{g_L}\right). \tag{1.7}$$

Since V_R is easily measured and I_b is not—assuming that the cell's internal ionic pumps are responsible for the bias current—we can rewrite equation 1.7 in terms of I_b as

$$I_b = (g_L V_L - g_L V_R). \tag{1.8}$$

Substituting 1.8 into 1.5 gives

$$C\frac{dV}{dt} = g_L(V_R - V). \tag{1.9}$$

So for practical purposes the actual values of V_L and I_b need not concern us; V_R subsumes both values into one easily-measured voltage.

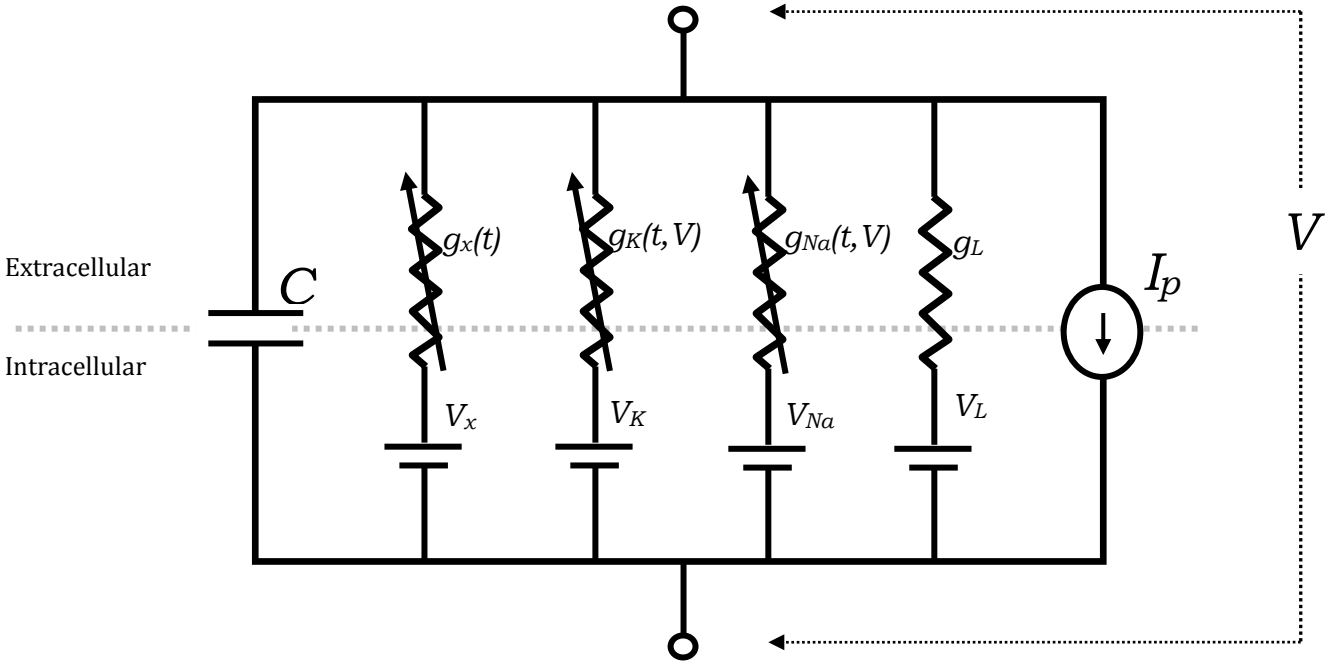

Figure 1-10. The equivalence circuit for a generic model neuron having multiple current sources and sinks.

Unfortunately for computational neuroscience, equations like 1.2 and 1.9 are far too simplistic to be of practical use: in real neurons conductances vary with time due to synaptic inputs. A more realistic model (of the sort shown in Figure 1-10 above) will have the general form

$$C\frac{dV}{dt} = g_L(V_R - V) + \sum_x g_x(t, t_o)\big(V_x - V(t)\big), \qquad (1.10)$$

where the conductances g_x may be excitatory or inhibitory, t_o is the time of onset of a pulse, and $g(t, t_o)$ dictates the temporal behaviour of the conductance during the time following the pulse, and hence of $V(t)$ itself.

This information will be put to use in Chapter 3 where, using a time-dependant conductance, a model will be postulated based upon simple observations and rudimentary assumptions of the sort provided above.

1.8 Summary

Successful communications between animals and insects require appropriate neural correlates, locations in their brains which process species-specific information and trigger suitable responses. Counting and, concomitantly, interval sensitivity would appear to play a major role in this process (in addition to being interesting topics in their own right). Despite ongoing interest in the subject of counting (or numerosity) and a recent spate of books and journal articles published on its behalf, the mechanism(s) by which species estimate the quantity of things remains largely unknown. Frequency-sensitive call-counting neurons in the anurans studied by Gary Rose and his colleagues would thus appear to present an important model system for the exploration of richly-coded auditory stimuli.

The physics that dictate the bioelectrical behaviour of individual neurons has been reasonably well understood for half a century, and this theoretical framework has been successfully applied to explain a wide variety of experimental observations. This first chapter has attempted to introduce this framework in preparation for the discussion that follows, as well as provide a justification for the research itself and the problems inherent in the subject, along with previous attempts at modeling the phenomena we call 'counting'. The problem that remains in the chapters that follow is to construct a comprehensive model linking the physics with the experimental data. Having introduced the former in this chapter, we turn now to the latter.

Chapter 2: The Experimental Evidence for Frequency-Dependent Call-Counting in Anurans

2.1 Introduction

The interval between the vocalizations of anurans (the *IPI*, or *interpulse interval*) is known to be regular and species-specific [29]. The discovery of interval-sensitive call-counting neurons in the *torus semicircularis* of two species of frog would thus seem to make anurans a model system for the study of interspecies communication in general and of counting in particular, since both the stimulus and response can be studied *in vivo*, in a controlled environment.

This chapter looks at the response of these neurons (one of which is illustrated in Figure 2-1) to a series of pulses, based on experimental evidence obtained by Dr. Gary Rose and his colleagues Christofer Edwards and Christopher Leary at the University of Utah, and subsequently published in *J. Neuroscience*, December 5, 2007 by *Edwards et al.*[2]. This journal article, along with supplementary data obtained from Gary Rose, forms the experimental foundation upon which subsequent chapters are based.

2.2 Methodology

Edwards et al. provides a concise description of the procedures involved in their experiment to identify call-counting neurons, the specific details of which need not concern us here. Indeed, this section provides only a brief summary of the most relevant results of the materials and methods section of that article, while the steps required to record from candidate neurons via a whole-cell technique are entirely ignored; the curious reader is advised to consult *Edwards et al.*, along with a few of Gary Rose's early works [30][31][32] for details. Nonetheless, a few comments from the materials and

methods section are relevant to later chapters of this manuscript, and are noted briefly in the paragraphs that follow.

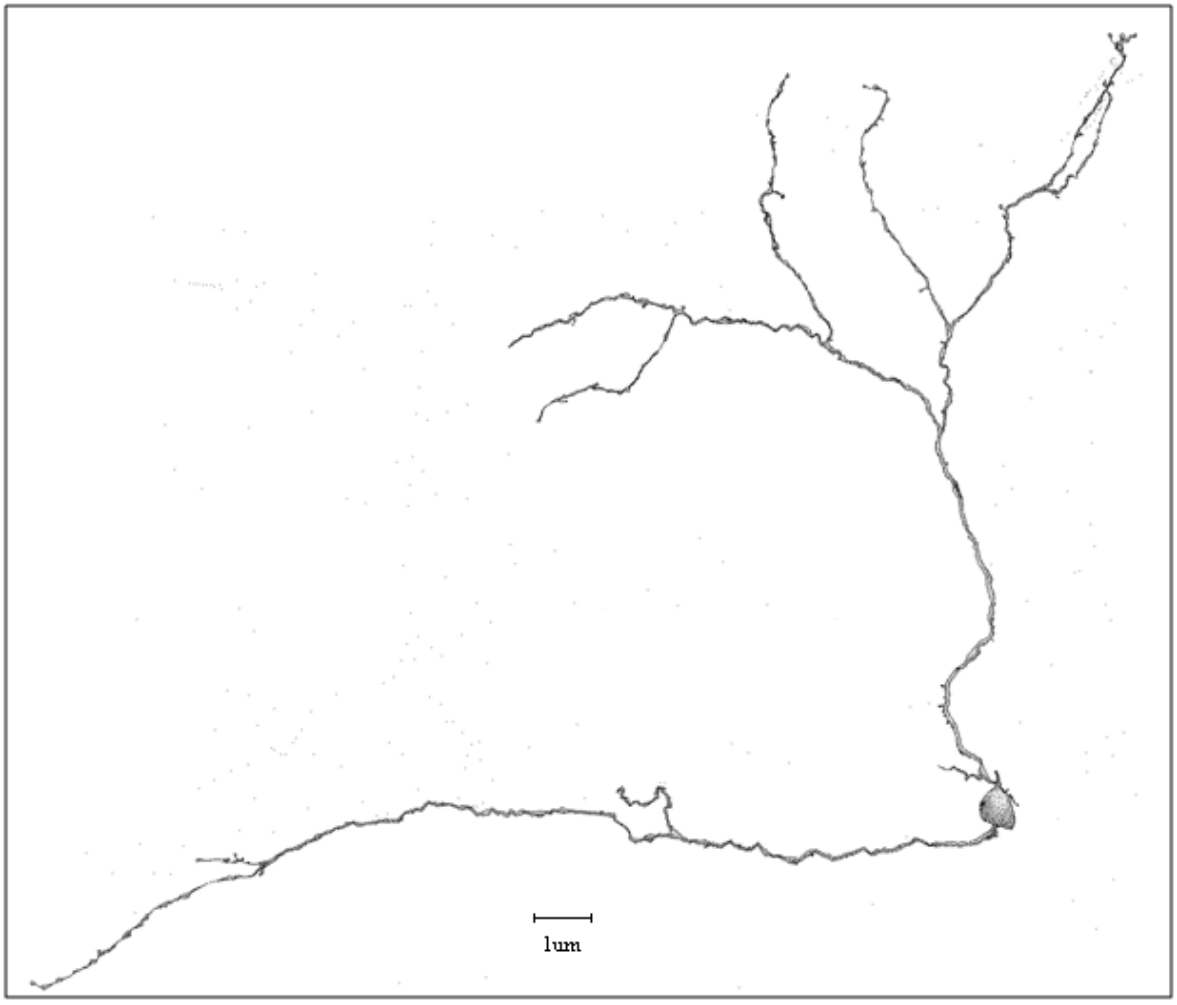

Figure 2-1: Drawing of a frequency-dependent call-counting neuron of the anuran *torus semicircularis*. Courtesy of Dr. Gary Rose.

In the preliminary analysis performed by *Edwards et al.* neurons were characterized according to their basic neurophysiological traits. Consideration was initially given to the question of *frequency tuning analysis* of the neurons. This consisted of presenting stimuli to anesthetized specimens in the form of either species-specific calls or brief white-noise *tone bursts* of 10-50 *ms* duration. This procedure was performed in both positive and negative *current clamp* mode, thus minimizing, in the former case, the excitatory current (i.e. V is raised to near the excitatory *reversal potential* V_e, and hence $g_e(V_e-V)\approx 0$) and in the latter case, the inhibitory current (V is lowered to near V_i, and so $g_i(V_i-V)\approx 0$.) As equation1.10 makes clear, the effects of an excitatory current cannot be fully isolated from that of an inhibitory current, since both are dependent on the voltage V inside the

neuron. However, by forcing a neuron to near either of its two reversal potentials, V_e or V_i, the effects of that current can be minimized. Experimentally, in both cases, the response to a single call or burst of calls was only weakly excitatory, followed by (in positive current clamp mode) a pronounced inhibitory response.

This operation was performed in preparation for a later analysis, the purpose of which was to address the question of whether the excitatory and inhibitory frequency response of counting neurons span an identical range, i.e. if excitation and inhibition could be isolated and driven independently, would they respond over the same range of input frequencies? (As a rough analogy, consider measuring the gain response of a leaky audio amplifier with and without a DC offset voltage applied.) If the frequency range of inhibition spans (i.e. starts at a lower frequency and extends to a higher frequency than) that of excitation then the excitatory current would be somewhat attenuated by the inhibition, further decreasing the apparent range of the excitatory response. This was found to be the case: the inhibitory range spans that of excitation, at least to the extent that this can be determined experimentally.

Also during this initial stage of the experiment, the baseline features of each cell were determined, including the best pulse repetition rate (PRR), interval-number threshold, and *best excitatory frequency* (*BEF*)—the fundamental frequency of each call or pulse, typically on the order of 800 Hz. Additionally, cesium fluoride was sometimes loaded into the neuron and the effects monitored. (Cs^+ effectively depolarize neurons by trapping positive charge inside the neuron, making the intracellular voltage less negative.) Its effects, while not quantitatively analysed at this stage of the experiment, were essentially to enhance EPSPs, decrease IPSPs, and broaden action potentials. A more detailed analysis of the consequences of Cs^+ loading is included later on in *Edwards et al.*, but the results can be summarized as follows: depolarization due to Cs^+ loading decreases interval-number thresholds, leading to spiking with lower call number. Put more succinctly still: an 8-counter without Cs+ loading becomes a 5- or 6-counter with loading, precisely as one would expect, since neurons are more likely to spike the closer they are to their excitation threshold.

One point of considerable interest—unfortunately not addressed in greater detail in the journal article—concerns an analysis of conductances in call-counting neurons using a method developed by Priebe and Ferster [33]. According to *Edwards et al*, enhancement of EPSPs (i.e. depolarization) due to repeated calls are mirrored by changes in the excitatory conductance, g_e. Furthermore, the data suggests that pulse-dependent

depolarizations are due to excitatory currents *only*, and *not* to a reduction in inhibitory currents. Additionally, when the experiment was performed in negative current clamp mode using optimal intervals (i.e. the best PRR) with a subthreshold number of pulses, EPSP duration (i.e. the breadth of the response) was not observed to increase, although EPSP amplitude (the height of the response) did. This again suggests that increases in excitatory current at optimum PRR are due to increased g_e, and are not enhanced by increases in V_e-V, the so-called '*battery term*' in equation 1-10. This observation will be commented upon later in more detail.

With this cursory overview behind us, we now turn our attention to actual results obtained by *Edwards et al.*

2.3 The Optimum PRR of Call-Counting Neurons

Figure 2-2 illustrates a feature of call-counting neurons mentioned earlier. When individual calls are presented to these neurons, the response is largely inhibitory, with IPSPs of perhaps a dozen millivolts or so. Complicating matters somewhat, the inhibitory stage is often preceded by a small EPSP of not much more than 1-2 *mV* (as indicated by the arrows). While this feature is barely above noise levels, it is reproducible enough that it can't be ignored.

As the PRR increases from 5 Hz to 30 Hz the neuron displays a time course consisting primarily of IPSPs interspersed with an occasional small EPSP; the overall behaviour remains largely inhibitory. As the frequency increases still further, EPSP size increases and the neuron begins to depolarize as excitation begins to dominate, typically somewhere above ~20 Hz. Finally, at the optimum PRR, the neuron reaches its spiking threshold and one or more spikes are observed.

Note that Figure 2-2 and the figures that follow are copied from *Edwards et al.*, and have in some cases been adapted for clarity. As explained below, neither the data upon which this journal article was based nor the diagrams published in *Edwards et al.* have been made available to us.

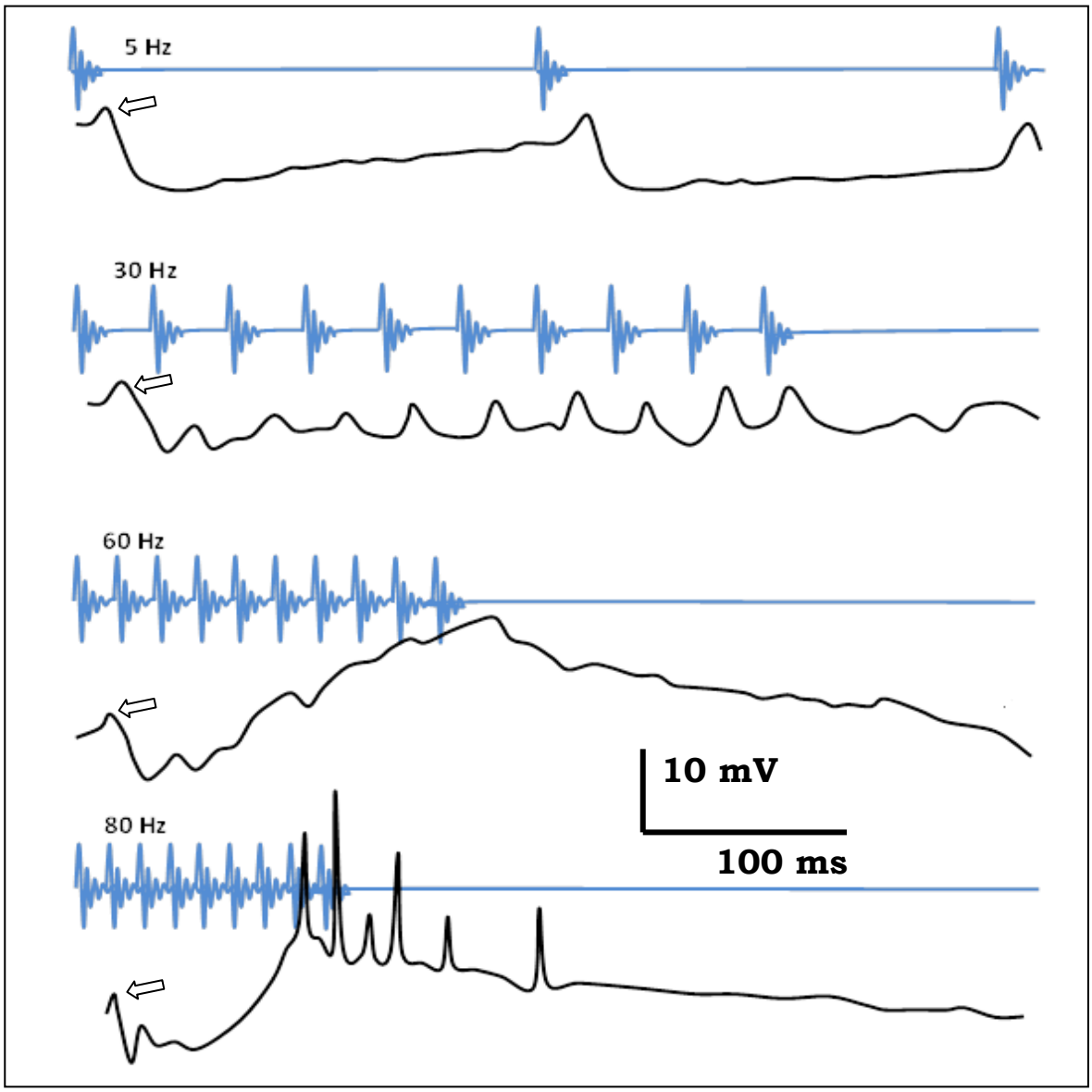

Figure 2-2. The voltage dependence of a frequency-sensitive counting neuron (in black) on input call frequency (in blue), over four separate call frequencies. Adapted from *Edwards et al.(2007),* Figure 1A, who uses the average of 10 pulses for each output trace. Because spikes do not occur precisely at the same time from trial to trial, averaging tends to attenuate spike size. The arrows signal the presence of a small EPSP present at the start of each call response, which is invariably followed by a broad trough of inhibition.

2.4 Counting

As seen in Figure 2-2, spiking depends entirely upon overcoming the natural tendency of the neuron towards inhibition (seen at low pulse repetition rates) with stimulus calls delivered in both sufficient number and at a sufficient rate. Consider the situation in

which a subthreshold number of pulses is delivered at optimum PRR, as in Figure 2-3 below. While the net depolarization may increase by a few millivolts, this will not generally be sufficient to generate spiking. For example, in the traces of the 5-counter shown in Figure 2-3 (taken from *Edwards et al.* Figure 2A) a net depolarization of only $\sim 7mV$ is seen after four calls; spikes are elicited only following the fifth call (not shown).

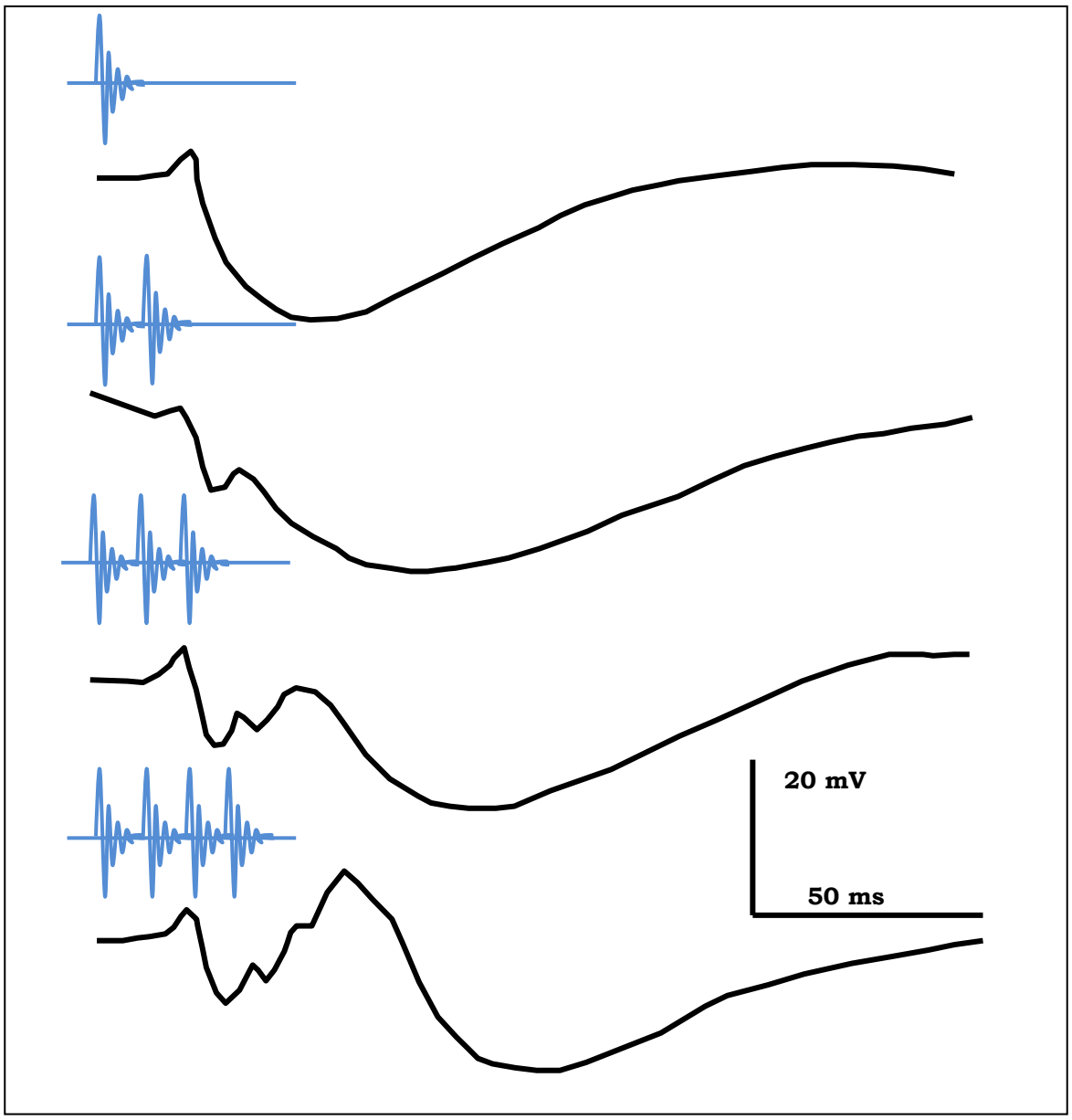

Figure 2-3. The dependence of a frequency-sensitive counting neuron (in black) on input call count (in blue) delivered at the optimal PRR. Adapted from *Edwards et al. (2007),* Figure 2A.

Additionally, it can be seen that each successive call extends the inhibitory time course of the neuron's response by approximately one call duration (~12.5 *ms*) up until the third call, at which point excitation begins to dominate the neuron's response. Indeed, while the first call depolarizes the neuron to -78 *mV*, the second call depolarizes the neuron still further to -81 *mV* at what must be very close to V_i, the reversal potential of the neuron. *Edwards et al.* notes that little or no *depression* of inhibition was observed during this stage from calls delivered at optimum PRR; in other words, the inhibitory conductance increase caused by each successive call is approximately the same. However, rate-dependent depression of inhibition could not be ruled out during the later excitatory time course when, after the third call, the situation begins to reverse. This again is due to the fact that excitatory and inhibitory currents are linked by the internal voltage of the neuron according to equation 1-10, and only under artificial experimental conditions can one or the other be more or less eliminated.

A strong case can thus be made that the purpose of these neurons is to act not just as a frequency-sensitive call filter, but as a number-sensitive counter as well, since spiking occurs only at both the correct PRR and the *interval number threshold*.

Additional corroborating evidence was obtained by hyperpolarizing neurons in negative-current clamp mode by -12 *mV* to -77 *mV* (not shown here), close to the inhibitory reversal potential of the neuron. The response of these hyperpolarized neurons to the first two calls was two EPSPs of approximately equal amplitude, followed as before with EPSPs of increasing size as additional calls were presented. The data offers additional support for the hypothesis that enhancement of EPSPs rather than changes in inhibition are responsible for the time-course observed.

It should be noted that the behaviour seen in Figure 2-3 is highly atypical of neurons in general. As a rule, one expects either a monotonic increase in membrane potential if a neuron has mainly excitatory synapses (as when *AMPA* and *NMDA* neurotransmitters predominate), or a monotonic decrease (for example, if *GABA* is the neurotransmitter present at the synaptic inputs). So perhaps the most curious feature of call-counting neurons is not so much that they count at a particular PRR frequency, but that, following a small depolarization, they strongly hyperpolarize—inhibiting spiking on the first few calls—before reversing and quickly depolarizing to a spiking potential. This conflicting behaviour opens the possibility that a rather complicated mechanism is perhaps at work.

2.5 Reset on Missed Calls

Missed calls play a critical role in determining the response of call-counting neurons. For example, when calls are paired with a small interval between each pair, the result is a mixture of small EPSPs and IPSPs, followed by a broad inhibitory time course, as shown in Figure 2-4. This occurs even when the average call-frequency is identical to the optimal PRR for the neuron, and the total number of calls exceeds the minimum required for spiking. The response of neurons to the mixed-interval regimen was similar regardless of the number of calls required to reach the spiking threshold at the optimal PRR. *Edwards et al.* suggests that the amplitude of the response indicates that the putative *afferents* (i.e. the neurons presynaptic to the call-counting neuron) respond only to the first call in the paired-call regime; the second call is ignored when calls are too closely spaced.

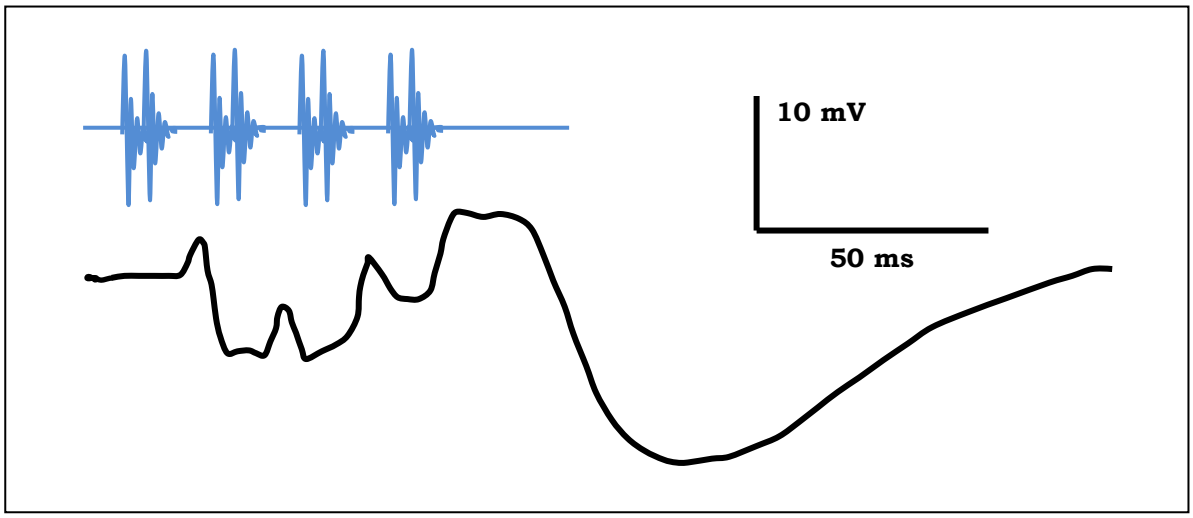

Figure 2-4: Pairing of calls produces a subthreshold response, even though the average call frequency equals the optimal PRR, and the total number of pulses exceed the number normally required to produce spiking. The neuron normally would spike on the 7th call. Adapted from *Edwards et al. (2007)*, Figure 2D.

Corroborating evidence is obtained by measuring the response of neurons stimulated at frequencies higher than the optimal PRR. For the neuron with an optimal PRR of around 80 Hz shown in Figure 2-5, the number of resultant spikes per stimulus response drops off at higher PRRs.

Edwards et al. suggests that as with the paired-pulse response, the frequency-dropoff, is simply due to the overlap between incoming calls. Thus a natural bandpass filter arises,

wherein the low-pass filtering is performed in the afferents which 'skip' input calls when they arrive too close together, and the high pass filtering is effectively performed in the call-counting neurons through a combination of excitation and inhibition which attenuate out the low frequency (i.e. low PRR) calls.

Another factor, not mentioned by *Edwards et al.*, may also account for the high-frequency attenuation above 80 Hz seen in Figure 2-5. The vertical axis displays spikes per call repetition, presumably because this is the most relevant parameter to measure: spikes out versus calls received per unit time. Thus if the number of spikes output tops out at a maximum PRR of say, 80 Hz, then the *absolute* number of spikes per millisecond can only drop off as the input call rate (or PRR) increases: the number of output spikes per stimulus *must* drop at higher PRR frequencies. So whether the neurons of the *torus semicircularis* perform an actual band-pass filter or just a high-pass filter may simply depend upon what one determines to be most relevant measure of output.

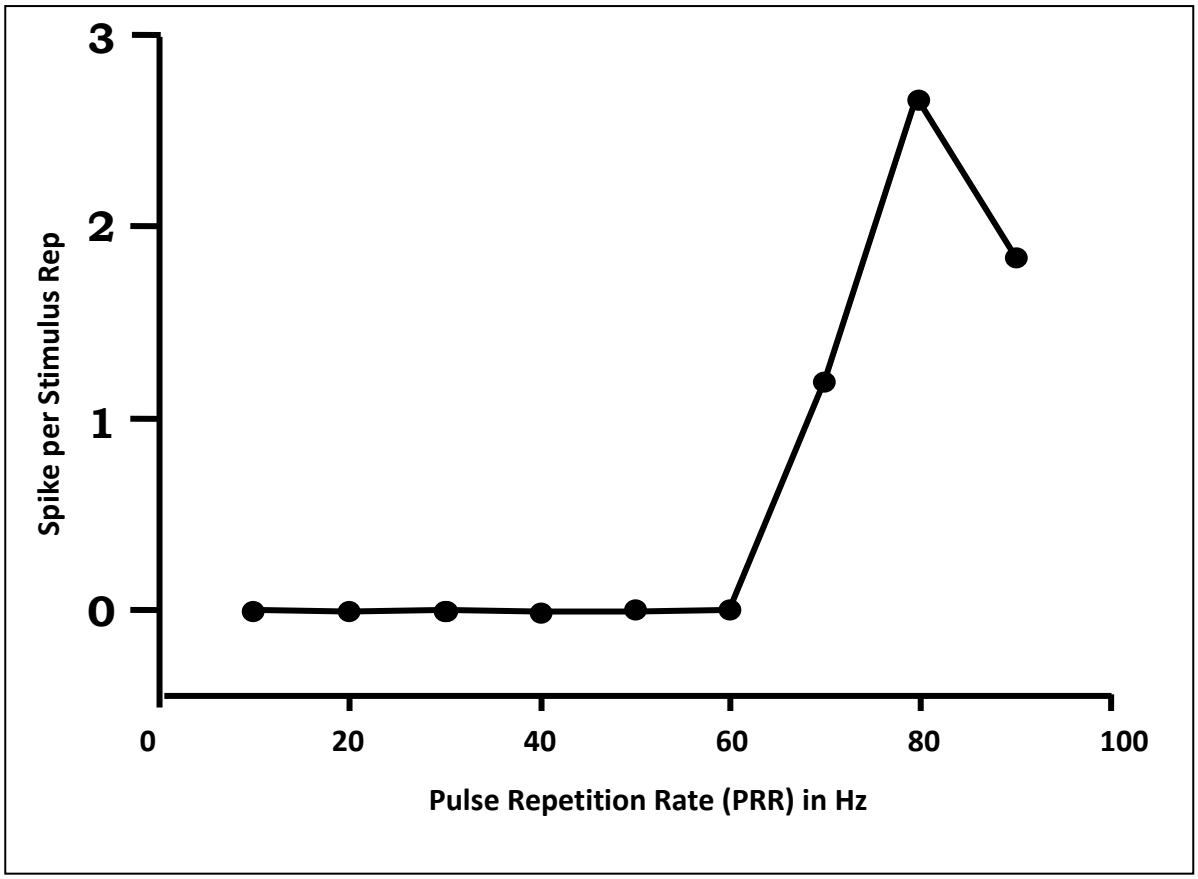

Figure 2-5: High frequency (i.e. >80 Hz) attenuation of spike production with increased call frequency (PRR). Adapted from *Edwards et al.* (*2007),* Figure 1B. The size of the errors associated with each point are unknown, hence the apparent peak at 80 Hz may be misleading. Other factors, described above, may also play a role.

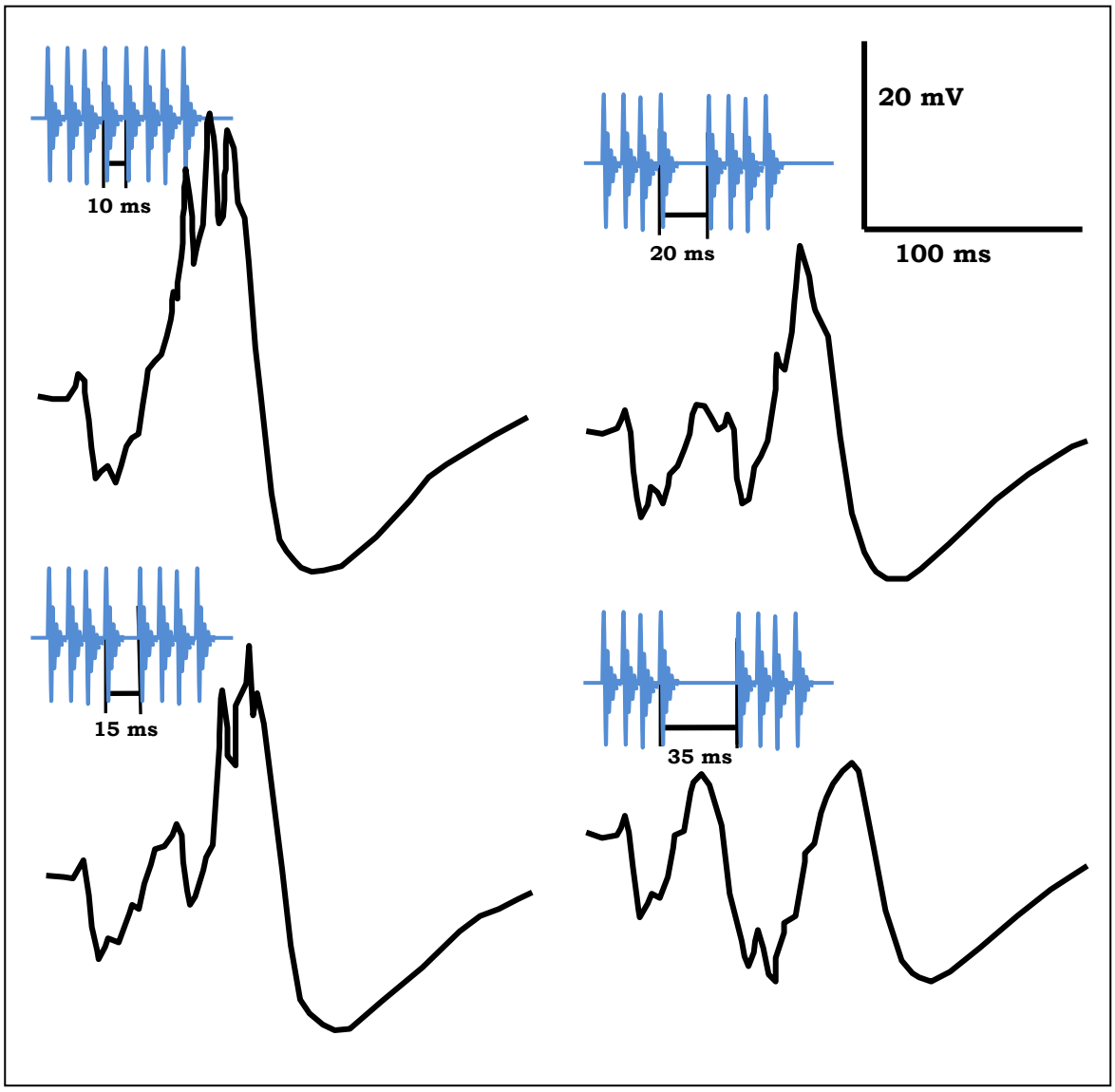

Figure 2-6: Dependence of a frequency-sensitive counting neuron (in black) on missed calls (in blue). Partial resetting is seen in the response of the neuron following the interval. Adapted from *Edwards et al. (2007),* Figure 2C. Note that averaging has the effect of removing spiking entirely, although for any small delay interval there will always be spiking present some of the time.

Even when calls are presented at optimal PRR, a delay interval of sufficient duration effectively resets the neuron so that counting must begin again, as shown in Figure 2-6. This effect is not complete, and spiking may still occur if the interval is sufficiently short. However, the probability of spiking decreases with increased interval length. The general results hold however. (As elsewhere in this chapter, figures shown are averages over ten trials, so while it may appear that no spiking occurs below a certain PRR, in actual fact spiking is simply less probable; because spiking times vary from trial to trial, averaging

flattens the spikes, and essentially removes them entirely when their probability of occurrence is low enough. For a reset period of >35 *ms*, *Edwards et al.* report that spiking still occurs 25% of the time immediately following the reset period, although the averaged output shown in Figure 2-6 would seem to indicate that no spikes occur at all.)

Table 2.1: Summary of information displayed in data set A

# of calls	Trials available in data	Exemplar
1	6	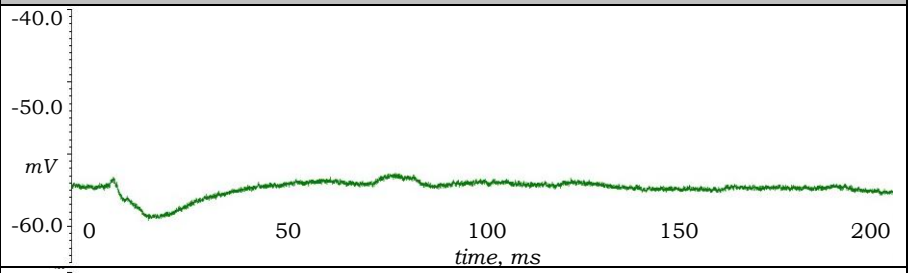
2	5	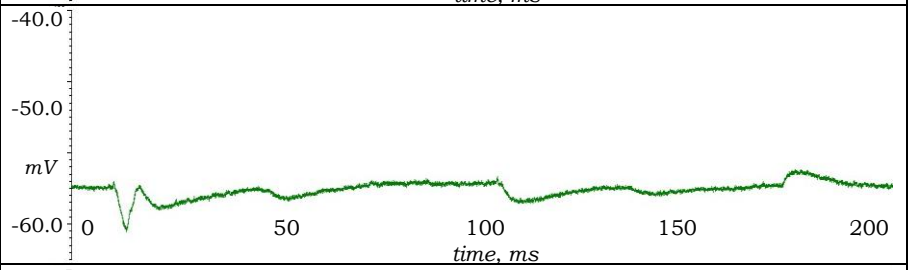
3	4	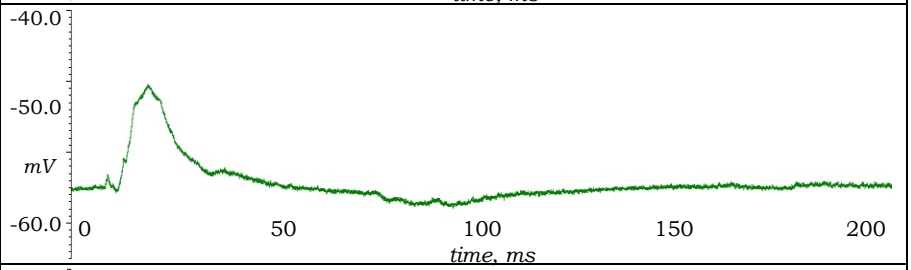
4	2	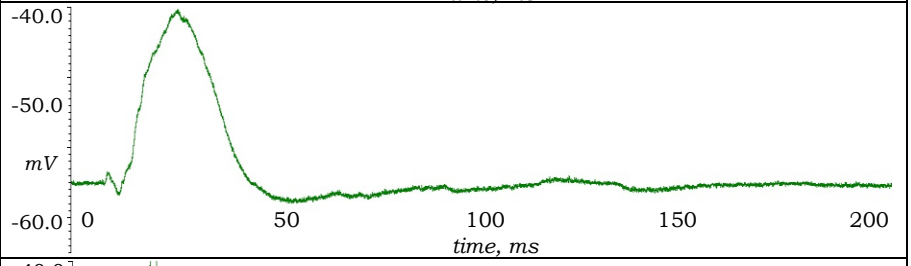
5	4	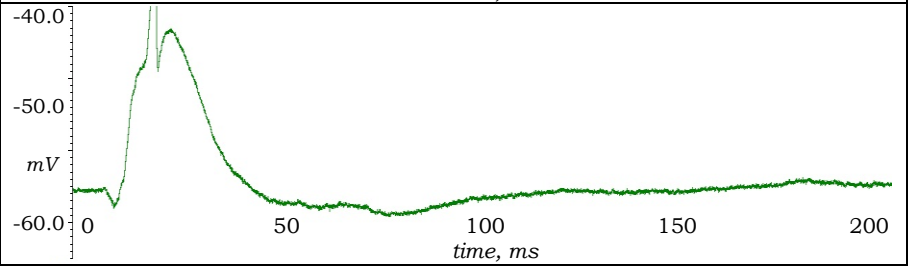

Furthermore, the response of a neuron to calls following a short reset period (typically equal to one or two call durations of 12.5 - 25 *ms*) is *not* comparable with the initial inhibitory response obtained when the neuron has been allowed to fully recover between trials, as a comparison between Figures 2-3 and 2-6 shows. Short intervals elicit, at best, a partial reset, albeit often one sufficient to temporarily quench an otherwise excitatory response, even when the number of calls is just one short of the threshold number.

2.6 Supporting Data

Two sets of raw data were provided by Gary Rose from recordings made November 5, 2005 which demonstrate the response of a single neuron to the input call count at optimal PRR. The first set, henceforth referred to as data set A, includes 31 trials consisting of 1 to 5 input calls each at a pulse repetition rate of 80 Hz, along with the recorded response of the neuron. Following each input of 1 to 5 calls, there is a 2-second recovery interval, during which time the neuron effectively resets to its resting value of -65 *mV*, making for a total of ~63-seconds of data. (Strictly speaking, one trial demonstrates the effects of an incomplete call, showing the failure of the neuron to respond when the call is interrupted before completion. Nine other samples include trials where spiking occurs, and are not immediately useful, except perhaps in the determination of the spiking threshold. So the total number of useful trials is 21.) This data is summarized above in Table 2.1.

From this data it is possible to construct a general output response curve for each of the four subthreshold call sequences; this is shown in Figure 2-7. Each response is averaged over the number of calls available according to the values shown in the second column of Table 2-1. For example, the 1-call average (in red) was generated from the six available 1-call responses provided in data set A, which are individually shown in Figure 3-7 below. The relative time of onset of the input calls is indicated by the colour-coded calls in the top left corner of the graph and is displayed solely for the purpose of giving a visual indication of the onset time of each call as it occurs. All four averaged plots have been heavily filtered with an 11^{th}-order Butterworth bandpass filter to remove the noise which is inevitably present when recording directly from neurons.

The actual latency time between the onset of a call and neuron's response is ~26 *ms* in the data, but in Figure 2-7 the input calls have been shifted so that the start of the first

call is aligned with the onset of the response it generates, i.e. the start of the first call (in red, near the top left corner) is aligned with the start of the brief EPSP it provokes; for the 2-call response (in green), the first call in the series starts again at 0 *ms* and the second call starts at ~13 *ms*. The 3-call and 4-call input calls and their responses are indicated in light blue and dark blue respectively in the top left of the figure.

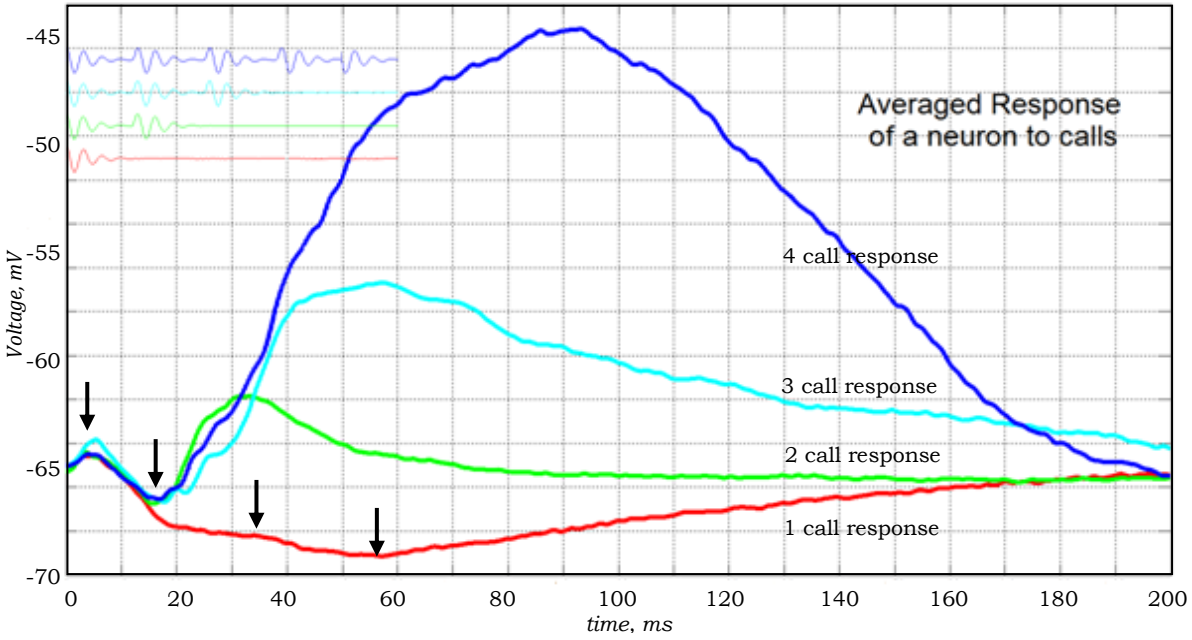

Figure 2-7: Average response of call-counting neurons to 1 (red), 2 (green), 3 (light blue) and 4 (dark blue) input calls at a PPR of 80 Hz and BEF of 800 Hz, from data set A. See text for information regarding the onset of calls (top left corner) and their response. Note: 4th order Butterworth filtered.

A second data set provided by Gary Rose, apparently recorded from the same neuron on the same day, also shows the effect of 1 to 5 input calls applied at a PPR of 80 Hz. For this second set, a -3 nA current has been applied to the neuron, and the inhibitory effects of this current depress the resting potential of the neuron to -73 *mV*, effectively preventing spiking. While some information can be gleaned from this 61-second recording (henceforth referred to as data set B), it is of less value than that obtained in data set A, which itself is rather limited in the scope of conditions it explores. (Both data sets were recorded at 10 kHz.)

Complicating matters further, there is a wide degree of variability seen in the data available in both data sets, as indicated in Figure 3-7. Unfortunately, despite repeated requests, no other data was provided. Therefore, the assumptions made in formulating

this thesis are based almost entirely on the three pieces of information available to us: the descriptions provided in *Edwards et al.*, discussed above, and the two data sets, A and B.

Data set A, while providing an exceptionally clear signal—although not without some noise—nonetheless demonstrates only one of the features found in *Edwards et al.*, that of the 'counting' of a neuron stimulated by a varying number of calls at its BEF at optimal PRR. The neuron is a '5-counter', spiking only after five consecutive calls at a PRR of 80 Hz. There is no data in this sample to indicate the response to lower PRRs, nor does the sample contain any data showing resetting due to one or more skipped pulses.

Furthermore, the neurons reported in *Edwards et al.* are exemplary, and have clearly been chosen to highlight particularly desirable traits in support of the thesis of that paper. The neuron whose output forms data set A is far from exemplary, and, while not contradicting *Edwards et al.* explicitly, demonstrates that the real world is full noise, jitter, and a large degree of ambiguity. In particular, Figure 2-7 shows a rather pronounced excitatory 'bump' peaking at ~32 *ms* in the single-call response data, just where the inhibitory trough should be deepest, which is not present in any of the data presented in *Edwards et al.* While it would be convenient to dismiss this as an anomaly, close inspection of the raw data reveals a similar broad EPSP in many of the 1- and 2-call recordings. Indeed, there are hints of this EPSP in the current-injected data set B as well.

Thus, of the two main sources of information available in support of this thesis, i.e. the paper by *Edwards et al.* and the data sets, the first may be characterized as consisting of exemplary, but inaccessible, data, at best only available in PDF format. This information is descriptive only, and does not provide an accurate time series for further analysis. Its chief benefit lies in the fact that it describes the ideal achievable output in broad terms—a qualitative target to shoot for. The second, in the data sets, is raw, precise, and of some value, but extremely limited in the scope of what is needed for a full analysis: it is a one-dimensional snapshot of a neuron functioning in a much higher dimensional parameter space.

It should be noted that while this situation is unfortunate, it is not necessarily unavoidable. The process involved in obtaining electrophysiological data from these neurons requires considerable expertise, patience, stamina, and a fair measure of luck; this is experimental electrophysiology at the cutting edge. Stable, low-noise signals like

those shown in Table 2-1 are difficult to obtain, and while a 'wish list' of possible trials has been suggested to Gary Rose, the probability of obtaining this information from a single neuron, requiring a total of approximately ten continuous minutes of data collection, is at present very low.

2.7 Summary

Recordings taken from neurons in the anuran *torus semicircularis* by Gary Rose and his colleagues exhibit a particular and unusual response when presented with a number of input calls delivered at a regular rate. When both the call number and their input frequency are of a particular, preset value, the neuron spikes; lesser values of either the call number or frequency result in a subthreshold response at best. Despite the presence of noise, the phenomenon is reproducible to a large degree, and appears to provide basic insight into some of the more complicated capabilities of the mammalian brain such as counting and communication.

The problem which thus presents itself, and which this thesis endeavours to address, is simply this: given a recorded output $V(t)$ like that shown in Figure 2-7, and the equation (1-10) which dictates the behaviour of $V(t)$, what reasonable assumptions must be made in order to reproduce the features observed in the call-counting neurons of the anuran *torus semicircularis*? The evidence provided by *Edwards et al.*, along with data outlined in Section 2.6, strongly suggests that any model relying on the simple summation of input pulses to the neuron will be inadequate; a more elaborate mechanism is needed to account for this behaviour.

The problem, then, is analogous to the situation in which one is presented with an electronic 'black box' whose behaviour is known, but whose internal structure—the number of components, their properties, and interconnections—is not. In the chapters that follow we present a case for a simple model involving a single neuron which is potentially capable of explaining the features of the data presented in this chapter.

Chapter 3: A Plausible Model

3.1 Introduction

Given the paucity of data available and its variability, is a model possible? Certain lines of evidence suggest that, despite the wide variation seen in the limited number of samples on hand, the situation may not be as intractable as first appears. This chapter examines two lines of evidence and proposes a simple model that, qualitatively for the moment, addresses both the observed behaviour of the averaged recorded output due to each additional call, as well as the variability seen in individual recorded signals. Additionally, the assumptions made in constructing the model impose limitations on its actual use, and these too are addressed.

In order to construct the model, we first consider the difference between the average response due to N calls and the average response from N-1 calls. The difference between the two averaged samples is just the effect of the N^{th} call minus the effect of the preceding N-1 calls—referred to here as the *N-(N-1) data*. Despite the complexity of any one signal, the difference between two averaged sets of signals shows a consistent pattern suggestive of a basic underlying mechanism.

The second line of evidence addresses the variability of the output. Given the model suggested by the N-(N-1) data, can we explain the variability in the two extant data sets? Again, a simple assumption helps elucidate the variety of output observed in the raw data. Together, the two lines of reasoning support the assumptions made in constructing the model itself. The actual effectiveness of the model relative to the actual *single-call response* data will be addressed in the following chapter.

3.2 The N-(N-1) Data

While a high degree of variability is seen in the response of call-counting neurons to individual stimulus calls (samples are shown in Section 3-5, Figure 3-7), even the *averaged* output due to a single call exhibits some rather unusual features. As seen in

Figure 2-7, a small initial EPSP is followed by a broad trough of inhibition, which is interrupted by the second EPSP, followed by a gradual return to V_R. The two-call response shows some equally unusual behaviour as well, and only when excitation truly kicks in on the third call does the second EPSP disappear—or perhaps it's merely swamped in the rising tide of depolarization.

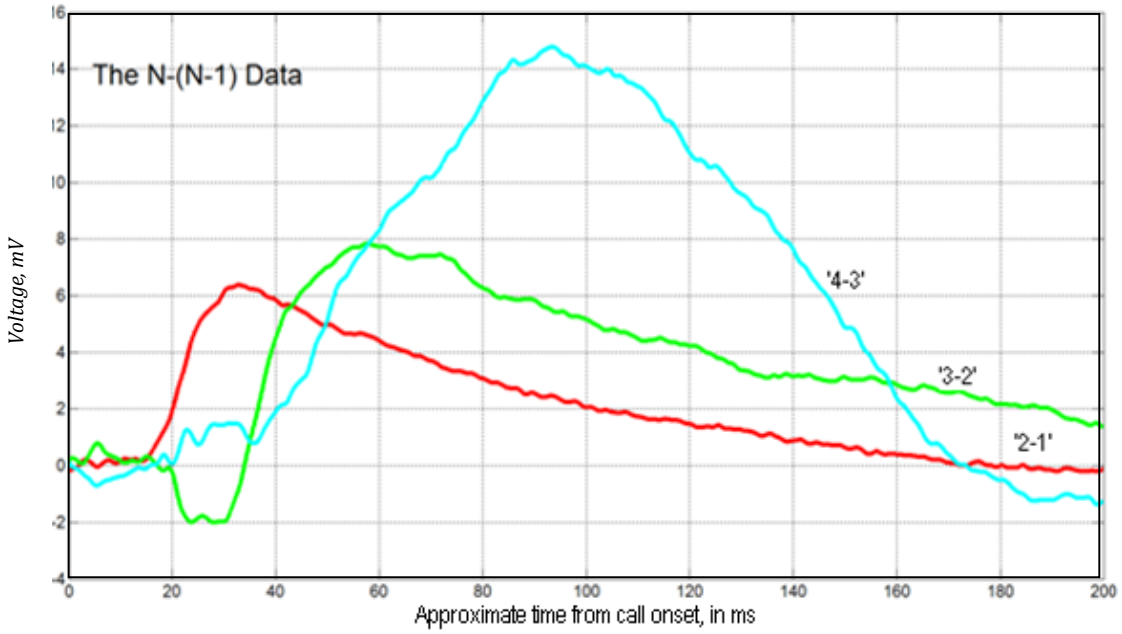

Figure 3-1: The N-(N-1) data. This graph, created by subtracting the average of the (N-1) data from the averaged N data, shows that the net effect of each additional call is to supply a small excitatory pulse to the neuron—and so a simple model involving only a single neuron could potentially suffice to explain the effects seen in Figure 2-7.

If we ignore for a moment these anomalies and look only at the broad picture or, alternately, focus on the graphs in Figure 2-3, we see a trough of inhibition that initially increases and then diminishes as N increases, and is eventually overcome by EPSPs from the latter input calls just prior to the onset of spiking. Therefore, in order to separate out the effect of a particular call from the calls preceding it—of the N^{th} call from the N-1 calls before it—it should suffice to subtract $V_{N-1}(t)$ from $V_N(t)$ for each t. In the resulting graph, shown in Figure 3-1 above, $V_{N|N-1}(t)$ is the 'N-(N-1) data'. This graph is derived by subtracting point by point the data displayed in Figure 2-7, which itself was constructed from the averaged and filtered response to N calls (where N=1,2,3,4, hence the three plots in the figure are '2-1' (in red), '3-2' (in green), and '4-3' (in blue)).

What emerges is a clearer picture of the data, one in which the difference of the two graphs has removed both the initial EPSP bump, and to a large degree, the second

excitatory bump as well. The chief benefit of this approach is to show that, despite the inherent complexity of the output seen in Figure 2-7, the actual effect of each additional call is simply to inject a small excitatory pulse into the neuron—no sophisticated network effects are required to explain the observed output. This suggests that the effects seen in Figure 2-7 are due *solely* to increasing excitation against an initial background of inhibition. This observation is in broad agreement with the conclusions of *Edwards et al.*, in which it is stated that "the interplay between inhibition and PRR-dependent enhancement of the excitation underlies the interval-counting properties of mid-brain auditory neurons" [2]. The one anomalous feature, seen in the '3-2' data, is a somewhat pronounced drop of ~2.0 mV seen 20-30 ms after the start of the plot. The effect does not appear to be significant in Figure 2-7, and is probably best explained as a combination of noise, instrumention drift and, in particular, low sample size: the three-call data is averaged over a total of five three-call responses; the two-call data over three responses.

These observations suggest that a simple model should suffice to explain the features observed, one having the general form (following equation 1.10)

$$-C\frac{dV}{dt} = g_L(V - V_R) + I_e(t) + I_i(t), \tag{3.1a}$$

where the synaptic currents I_e and I_i are given by:

$$I_e(t) = -g_e(t)\big(V_e - V(t)\big) \tag{3.1b}$$

and

$$I_i(t) = -g_i(t)\big(V_i - V(t)\big). \tag{3.1c}$$

We can combine these three equations into the following form:

$$C\frac{dV}{dt} = g_L(V_R - V) + g_e(t)\big(V_e - V(t)\big) + g_i(t)\big(V_i - V(t)\big). \tag{3.1d}$$

(We ignore, for now, the question of the delay time between a call and the actual onset of its effects.) Additionally, $g_e(t)$ and $g_i(t)$ will change with call number, increasing or decreasing according to the number and frequency of stimulus repetition. For example, facilitation of the excitatory current will be required in order to explain the rising tide of excitation that results from multiple calls as seen in Figure 2-7. This is a subject for a

later chapter. For the present, we require a way to model the synaptic conductances $g_e(t)$ and $g_i(t)$ in response to a single call.

3.3 One- and Two-Parameter Alpha Functions

In order to model the synaptic currents such as those found in equation 3.1d, we require a function $g_x(t)$ which itself accurately models the change in synaptic conductances with time. An *alpha function* performs just such a task. Introduced into neuroscience by Rall in 1967 [34], its chief benefit lies in its ability to model the rapid delivery of neurotransmitter into the synaptic cleft, peaking quickly to a maximum at time τ, followed by the slow uptake of neurotransmitter at the post-synaptic binding site [35][36]. (The properties of alpha-functions, along with a more-detailed mathematical argument for their use, are addressed in Appendix A.)

Mathematically, the conductance represented by a single-parameter alpha function will have the form

$$g_x(t) = A_x t e^{-t/\tau_x}, \tag{3.2}$$

where A_x and τ_x are constants that characterize the overall behaviour of the function, as shown in Figure A-1, and x stands for either excitation or inhibition, as before. The conductance $g_x(t)$ reaches a maximum value of $A_x\tau/e$ at time τ, a fact of some use in the next chapter.

The release of neurotransmitter vesicles at synapses is quantized and irregular; at best, the alpha function described by equation 3.2 gives only a rough approximation of the conductance changes due to neurotransmitter release at the synapses. While it provides the requisite functional behaviour, nothing guarantees that a particular synapse will behave according to this model. Collectively however, a large number of synapses should approximate this behaviour, and so despite their limitations alpha functions perform reasonably well in modeling average synaptic conductances with time.

The overall shape of equation 3.2 is defined by a single parameter, τ_x, but in many cases where this is too restrictive, a two-parameter alpha function is required of the form

$$g_x(t) = A_x(e^{-t/\tau_{xd}} - e^{-t/\tau_{xr}}), \quad (3.3)$$

where τ_{dx} and τ_{rx} are parameters responsible, respectively, for the decay and rise of the function [37][38][39]. Note that, since $g_x(t) > 0 \; \forall t$, $\tau_{xd} > \tau_{xr}$. In the limit where $\tau_{xd} \rightarrow \tau_{xr} \rightarrow \tau$, equation 3.3 reduces to equation 3.2 (as shown in section A-1 of the Appendix). Using the notation $a_x = \tau_x^{-1}$, equation 3.3 can be written as

$$g_x(t) = A_x(e^{-\alpha_{xd}t} - e^{-\alpha_{xr}t}). \quad (3.4)$$

Letting $a_{xr} = a_{xd} + \Delta a_x$, this becomes

$$g_x(t) = A_x e^{-\alpha_{xd}t}(1 - e^{-\Delta a_x t}), \quad (3.5)$$

with the maximum of $g_x(t)$ occurring at time

$$t_{gmax} = \frac{1}{\Delta a_x} ln\,(\mathrm{a}_x), \quad (3.6)$$

where $\mathrm{a}_x = a_{xr}/a_{xd} = \tau_{xd}/\tau_{xr}$ and $\Delta a_x = a_{xr} - a_{xd}$ as before. The value of g_x at this time will be:

$$g_x(t_{gmax}) = A_x {a_x}^{-\alpha_{dx}/\Delta\alpha_x}(1 - {\mathrm{a}_x}^{-1}). \quad (3.7)$$

Thus equations 3.5 and 3.7 symbolically mirror each other, with $e \longrightarrow \mathrm{a}_x$ and $t \longrightarrow 1/\Delta a_x$ —the same relationship holding true in equation 3.6, but with the arrows reversed in the above substitution.

3.4 An Intuitive Model Based on Alpha Function-like Conductances

Given equation 3.1d and the alpha functions described above, is it possible to generate output similar to the single-call response seen in Figure 2-7 (the red line), provided

suitable values of V_R, G_L, V_e, V_i, A_e, A_i, τ_e, and τ_i can be found? A simple mathematical argument suggests that it cannot, at least not without some modification.

Note that a single call response with two EPSPs, the second appearing at the bottom of an inhibitory trough—the situation described above—will have four *extrema* (local minima or maxima). In the data seen in figure 2-7, these occur at approximately 5, 18, 35, and 57 *ms*, as indicated by the arrows (averaging has somewhat flattened the curve; the individual data provides a better indicator of where these extrema appear to occur. An extreme example is found in sample 1-d in Figure 3-7). Extrema correspond to situations in which $dV/dt=0$ in equation 3.1d. Furthermore, to describe these four extrema, the second derivative of 3.1d must be alternately negative, positive, negative and positive at these four points. Taking the derivative of 3.1d we get:

$$C\frac{d^2V}{dt^2} = g'_e(t)(V_e - V) + g'_i(t)(V_i - V) - (g_L + g_e + g_i)\frac{dV}{dt}. \qquad (3.8)$$

The last term on the right of the equation vanishes, since $dV/dt=0$ at all minima and maxima. Practically speaking, the battery term (V_e-V) is always positive, (since $V<V_e$), at least outside of spiking conditions. And since V_i is assumed to be ~-80 mV, $V>V_i$ throughout the time course seen in Figure 2-7. We can rewrite equation 3.8 very generally as

$$C\frac{d^2V}{dt^2} = V_+ g'_e(t) + V_- g'_i(t), \qquad (3.9)$$

where V_+ and V_- are respectively positive and negative values reflecting the value of the two battery terms in equation 3.8. For a generic single parameter alpha function in the form $g_x(t) = A_x t e^{-t/\tau_x}$ as given above, its derivative $g'_x(t)$ starts positive at A_x when $t=0$, then crosses the x-axis at $t=\tau_x$, and remains negative thereafter, returning to 0 as $t\to\infty$. As Figure 3-2 shows, the two curves for $V_+g'_e(t)$ and $V_-g'_i(t)$ can at best cross only once in a finite amount of time, and at most, can only give rise to *three* separate extrema: Cd^2V/dt^2 may be negative-positive-negative, or positive-negative-positive. So equation 3.1 is not sufficient to explain the behaviour of the one-call response output.

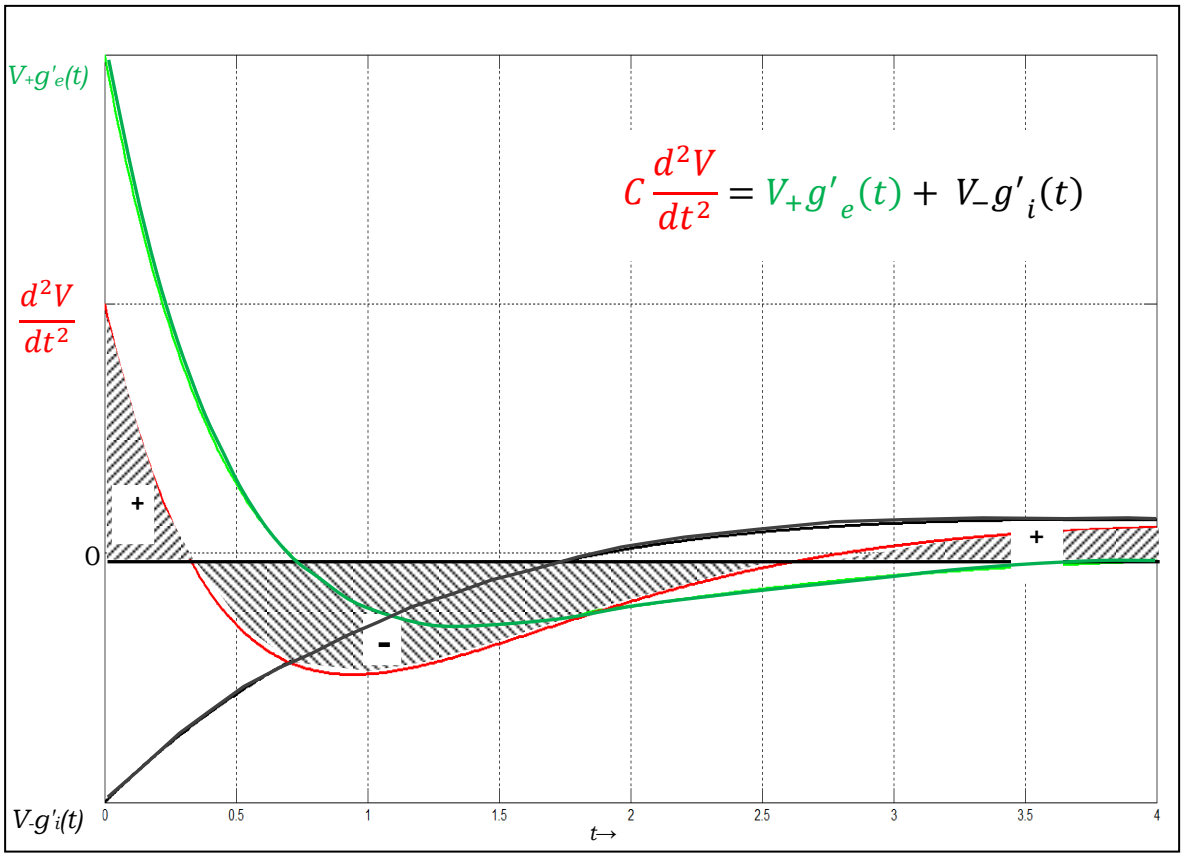

Figure 3-2: d^2V/dt^2 versus time according to equation 3-9. The green line shows the behaviour of $V_+g'_e(t)$, the black line $V_-g'_i(t)$. The red line is the sum of the two, and crosses the axis twice, demarcating three separate regions, from positive to negative to positive. So four extrema are not possible with the model described by equation 3-9.

There is a quicker, but less accurate way of looking at equation 3.1d which, despite its limitations, gives a more intuitive picture of the situation at hand. Three assumptions are required. First, that g_L is so small that the leak current is essentially negligible, and so the two synaptic currents I_e and I_i therefore dictate the voltage behaviour of the neuron entirely. Experimental evidence suggests that this is generally true: since g_L is on the order of 0.02 ±0.01 $\mu F/ms$ (to be shown in chapter 4), and (V_R-V) is typically on the order of a few millivolts over the range covered by the single-response data (i.e. $V(t)$ only varies from ~-64 to ~-70 mV), the leak current $g_L(V_R-V)$ will be small compared with the effects of I_e and I_i.

Second, since the inhibitory current is always (for practical purposes, as explained above) negative, and the excitatory current positive, at least over the region of interest, we can plot the two currents in the positive direction with the understanding that dV/dt will be represented by the difference between the two currents at all times; specifically, that the inhibitory current is to be subtracted from the excitatory current. This has the advantage

that the cross-over points between the two lines, where I_e=-I_i, are immediately obvious. Since $dV/dt \propto I_e + I_i = 0$ at this time, extrema in plots of $V(t)$ based on Figure 3-4 as well as in the experimental data seen in Figure 2-7 must correspond to cross-over points as well.

It's worth noting that due to this simplification we may treat the distance between the two lines in Figure 3-4 as determining how fast the slope of $V(t)$ rises or falls—another advantage of the graphical approach. When the black line is far above the green line, the neuron is flooded with more negative charge than positive charge, resulting in a large (negative) dV/dt and therefore a large hyperpolarization. When the situation is reversed, $dV/dt>0$ and $V(t)$ rises; as before, the greater the separation between the lines, the faster the change.

The final assumption is somewhat riskier. Currents are treated as though they depend entirely upon conductance alone; the effect of varying voltages is to be neglected. But to a good approximation, this should at least be true of the excitatory current following a single call, since, as V_e is assumed to be close to zero, the value of (V_e-V) in equation 3.1 remains roughly constant (to within ±10%) over the time course of the single-call response. If the excitatory conductance can be described by an alpha function, then the excitatory current (in green, in Figure 3-4 below) should behave likewise, to within ±10%. So the excitatory current will always look something like an alpha function, provided $V<<V_e$.

No such argument can be reliably made for the inhibitory current (in black). Only ~15 mV separate V_R from V_i, the presumed 'floor' for all voltages in equation 3.1d. The battery term ($V_i - V$) for the inhibitory current may thus vary by 30% or more as the voltage changes, and an alpha function will only provide a crude approximation to the actual shape of $|I_i(t)|$. So when considering the black line in plots like Figure 3-3 one must take into account the fact that whenever the neuron depolarizes (as for example, during the initial EPSP in Figure 2-7), $(V_i-V(t))$ becomes more negative as $V(t)$ increases, with the result that the current, $|I_i| = |g_i(t)(V_i-V)|$, looks like a distorted alpha function but with larger values of $|I_i|$ than we would expect from the alpha function-like plot of $g_i(t)$ alone. As V increases and the inhibitory term starts to dominate equation 3.1d, negative current enters the neuron causing increased hyperpolarization. As V falls, the effect of (V_i-V) decreases, causing the alpha function to attenuate somewhat. Closer to the resting potential, V will be somewhat smaller and flatter than we would expect from a pure alpha function-driven circuit. As a general rule, the inhibitory current rises and falls faster than a pure alpha function would when excitation dominates, before flattening out as V

decreases. The assumption that inhibitory current behaves like an alpha function is therefore a very crude approximation.

Broadly speaking then, the behaviour of the excitatory current is governed by $g_e(t)$ to a good approximation, and so an alpha function should accurately model the behaviour of I_e. But the behaviour of the inhibitory current is governed not just by $g_i(t)$, but by $V(t)$ as well, and therefore to a limited extent by $g_e(t)$ also. In the tug-of-war between inhibitory and excitatory synaptic currents, the relative values of $|(V_e-V)|$ and $|(V_i-V)|$ dictate that since the former is typically about five times larger than the latter, $g_e(t)$ will tend to dominate equations 3.1.

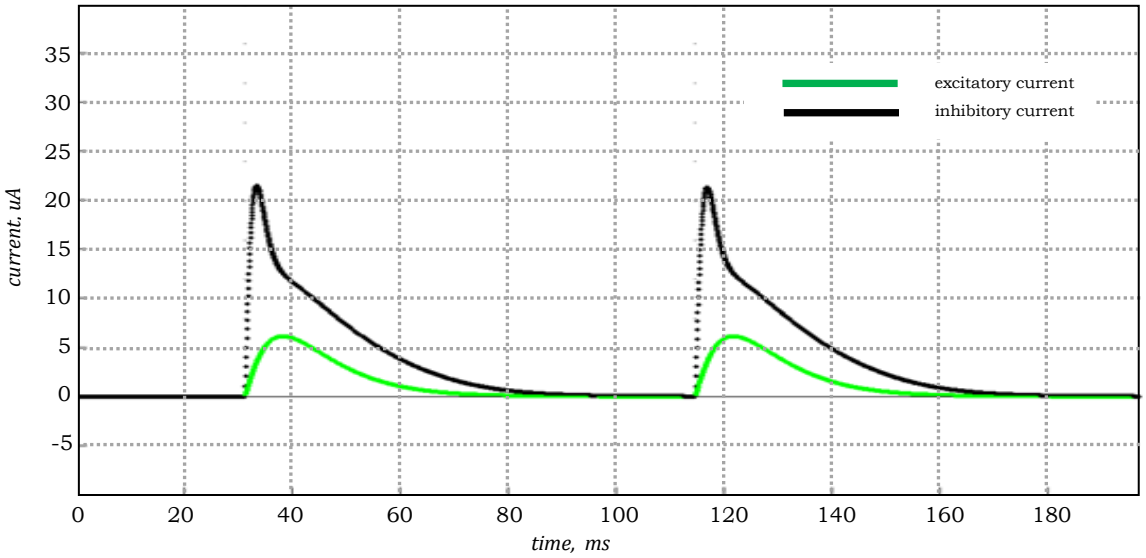

Figure 3-3: Inhibitory current (in black) follows excitatory current (in green) in this simulation based on equation 3.1d. (Note that $V_e \sim 0$ mV and $V_i = -80$ mV, but both currents are normalized to zero here, as described above in the text. Even though $A_i >> A_e$ and $\tau_i \approx \tau_e$, the inhibitory current is distorted by the excitatory current, which dominates the behaviour of $V(t)$. Clearly, I_e behaves much more like an alpha function than I_i.

As an example, consider Figure 3-3, taken from a simulation using real values derived from Figure 2-7. The amplitude of the excitatory current alpha function (A_e) is set about five times *smaller* than the amplitude of the inhibitory current alpha function (A_i), in order to balance out the relative values of the two battery terms, (V_e-V) and (V_i-V), over the voltages covered by the single-call data. Initially, the two currents just balance out. Input spikes are triggered at ~30 *ms* and ~115 *ms*. While the excitatory current (in green) follows an alpha function closely, the inhibitory current (in black) is highly distorted. This distortion is due to the fact that, while $|I_i(t)|$ initially rises quickly due to its larger A_i (or rather, since $I_i(t)$ is a negative current plotted in the positive direction, the negative

current drops more rapidly), then, as the voltage decreases, $|I_i(t)|$ weakens quickly while $|I_e(t)|$ strengthens slightly. The excitatory current of positive charge quickly overwhelms the weakened inhibitory current, with the result that even though both currents are modeled on alpha functions, the inhibitory current, despite its larger A_i, will be held 'in check' by the excitatory current.

In order to liberate the inhibitory current and restore to it a response somewhat more closely resembling an alpha function, it is necessary to introduce a second parameter into the alpha function, one which controls the decay rate independent of the rise and the peak times, as seen in equation 3-3. This second parameter allows us to 'coerce' our inhibitory current, but introduces yet another parameter into equations 3.1.

Armed with these three approximations and a two-parameter inhibitory alpha function, is it now possible to graphically generate the four extrema needed to generate the outputs seen in Figure 2-7? Using the graphical method just described, the answer is certainly 'no': the graphs can obviously be made to cross only twice, as shown in Figure 3-4 below. Charitably, we might allow for a third crossing owing to the effect of the slow leak current at a time when the other two currents have died away. This is shown as a third potential crossing point to the far right in Figure 3-4.

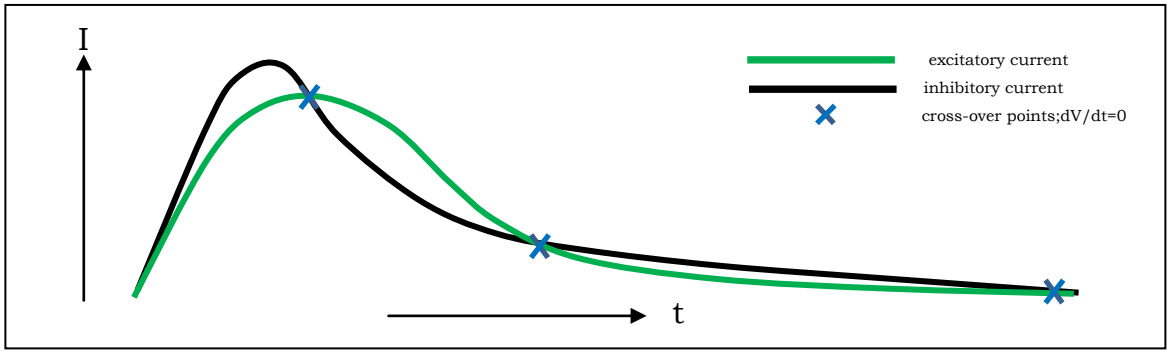

Figure 3-4: Excitatory current (in green) and inhibitory current (in black) using generic alpha function-type conductances. If both currents are dominated by alpha function-type conductances, there can be, at most, two extrema in the resultant plot of $V(t)$ for non-zero values of I_e and I_i. The return to V_R owing to the leak current allows for a third possible extrema.

One additional feature is therefore required to generate the four extrema. The simplest assumption to make—one, however, with profound implications as well shall see—is that a small time delay between the onset of the two currents nicely explains the four extrema seen in the data. This is noticeable if we offset the two curves in Figure 3-4 by some small time Δt. The effect is shown in Figure 3-5.

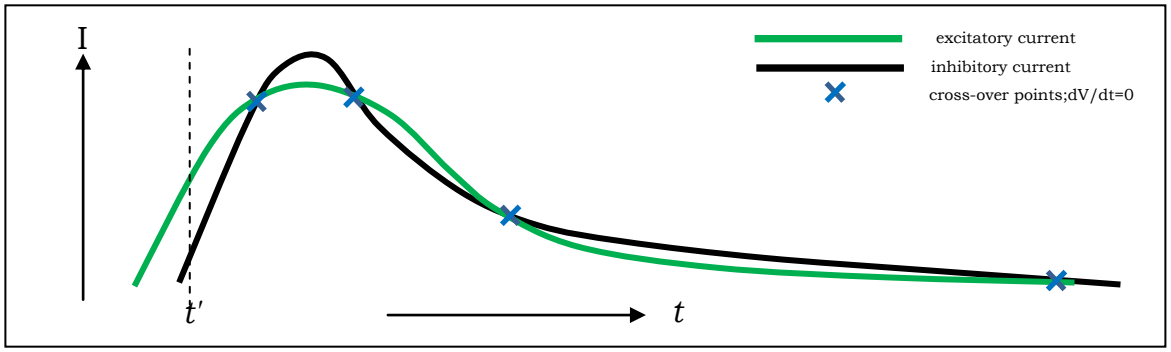

Figure 3-5: The effect of shifting the excitatory current (in green) relative to the inhibitory current (in black). It is now possible to generate four extrema in the resultant plot of *V(t)*. The sample inhibitory and excitatory plots are identical to Figure 3-4; only the delay is altered. The significance of the vertical line at *t'* is explained below in Section 3-6.

Figure 3-6 shows the effect of this time shift on *V(t)*. In Figure 3-6a, excitation precedes inhibition by several milliseconds, and the spread of the two curves tells us that we would expect a large depolarization from the excitatory current followed by a broad trough of inhibition. There are, at most, two cross-over points and hence two extrema.

As the delay between the curves decreases, the graph of *V(t)* alters radically. Figure 3-6b is just Figure 3-5 again, but now with four extrema possible we can generate something resembling the single-call response seen in Figure 2-7 (i.e. the red line). Shift the curves again, and in Figure 3-6c they very nearly overlap; the response of *V(t)* is comparatively flat since the separation between the curves is at a minima. Only three extrema are possible, but now inhibition dominates the initial phase, with depolarization following a few milliseconds later. Finally, in Figure 3-6d, inhibition predominates so completely that the belated excitatory current diminishes to zero before it can generate any depolarizaton, and only the leak current accounts for the final return of the membrane potential to V_R.

3.5 Implications of the Model for the Single-Call Response Data

As indicated in Section 2.6, a wide variety of output is observed in data sets A and B. A quick look at the six single-call responses available in data set A, shown in Figure 3-7 below, shows just how variable this output actually is.

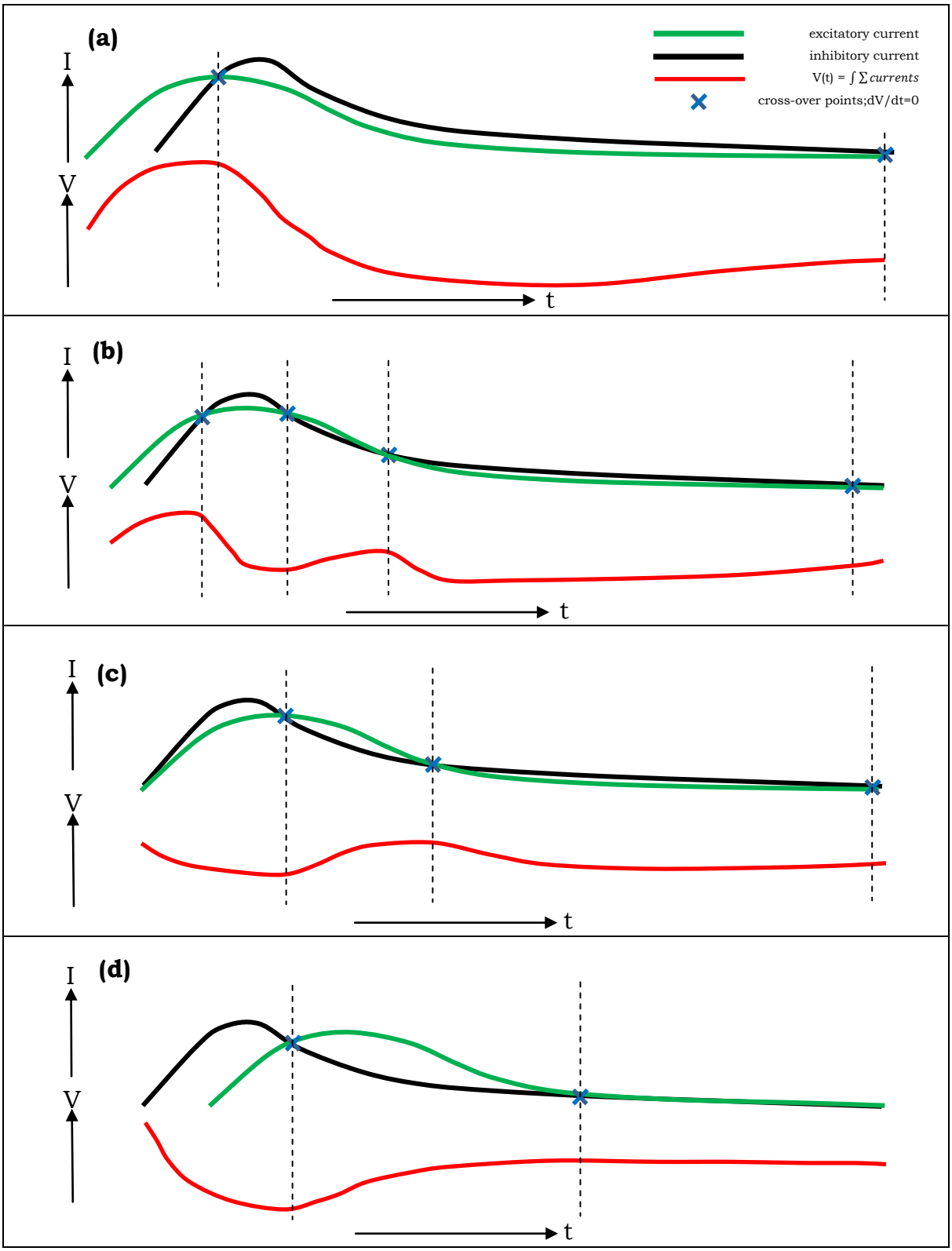

Figure 3-6: The effect of shifting the excitatory current (in green) relative to the inhibitory current (in black) on *V(t)* (in red). The inhibitory and excitatory plots are identical to those in Figures 3-4 and 3-5. Vertical lines indicate cross-over points/extrema.

At first glance it is difficult to see anything reproducible in the data; from one sample to the next there is virtually no consistency. But here again, the model described in the previous section helps explain the seeming randomness, since the model is clearly sensitive to the presumed delay between currents, Δt. If we assume the existence of a small amount of *propagation jitter* between the two competing currents along the *dendrites* of the neuron, we can at least qualitatively explain much of the variation in the single-call responses shown below in Figure 3-7.

Sample	Single-Call Response
1-a	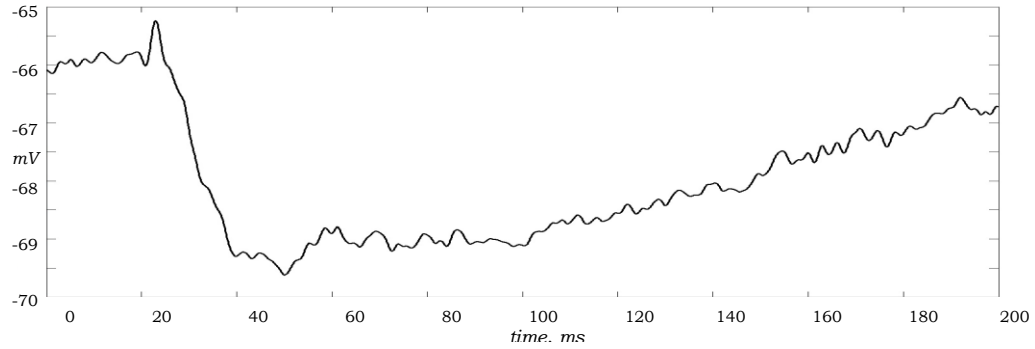
1-b	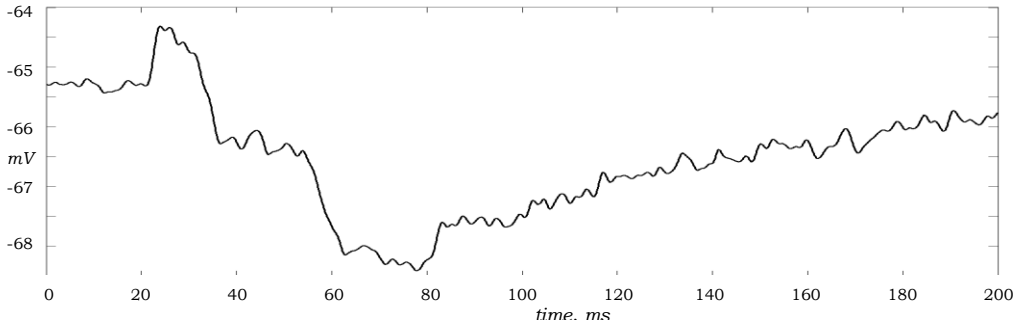
1-c	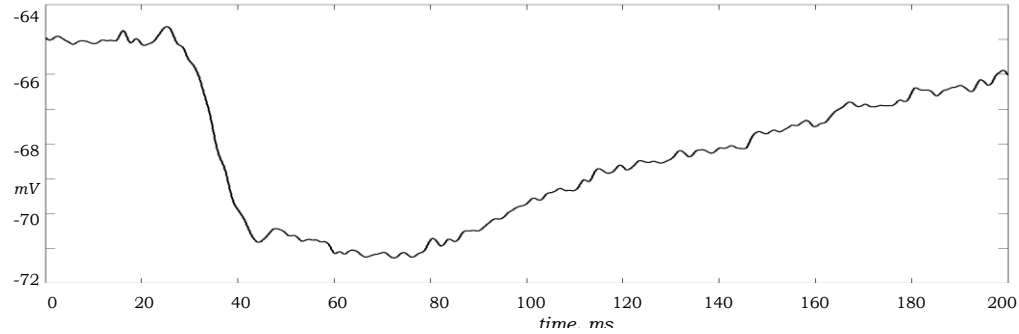

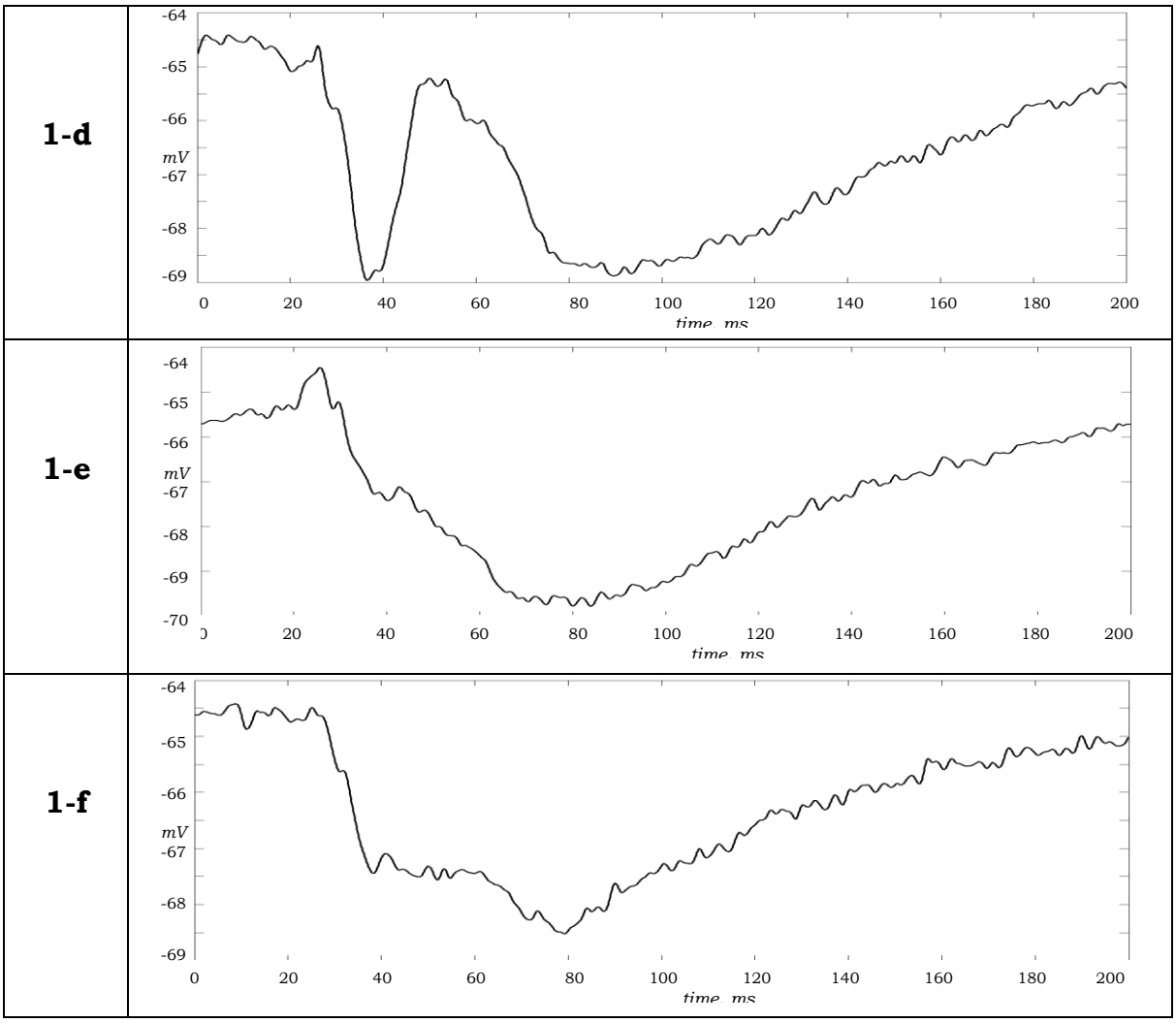

Figure 3-7: Response to a single-call recorded from call-counting neurons, from data set A, courtesy of Gary Rose.

Hence, a menagerie of possibilities exists depending on the value of Δt. Biological variability being a natural feature of all neural systems, a small amount of noise in any of the remaining variables will play havoc with the shot-to-shot reproducibility [40]. For instance, a small amount of noise added to A_e or A_i will affect the initial slope of $V(t)$, the size of the initial EPSP or IPSP and the peak of conductance of the alpha function, as outlined in Section 3.3.

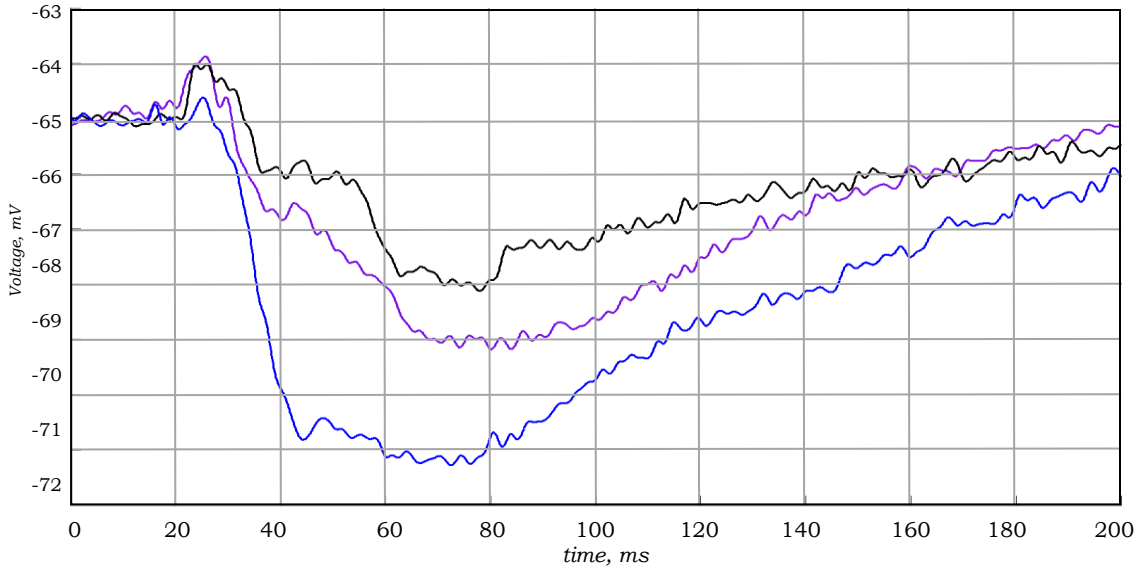

Figure 3-8: Three sample outputs taken from Figure 3-7 (black='1-b', blue='1-c', purple='1-e') where the offset has been set to -65 *mV*, nullifying the effects of drift during data collection. The data is heavily filtered with an 11th order Butterworth filter. A smaller initial EPSP, defined as the apparent width of the EPSP at around 26 *ms*, would appear to be correlated with a shorter recovery time, defined as a shorter time to return to V_R. Given the low number of samples available, this is highly speculative.

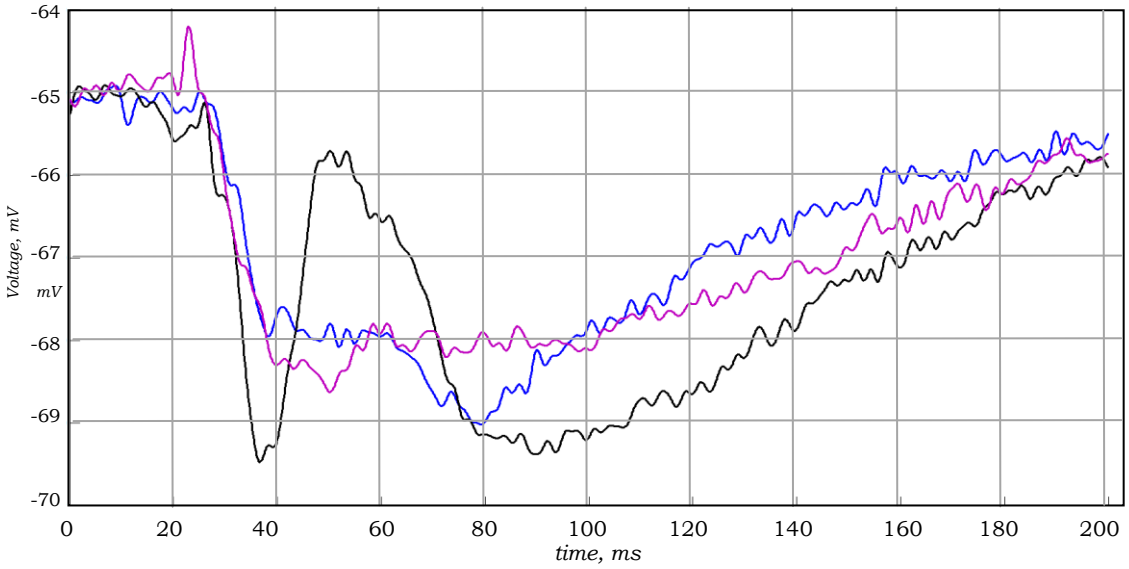

Figure 3-9: Three sample outputs from Figure 3-7 (purple='1-a', blue='1-f', black='1-d') with their offset normalized to -65 *mV* to account for drift during data collection.

Despite the simplicity of the model, certain qualitative predictions can be made which are generally verified by the limited experimental data available (which does not, of course, rule out other possibilities). In general, a large initial depolarization should be correlated with a large *propagation delay* and larger voltage swings (i.e. as demonstrated in Figure 3-6(a)). Figure 3-8 shows this effect using three selected samples from Figure 3-7. There

are hints of a possible negative correlation between the size of the initial EPSP, defined as the width at half maximum, and the depth of the inhibitory trough that follows, and the time required to return to V_R. But this is largely speculation, given the relatively high noise levels and low sample size.

Propagation delay may also account for situations like those shown in Figure 3-9. As the excitatory pulse arrives later, situations such as those seen in Figure 3-6(b) can be expected. Presumably, the black trace in 3-9 is caused by a slightly larger propagation delay than is found in either of the other two traces, which helps somewhat explain the pronounced EPSP at around 55 *ms*, where the inhibitory trough should be the deepest.

This evidence suggests that the exemplars of *Edwards et al.* are perhaps just neurons in which propagation jitter is less of a factor: exemplars merely behave more consistently than do 'less-exemplary' neurons. (No secondary excitation peak is mentioned in *Edwards et al.*, suggesting that excitation in exemplars precedes inhibition to such an extent that only one crossing of the $|I_e(t)|$ and $|I_i(t)|$ curves is possible.) Again, given the limited data available for study, this is speculative, but the suggestion is plausible.

3.6 Propagation Jitter and its Complications

While the assumption of propagation jitter helps explain output variability, it introduces an unsettling complication (beyond simply introducing an additional parameter) into the model. The situation is perhaps best described with the help of the two-current graphical model just introduced.

Using the assumptions made above, equation 3.1d can be written in the form:

$$-C\frac{dV}{dt} = I_e(t) + I_i(t-\Delta t), \tag{3.13}$$

where $I_i(t-\Delta t)=0$ for $t<\Delta t$. Also, we have assumed that the pulse that triggers the excitatory alpha function conductance begins at time $t = t_o = 0$. Assume for simplicity that I_e and $I_i(t-\Delta t)$ both vary linearly with time and have the same rate of increase G (i.e. $G = dI/dt = constant$), at least over the period of interest. Since $I_i(t-\Delta t)$ will have the opposite sign from I_e, we can write this as

$$-C\frac{dV}{dt} = G \cdot t - G \cdot (t - \Delta t) = G \cdot \Delta t. \qquad (3.14)$$

Under these circumstances, the rate at which the voltage changes with time will vary with both the rate of change of current *G and* the propagation delay between the two currents. Thus $I_e(t)$ and $I_i(t-\Delta t)$ are capable of producing identical values of $V(t)$ provided the product $G\Delta t$ remains constant.

To see this effect, consider again Figure 3-5. The value of dV/dt at the time *t'* (indicated by the vertical line) is a function of the vertical separation of the two currents. If the values of I_e and $I_i(t-\Delta t)$ were amplified by a factor of ten (i.e $10*A_e$ and $10*A_i$), but the time delay was decreased by one tenth, the separation of the green and black lines would remain roughly constant over the initial part of the curve, and $V(t)$ would remain virtually identical for both situations, except perhaps near the points where $dV/dt=0$, where we would expect subtle differences. Of course, when currents change faster, that change will be of shorter duration. However, this can be offset somewhat by increasing τ_e or τ_i by an equal amount, effectively counteracting the shorter duration by introducing an expanded time scale into either equation 3.1b or 3.1c.

Of course, equations like 3.14 are unrealistic; fluctuating potentials, noise, and varying synaptic conductances guarantee that currents will never be linear for long. But the example conveys a general warning: if two competing currents have linear behaviour over short periods of time then, even *if* the two currents have different slopes, both the alpha function amplitudes (A_e and A_i) and the time delay can be altered in such a way as to yield very similar forms of dV/dt—and hence $V(t)$—at least over short intervals. Unfortunately, alpha functions are roughly linear for small (i.e. initial) values of *t*, and only changes in voltage with time (according to equation 3.1d) guarantees that I_e and $I_i(t-\Delta t)$ will not vary linearly in this range. Still, the effect due to the battery term of equation 3.1 is relatively small against a background of noise, and so unfortunately our alpha functions turn out to be least informative in exactly the range where they are tractably linear, since an increase in $V(t)$ may in fact be due not to increased A_x, but to increased propagation delay.

Thus, the inclusion of propagation delay into the model introduces a complication. While differing values of A_e, A_i, τ_e, and τ_i, may reasonably be expected to produce relatively unique curves, Δt offers the possibility of introducing whole *families* of solutions to

equations 3.1 with potentially similar output, differing only at the crossover points. The battery terms (V_e-V) and (V_i-V) help ensure that this simplified situation cannot take place in reality. Unfortunately, while the data provided by Gary Rose is relatively noise free, there is still enough noise in $V(t)$ to obscure whatever benefits the battery term would bring in clarifying the ambiguity introduced by the presence of propagation jitter in data set A.

3.7 Summary

Despite a shortage of data, progress has been made in constructing a plausible model consistent with some of the attributes of counting neurons described in *Edwards et al.* The N-(N-1) data suggests that a simple model based on excitation and inhibition alone should suffice to explain the behaviour of counting neurons. This conclusion is broadly supported by the experimental evidence presented in *Edwards et al.*

While a conductance model using simple one-parameter alpha functions is insufficient to account for the behaviour of the averaged single-call response, the assumption of a propagation delay, in conjunction with two-parameter alpha functions, suggests a way to preserve this basic model without undermining the conclusions drawn from the N-(N-1) data. The resulting model explains not just the features seen in the averaged single-call response data, but potentially elucidates the variability seen in the samples found in data set A. Ideally, the model should eventually be able to reproduce not just the original data seen in Figure 2-7, but the N-(N-1) data in Figure 3-1 as well.

However, the assumption of propagation jitter, while clarifying the situation somewhat, is not without its complications. As we have seen in the previous section, Δt, A_e, A_i, τ_e, and τ_i may interact in ways which generate similar output voltage despite having very different values. Additionally, a number of other complications exist, and these will be described in the next chapter.

Chapter 4: The Single-Call Response Model

4.1 Introduction

In the previous chapter evidence was presented suggesting that a simple mathematical model involving competing inhibitory and excitatory synaptic currents is responsible for the behaviour of call-counting neurons. This in itself represents a step forward, since—aside from general comments in support of the experimental evidence for the interplay between excitation and inhibition—nothing in *Edwards et al.* suggests any particular neural mechanism to explain counting in anurans.

As shown in Chapter 3, single parameter alpha function-type conductances will, at best, allow $I_i(t)$ and $I_e(t)$ to cross only once, assuming that there is no propagation delay between their onset. This means that the simplest model can have at most two extrema, the second being provided by the gradual return to the rest current seen in equations 1.6 to 1.9. A two parameter inhibitory function allows for an additional extrema, and the assumption of a propagation delay provides the final fourth additional extrema. This simple model helps explain some of the features seen in the single-call responses in data set A, shown in Figure 2-7.

At this point, nothing precludes the possibility that other factors play a role. For example, a two-parameter alpha function may be required to model the excitation, just as two-parameters appear to be necessary for the inhibition. The second EPSP, while it can be theoretically explained by the model, could also be the result of a second, delayed excitatory synaptic pulse, although this seems unlikely.

Three lines of reasoning suggest that, for now, the model need not be augmented further with purported mechanisms and additional parameters: (1) the model presented appears to adequately explain what has been observed, at least quantitatively, (2) it is entirely consistent with the experimental evidence discussed in Chapter 2, and (3) additional parameters invite overfitting of the data.

If the assumptions underpinning the model are correct, then all that remains is to determine a set of parameters that generates output similar to the single-call response

data presented in Figure 3-7 (with the averaged data shown in Figure 2-7 in red), and then broaden this out to a multiple call response model (the subject of Chapter 5). Some parameters can be estimated directly from the data, and may be taken as reliable values. Unfortunately such cases are the exception rather than the rule. For the most part, values must be extracted from the data using rough approximations of the theory, and for any one variable so determined, the range of possible values varies widely. Even when this is possible, additional complications beyond those introduced in the last chapter introduce serious practical limitations on the accuracy of any of these parameters. Given the limited data set available for analysis and the very nature of the model itself, substantiating the validity of this model will naturally prove to be difficult. This chapter therefore discusses the model and its limitations before presenting a 'best-fit' data set.

4.2 A Mathematical Description of the Single-Call Response Model

Based on the information presented in Chapter 1, the results of *Edwards et al.* outlined in Chapter 2, and the qualitative model proposed in Chapter 3—including the theoretical alpha function-based conductance model—we can state the complete model thus far in mathematical terms, using equations 3.1d, 3.2, and 3.4 as

$$\begin{aligned} C\frac{dV}{dt} &= A_e(t-t_o)e^{-\alpha_e(t-t_0)}\,(V_e - V(t-t_o)) \\ &\quad + A_i(e^{-\alpha_{id}(t-t_o-\Delta t)} - e^{-\alpha_{ir}(t-t_o-\Delta t)})(V_i - V(t-t_o)) \\ &\quad + g_L(V_R - V(t-t_o)), \end{aligned} \tag{4.1}$$

where t_o is the time of onset of the pulse, and $A_i=0$ for $t-t_o<\Delta t$. This equation embodies all of the features introduced in the previous chapter: the two alpha functions needed to generate two of the extrema, including a one-parameter alpha function for the excitatory current and a two-parameter alpha function for the inhibitory current; the time delay needed to generate a third potential extrema; and finally the leak current, to account for a fourth extrema.

Technically, this is a time-delay differential equation, but not one of the sort typically encountered in control systems involving feedback. The current at each moment in time depends only on the product of the conductance and the voltage difference *(Vi-V)*; the former is delayed i.e. $g_e(t-\Delta t)$, but not $V(t-\Delta t)$. The delay *only* appears in the non-autonomous term $g_e(t-\Delta t)$, and so there is no feedback involved. While nothing prevents some form of feedback from occurring, there is nothing to particularly suggest it needs to be included either. This does not rule out the possibility that feedback plays a factor in assisting excitation following multiple calls, but as we shall see in the following chapter, that assumption is not required either.

Note also that synaptic conductances depend only *on* the time that the neurotransmitter is released from the presynaptic side of the synapse and *not* on the voltage at the synapse; the voltage at the synapse plays no role in determining the amount of neurotransmitter released. Slow-acting NMDA-mediated synapses can be voltage dependent, but this does not appear to play a role here, where the characteristic features of the neuron are present in the first 30 ms or so. This is indeed fortunate, since the assumptions made in the constructing the graphical model in Section 3.4 would not have been possible if conductance was a function of both *t and V*.

4.3 Assumptions, Approximations, and Inherent Limitations of the Model

A number of assumptions have been made in the construction of the model so far described. These include:

(1) Preprocessing of calls is entirely ignored. Evidence is presented in *Edwards at al.*, as well as in one of the trials in data set A, that incomplete calls are treated as missed calls. Our model presumes that a preprocessing unit determines the validity of incoming calls and transmits this information in the form of a single spike, thereby changing the synaptic conductivity of the call-counting neurons, giving rise to the voltage changes described by equation 4-1. This is an assumption, and no attempt is made here to explain call preprocessing in the putative afferents of the counting neurons. (The relevant data have not been recorded to our knowledge.) Similarly, no attempt has been made to address

questions such as the effects of call signal strength, filtering, or blind call processing.

(2) The time delay between the onset of a call and the onset of its effects cannot be made with great accuracy. In practice, a reasonable estimate has been made, based on the apparent first indication of an incipient EPSP or IPSP, but noise limits this value to perhaps ±1 *ms* at best. In diagrams in Chapter 3 this was assumed to be 26 *ms*, but the actual number cannot be measured precisely. This effectively complicates the consequences of propagation jitter still further.

(3) The assumption is implicitly made that only two synapses, one excitatory and one inhibitory, are attached to each call-counting neuron, and that the conductances of each synapse are dictated by an alpha function of either the one- or two parameter variety. As mentioned previously, this is a gross oversimplification of reality. The actual behaviour of the conductance at each synapse is random and should ideally be treated stochastically. Moreover, for each of the two types of presumed synapse, there are possibly hundreds or thousands of actual synapses impinging on the neuron, each with its own synaptic strength and propagation delay time—and this complex behaviour in its entirety has been condensed into a single alpha function.

(4) In pooling the various responses used in the construction of Figure 2-7, we have implicitly assumed that, given the small data set, this is not an unreasonable thing to do. However, where nonlinear differential equations are concerned, averaging over samples may have the effect of introducing artefacts which can never exist in reality. For example, consider Figure 4-1. Here it is assumed that the output, $V(t, a)$, of a nonlinear differential equation is critically dependent upon some noisy parameter, called a, upon which the delay time of the output voltage depends. The output samples, labeled $V_1, V_2 \ldots V_N$, fall into two groups on either side of t_o, according to the value of a. As seen on the right side of Figure 4-1, in taking the average of these samples, we have inadvertently created a 'shelf' in the data where none exists in reality. Any attempt to model this feature will be met with frustration since there is no value of a capable of recreating this specific output, despite the fact that it has been derived from the average of perhaps hundreds of samples. Where nonlinear differential equations (NDEs) are concerned, the average of the outputs is not guaranteed to actually exist as a specific solution to any one NDE.

In addition, the very nature of the model makes it exquisitely sensitive to small fluctuations in many of the variables. Specifically:

(1) The rate of change of voltage with time is directly related to the sum of the excitatory and inhibitory currents (again, neglecting the effects of leak current). So the actual voltage at any time is not just proportional to the two currents, but rather the integral of the sum of the two currents over a period of (typically) dozens of milliseconds. Small amounts of noise in any of the parameters that contribute to the currents, and particularly those affecting the exponential terms in the alpha functions, can therefore have a considerable effect on *V(t)*. The fine interplay between excitation and inhibition incorporated into the model, and their dependence on alpha functions, makes the model highly susceptible to noise of this sort.

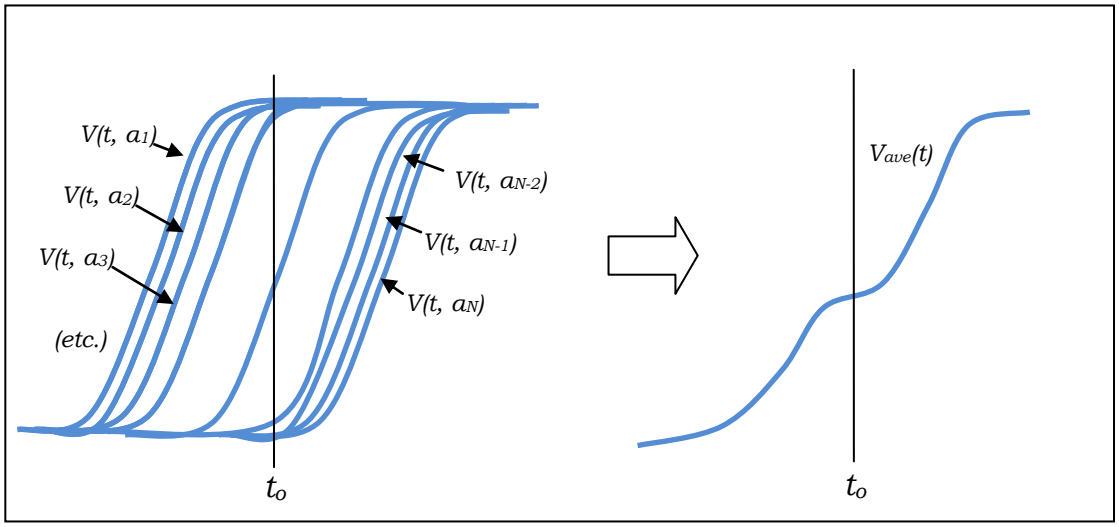

Figure 4-1: The averaging of a number of trials (at left) whose time delay is critically dependent upon some noisy parameter *a* creates an artifact in the average which does not exist in the original data set.

(2) From a theoretical perspective, alpha functions present two major challenges, both related to the exponential dependence of $g_x(t)$. First, consider the practical consequences of using alpha functions to represent conductances in equation 4-1. From equation 4-1 we have

$$\frac{dV}{dt'} = \frac{1}{C}\left[A_e t' e^{-\alpha_e t'} V_e - A_e t' e^{-\alpha_e t'} V(t') \right.$$

$$+A_i\left(e^{-\alpha_{id}(t'-\Delta t)} - e^{-\alpha_{ir}(t'-\Delta t)}\right)V_i$$
$$-A_i\left(e^{-\alpha_{id}(t'-\Delta t)} - e^{-\alpha_{ir}(t'-\Delta t)}\right)V(t') + g_L V_R - g_L V(t')\Big], \quad (4.2)$$

where $t'=t-t_o$ for simplicity. This can be rewritten in the form

$$\frac{dV}{dt'} + P(t')V(t') = Q(t'), \quad (4.3)$$

where

$$P(t) = \left[A_e t' e^{-\alpha t'} + A_i\left(e^{-\alpha_{id}(t'-\Delta t)} - e^{-\alpha_{ir}(t'-\Delta t)}\right) + g_L\right] \cdot V(t')/C \quad (4.4a)$$

and

$$Q(t) = \left[A_e t' e^{-\alpha t'} V_e + A_i\left(e^{-\alpha_{id}(t'-\Delta t)} - e^{-\alpha_{ir}(t'-\Delta t)}\right)V_i + g_L V_R\right]/C. \quad (4.4b)$$

This has a solution of the general form [41]

$$V(t') = e^{-\int_{t_o}^{t'} P(t')dt'} \int_{t_o}^{t'} Q(t') e^{\int_{t_o}^{t'} P(t')dt'} dt'. \quad (4.5)$$

Since *P(t')* contains exponentials, then $e^{-\int P(t')dt'}$ will have exponentials of exponentials, and *V(t)* will have the general form

$$V(t) \propto e^{-f(e^{-\alpha t'})}. \quad (4.6)$$

V(t) depends upon the exponent of an exponent of time. Consider what happens then if we attempt to plot *ln(ln(V(t)))* versus time in order to obtain a value of α, applying (presumably) suitable approximations that essentially allow us to read α as the slope of straight line (as is performed in the next section). *V(t)* varies by only a few millivolts over the time course of interest, and the *ln(ln())* operation effectively makes any result meaningless; the plot of *ln(ln(V(t)))* is almost a flat line with a very large uncertainty involved in the estimation of its slope.

This is exactly the problem that arises if we attempt to extract τ_e (or α_e) from data set B. With $V_i \approx V_R$ = -78 mV, the latter two terms on the right hand side of equation 4-1 are essentially equal to zero, and the equation effectively becomes:

$$C\frac{dV}{dt'} = A_e t' e^{-\alpha_e t'}(V_e - V(t')). \tag{4.7}$$

This equation has an exact solution with the general form of equation 4.6. Averaged over perhaps a few hundred samples, it might be possible to obtain a reasonable estimate of α_e, and perhaps even A_e (from the intercept), from a graph of $V(t)$ versus t. But the limitations just described prevent such an accurate determination. The only solution to this problem is to linearize the equation by considering only the situation around the time $t \approx 0$, before the exponential term has any chance to really take effect.

Attempts to use the slope dV/dt in Figure 2-7 are also problematic. The initial EPSP rises by only ~1 mV against a noise background perhaps half as large, and so for the first ~5 ms the noise background is too large to put the small signal change to any use. Following the peak of the EPSP, there is a linear interval of hyperpolarization lasting perhaps 10 ms. Unfortunately, this section is so linear that taking $ln(dV/dt)$, as equation 4.7 suggests, again does not provide enough information to be of any real service.

As a second general comment on the difficulties that result from using alpha functions, it should be noted that the exponential dependence of the functions naturally gives rise to transcendental equations, thus incurring a heavier computational burden. Say, for example, we attempt to express one parameter, α_e, as a function of other the parameters, $f(V_i, V_e, A_e, A_i, \Delta t, \ldots)$ in order to help limit the range of values of α_e over which to search for any given set of parameters $\{V_i, V_e, A_e, A_i, \Delta t, \ldots\}$. The time t_m at which $dV/dt = 0$ serves as a convenient reference point because minima and maxima are easily identified and may be accurately assessed, and t_m and V_m ($\equiv V(t_m)$)can then be read directly from the data. From equation 4-1, we have

$$A_e t_m e^{-\alpha_e t_m}(V_e - V_m) = -A_i(e^{-\alpha_{id}(t_m - \Delta t)} - e^{-\alpha_{ir}(t_m - \Delta t)})(V_i - V_m) \tag{4.8}$$

where here, as before, the leak current is assumed to be negligible since V_m is close to V_R. This leads to an expression for α_e in terms of the other parameters:

$$\alpha_e = \left(\frac{1}{t_m}\right) ln\left\{\left(\frac{A_i}{A_e t_m}\right)\left(\left|\frac{[V_i - V_m]}{[V_e - V_m]}\right|\right)\left[1 - e^{-\alpha_{ir}(t_m - \Delta t)}\right]\right\}. \quad (4.9)$$

Here, we have assumed that $\tau_d >> \tau_r$, hence $e^{-\alpha_{id}(t_m - \Delta t)} \approx 1$ for relatively small values of $(t_m - \Delta t)$, i.e. immediately following the onset of a pulse. The absolute value sign reflects the fact that since $V_e > V_m$ and $V_i < V_m$ for all values of V_m over the range of interest, the ratio of the voltages in the second set of brackets, combined with the negative sign in equation 4.8, will always resolve to a positive value.

Notwithstanding the concerns previously expressed regarding the effect of propagation jitter and signal onset time on t_m, Δt, and V_m, this equation may provide a rough estimate, to within an order of magnitude, of possible values of α_e–a 'ball-park figure' for any given set of A_i, A_e, α_e and Δt.

Since we often have more than one extrema to work with, it is tempting to try to remove α_e from consideration altogether by assuming that the value of α_e measured at one maxima at time t_{m1} should be the same as the value α_e measured at another minima at time t_{m2}—since equation 4-9 presumably holds whenever $dV/dt = 0$—provided we can obtain accurate readings of t_m and V_m. Using two pairs of experimentally determined data points (t_{m1}, V_{m1}) and (t_{m2}, V_{m2}), equation 4.9 becomes:

$$\left(\frac{1}{t_{m1}}\right) ln\left\{\left(\frac{A_i}{A_e t_{m1}}\right)\left(\left|\frac{[V_i - V_{m1}]}{[V_e - V_{m1}]}\right|\right)\left[1 - e^{-\alpha_{ir}(t_{m1} - \Delta t)}\right]\right\}$$
$$= \left(\frac{1}{t_{m2}}\right) ln\left\{\left(\frac{A_i}{A_e t_{m2}}\right)\left(\left|\frac{[V_i - V_{m2}]}{[V_e - V_{m2}]}\right|\right)\left[1 - e^{-\alpha_{ir}(t_{m2} - \Delta t)}\right]\right\}. \quad (4.10)$$

Assuming it is the other exponential parameter α_{ir} which we now wish to express in terms of the remaining variables A_i, A_e, and Δt, we can at best arrive at an expression which is only slightly less intractable and is not worth reproducing here; equation 4-10 lacks a closed solution. Furthermore, it doesn't matter

whether we choose points $(t_{m1}, V_{m1}(t_{m1}))$, $(t_{m2}, V_{m2}(t_{m2})...)$ at which $dV/dt=0$ or a set of points at which the slope dV/dt is relatively constant and therefore easily measured, the problem remains the same. Even with accurate, noise-free values of $V(t)$ at our disposal, transcendental equations arise naturally whenever the right side of equation 4.1 contains a term such as $Ate^{-\alpha\Delta t}\Delta V$. These must be resolved computationally. And often, even when these equations can be written in closed form, they do not convey ideas any better than the graphical representations they are intended to replace.

With these limitations understood, we turn from the subject of what can't be determined to what can be determined, or at least approximated to varying degrees, from the data.

4.4 An Analytical Estimation of the Parametric Values Derived from the Available Data

Equation 4-1 contains two variables, t and $V(t)$, and eleven parameters: C, A_e, α_e (or τ_e), V_e, A_i, α_{id} (or τ_{id}), α_{ir} (or τ_{ir}), V_i, Δt, g_L, and V_R. Of these parameters, only V_R, the resting potential, can be read directly from the data. From data set A, its value can be determined as -65 mV (although there is an apparent instrumentation drift of about 1 mV in some of the data). The value of C, the membrane capacitance, is unknown, but a value of 1.0 uF may be reliably assumed [42][43]. Furthermore, we can effectively remove one parameter from the equation by using a non-dimensional parameter C'=C/1 μF and scaling the values on the right side of the equation appropriately. So taking C'≡1 on the left side of the equation, even if incorrect, poses no serious consequences for the validity of the model: we need only scale A_e, A_i and g_L appropriately and the model would still hold. The value of C≡1 will be assumed from this point onwards, and the capacitance effectively drops from the equation. The missing factor of 10^{-6} on the left side of equation 4.1 is effectively dealt with by using mV and ms on the right side.

The two Nernst reversal potentials, V_i and V_e, have been determined experimentally by Gary Rose [44]. V_e may be taken to be ~0 mV, and here too the consequences of choosing a bad value have minimum impact, since the excitatory current will only change by a few percent if the value of V_e were changed by a few millivolts. The model is somewhat less forgiving where the value of V_i is concerned, as discussed above in section 3.4. A value of

-78 mV has been reported, and values close to it have been used throughout most of the trials conducted using the model, described below.

Of the remaining seven parameters, three may be estimated from the data with varying degrees of accuracy, with large uncertainties being the rule rather than the exception. We'll look at each of these in turn.

First, the leak current, $g_L(V_R\text{-}V(t))$, may be assumed to dominate equation 4-1 when the effects of $g_e(t)$ and $g_i(t)$ have either diminished or canceled each other off. The solution to 4.1 with $g_e(t) = g_i(t) \approx 0$ is

$$ln\left[\left(V_R - V(t)\right)\Big/\left(V_R - V(t_o)\right)\right] = -g_L t. \qquad (4.11)$$

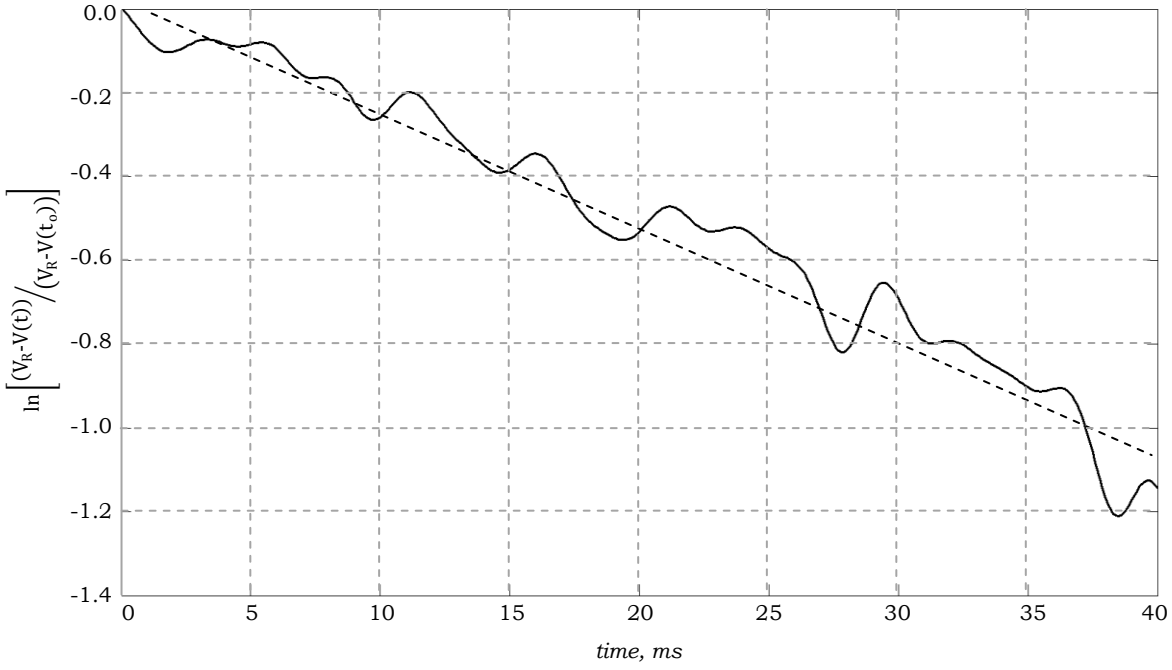

Figure 4-2: The determination of g_L from a plot of $ln[(V_R - V(t)) / (V_R - Vo)]$ versus $-g_L \cdot t$ using single-call response data (6 samples). The raw data has been heavily filtered with a 15th order Butterworth filter. '0' on the horizontal scale corresponds to time t_o, which occurs at ~140 ms following the onset of a call. The trend line has a slope of ~-0.026 ms^{-1}.

Note that we are really estimating g_L/C, which has units of inverse time, i.e. g_L/C is the membrane time constant. When this is plotted using data from data set A using times

t_o>140 *ms*—the presumed time it takes for the effects of $g_e(t)$ and $g_i(t)$ to diminish to zero—a relatively straight line is obtained, shown in Figure 4-2. The slope of the line indicates that g_L is approximately 0.026 $\mu F \bullet ms^{-1}$.

A second parameter, A_e, may be obtained from data set B. With a -3 nA current applied, the neuron is effectively depolarized to V_R=-78 *mV*, close to the reversal potential V_i. Both the inhibitory and leak currents may be treated as essentially zero. For the situation in which $\alpha(t - t_o) << 1$ equation 4.1 becomes

$$\frac{dV}{dt} \approx A_e(t - t_o)(V_e - V(t - t_o)), \tag{4.12}$$

where A_e has units of ms^{-2}, and t_o, as before, is the time of onset of the call. This has the solution

$$V_e - V(t - t_o) \approx (V_e - V_o)e^{-A_e(t-t_o)^2/2}, \tag{4.13}$$

or

$$\left[ln\left(\frac{V_e - V_o}{V_e - V(t-t_o)}\right)^2\right]^{1/2} \approx (A_e)^{\frac{1}{2}}(t - t_o). \tag{4.14}$$

Plotting the left side of equation 4.14 versus time (Figure 4-3) we obtain from the slope of the line a value of $A_e \approx 0.0013$ $\mu F \bullet ms^{-2}$. Given that less than 2 *ms* of data was used in the determination of this value, its accuracy must be considered somewhat suspect. However, unlike every other calculation derived from the data, this one is based on all 25 samples in data set B. (Since the initial response of the putative excitatory synapse to a single call following a rest period should be exactly the same—regardless of the total number of calls eventually presented—we can reasonably pool the first-call information in data set B to obtain a graph of the average response.) Despite the data set size, the value obtained could easily be an order of magnitude higher or lower, given the uncertainties involved and the nature of the calculation performed.

Finally, the value of A_i may be crudely approximated by first selecting from amongst the samples in data set A those responses in which inhibition initially predominates, with little or no evidence of an initial EPSP. One candidate, 1-c in Table 3-1, fits this criterion.

Assuming I_e is initially absent and the leak current negligible, equation 4-1 can be approximated as:

$$\frac{dV}{dt} \approx A_i(1 - e^{-\alpha_{ir}(t-t_o)})(V_i - V(t - t_o)), \tag{4.15}$$

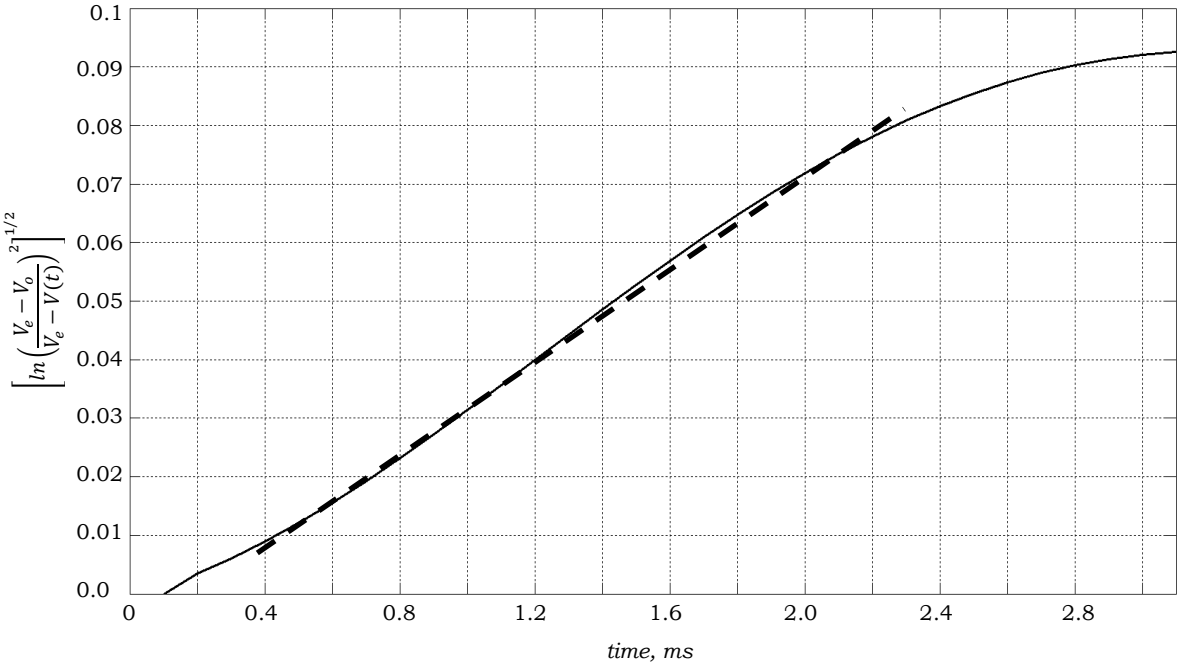

Figure 4-3: The determination of A_e from equation 4.14. While the interval of interest is only <2 *ms* long, the data set used consists of every trial in data set B—25 samples in total. The trend line has a slope of $(A_e)^{1/2} \approx 0.036\ ms^{-1}$.

where we have here assumed, as in equation 4.9, that $\tau_d >> \tau_r$ and hence $e^{-\alpha_{id}(t_m - \Delta t)} \approx 1$ during the initial phase of the response when $\alpha(t - t_o) << 1$. Also note the absence of Δt; because inhibition precedes excitation in this particular case (the sample was chosen exactly because it lacks an initial EPSP), we may assume that the time measured is with regard to the onset of inhibition alone. This is perhaps wishful thinking, but it's the only reasonable assumption that can be made under the circumstances. Equation 4.15 has the solution

$$ln\left(\frac{V_i - V_o}{V_i - V(t - t_o)}\right) \approx \frac{A_i}{\alpha_{ir}}(\alpha_{ir}(t - t_o) + e^{-\alpha_{ir}(t-t_o)} - 1). \tag{4.16}$$

where V_o is the initial value at time t_o. For values of t just slightly greater than t_o, we can approximate $e^{-\alpha_{ir}(t-t_o)} \approx 1$. And so the slope of the plot of the left hand side of the equation versus time should give a crude value of A_i.

The value of A_i obtained from the plot shown in Figure 4-4 is 0.0035 $\mu F \bullet ms^{-1}$, but this should be greeted with a high degree of skepticism, given the assumptions made in its determination—in particular the fact that it is based on a single piece of somewhat-noisy data. Realistically, given the presumed presence of some excitatory current, this value should be taken as a minimum.

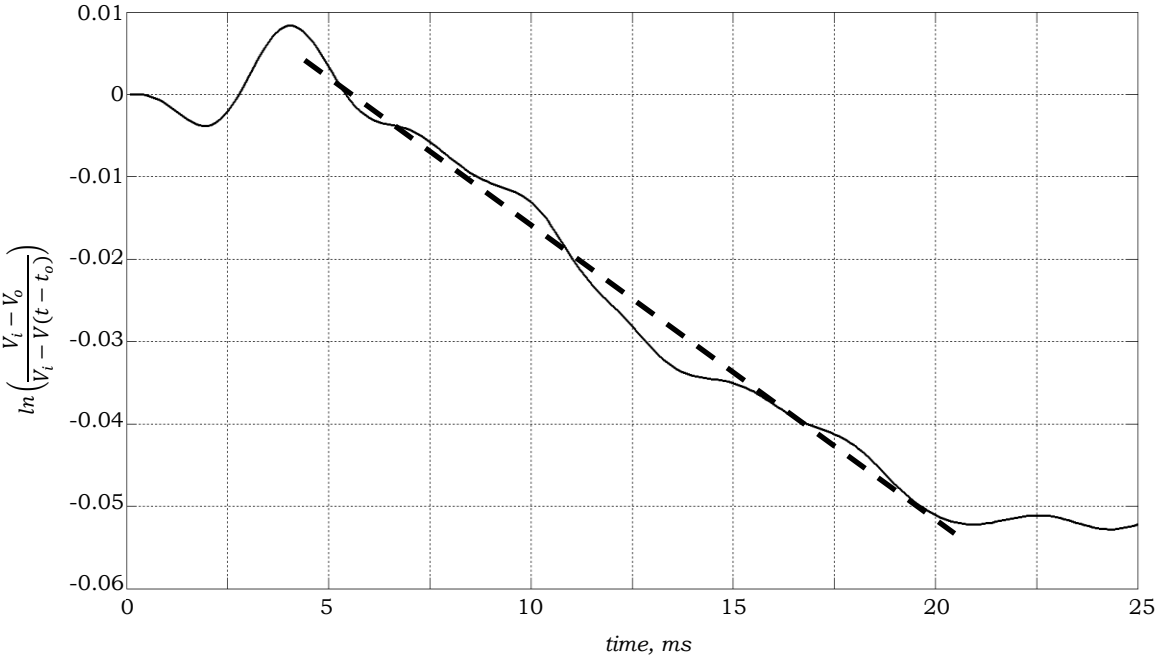

Figure 4-4: The determination of A_i, approximated from equation 4.16, using sample 1-c from Table 3-1. An offset time of ~25 *ms* is assumed from the start of the call. The trend line covers the region where the inhibitory current is presumed to dominate, although there is potentially some excitatory current mixed in. The measured value of A_i is ~0.0035 ms^{-1}.

The question may be asked as to whether the intercepts of these graphs could also be used to provide information for parameters such as V_e or α_{ir}. Attempts were made at extracting values from the intercepts. Unfortunately, given the uncertainty in the onset time of the pulse, the noise in the data, and the inherent unreliability of the calculations used in determining the actual slopes of the graphs above, the values obtained were found to be no better (and typically worse) than a reasonable guess based on simple deductions, like those used below.

It should be noted that equations 4.11, 4.14 and 4.16 each contain terms in the form $(V_x - V(t_o))/(V_x - V(t))$ (or some variation) where the actual onset time, t_o, is unknown, the voltage differences are typically on the order of a few millivolts, and each voltage measurement could have about a half a millivolt of noise associated with it. Despite the flattening effect of the logarithmic function, the natural output of these three equations is sufficiently fuzzy that a linear fit is impossible without some filtering. The Butterworth filter has the advantage that it has a flat response in the pass band, and a sharp cut-off above a set frequency. The order of the filter determines the sharpness of the cut-off, and for the most part a 11th- or 15th-order filter was found to be necessary to sufficiently tidy up the output so that a trend line could be established.

So equations 4.11, 4.14, and 4.16 allow us to determine three values. Of the four remaining variables, α_e, α_{id}, α_{ir}, and Δt, there appears to be no way to calculate them directly from the data, This is unfortunate, since these are exactly the values which have the greatest possible impact on the qualitative behaviour of the model. However, limits can be deduced on the range of values possible. In the single-call response data, the maxima of the first EPSP (where one exists) must occur after Δt. The latest EPSP peak occurs at ~5 *ms*, hence we would expect that $0 < \Delta t < 5$ *ms*.

Furthermore, if we linearize the one- and two-parameter alpha functions used in equation 4-1 (i.e. assume that $t - t_o < \tau_e$, and therefore $e^{-\alpha_e(t-t_o)} \approx 1$), we obtain, at the peak of the EPSP in the averaged one-call response,

$$A_e t_m (V_e - V_m) \approx -A_i \alpha_{ir} (t_m - \Delta t)(V_i - V_m) \tag{4.17}$$

or

$$\frac{A_e(V_e - V_m)}{A_i(V_i - V_m)} \approx \alpha_{ir} \left({}^{\Delta t}/_{t_m} - 1 \right), \tag{4.18}$$

where again, t_m is the time of the peak of the first maximum, and $V_m \equiv V(t_m)$. Using the values previously obtained (or assumed) on the left hand side of the equation, we can establish (somewhat skeptically) the following relationship:

$$\alpha_{ir} \approx \frac{1.7}{\left(1 - {}^{\Delta t}/_{t_m}\right)}. \tag{4.19}$$

Since t_m is reached at about 5 *ms*, we might alternately write this equation as

$$\tau_{ir} \approx 0.6\left(1 - {}^{\Delta t}/_{5}\right) \tag{4.20}$$

with the understanding that this is only a very crude approximation; the equation would seem to indicate that largest value of τ_{ir} would appear to be a fraction of a millisecond, when realistically we might expect a value an order of magnitude larger. Note that equation 4.20 conforms to our expectations about the relationship between Δt and τ_{ir}: for a given time t_m, which corresponds to the crossover point of the inhibitory and excitatory currents, the later the onset of inhibition, the steeper the rise of the inhibitory current required to overtake the excitatory pulse.

Also, the qualitative model (introduced in Chapter 3, and best expressed in Figure 3-6) predicts that, where an initial EPSP is present, τ_e should be greater than τ_{ir}, or α_e approximately less than α_{ir}. For a single-parameter alpha function, τ_e is the time at which $g_e(t)$ reaches a maximum. In the pooled single-call data seen in Figure 2-7, the second EPSP occurs at ~30 *ms* after the start of the response; inhibition still plays a role at this point, so we might assume a value of 20 $ms < \tau_e <$ 40 *ms*. The assumption that $\tau_e > \tau_{ir}$ implies that τ_{ir} <40 *ms*, but this would seem to be far too generous; if the model is correct, the peak of the inhibitory current must occur prior to the onset of the second EPSP, which occurs at ~25 *ms*. Reasonably, we might expect that 2 $ms < \tau_{ir}$<25 *ms*.

Finally, as was previously mentioned, the fact that conductances are always greater than zero implies that $\tau_{id} > \tau_{ir}$. Since τ_{ir} varies from 2 to 25 *ms*, we might expect a minimum τ_{id} of perhaps 15 *ms* and possibly much larger.

Table 4-1: Summary of the Variables used in the Model

Variable	***Presumed Value/ Range***	***Assumption based on***
V_R	*-65 mV*	Accuracy affected only by drift and noise in the electronic apparatus used to record the signal. Probably accurate to ±1 *mV*.

V_e	*~0 mV*	Determined experimentally; certainly not less than -20 *mV*; the exact value does not have an substantive affect on the validity of the model
V_i	*-78 mV*	Possibly <-78 *mV*, but not more than a few millivolts. Changes in this value would have a more substantial affect on the performance of the model.
C	*'1'*	Determined experimentally; this is the value traditionally used, and may be considered reasonably accurate. If this assumption is incorrect, the consequences only affect the value of other variables, but not the validity of the model itself.
g_L	~ 0.026 $\mu F \bullet ms^{-1}$	Determined from the average one-call response. Assumed reasonably accurate, probably to not worse than ±20%
A_e	~0.0013 $\mu F \bullet ms^{-2}$	Determined from the pooled data in data set B. Probably not very accurate; the actual value could be an order of magnitude higher or lower.
A_i	~0.0035 $\mu F \bullet ms^{-1}$	Determined from a single exemplar in data set A; given the approximations made in its determination it should not be judged to be at all accurate.
Δt	< 5 *ms*	Based on the assumption the propagation delay between currents must be less than the time to the first EPSP peak seen in the averaged one-call data.
τ_e (α_e)	20 *ms*< τ_e <40 *ms*	Based on assumptions about the second EPSP peak in the averaged single-call data
τ_{ir} (α_{ir})	2 < τ_{ir} < 25 *ms*	Based on the assumption that $\tau_e > \tau_{ir}$
τ_{id} (α_{id})	$\tau_{id} > \tau_{ir}$	Based on the fact that since conductances must be greater than zero, $e^{1/\tau id} < e^{1/\tau ir}$

4.5 Computational Methodology and Modeling

As shown in the Appendix, the discrete analogs of equation 4.1 may be written as:

$$h_e(t+dt) = h_e(t) - dt\left[\left(\frac{g_{e(t)}}{{\tau_e}^2}\right) + 2h_e(t)/\tau_e\right] + \delta(t) \quad (4.20a)$$

$$g_e(t+dt) = g_e(t) + dt \cdot h_e \quad (4.20b)$$

$$h_i(t+dt) = h_i(t)(1 - \frac{dt}{\tau_{ir}}) + \delta(t - \Delta t) \quad (4.20c)$$

$$g_i(t+dt) = g_i(t)\left(1 - \frac{dt}{\tau_{id}}\right) + dt \cdot h_i \quad (4.20d)$$

$$V(t+dt) = V(t) + dt[(g_L(V_R - V) + A_e g_e(t)(V_e - V) + A_i g_i(t)(V_i - V)] \quad (4.20e)$$

where dt is the time step size used in the iteration and $\delta(t)$ is one or zero depending on whether a spike occurs in a particular time step or not—the integral of a Dirac delta function. (Δt is the delay time, as before). Equations 4.20(a-d) model conductances, and their relationship to the alpha functions of equations 3.2 and 3.3 is addressed in Appendix A. Two variables, g and h, are used, their advantage being that they produce alpha functions without incurring the computational burden involved in evaluating exponentials directly at every time step of the numerical integration.

Equations 4.20 were implemented in two different computer programs. The first was built using Matlab software (V7.8.0, R2009a) and was designed to display graphically the effects of changing parameters, including the facilitation parameters covered in the next chapter. While this proved valuable in proving that certain features of the experimental data could be generated—counting, frequency-dependence and reset on missed pulses were all observed, and are discussed in Chapter 5—it was not possible to locate one set of parameters that were able to generate all three features while having values remotely similar to those shown in Table 4-1 above. This is because the sensitivity of the model to subtle changes in parameter is very high, as was discussed earlier in this chapter.

In addition to proving the efficacy of the equations and the correctness of the code, the program revealed certain counter-intuitive features of the model: for example, increasing τ_e has the effect of increasing the peak of excitatory conductance as outlined in Section 3.3, and so would reasonably be expected to lessen inhibition. However, increasing τ_e also has the effect of shifting the peak of excitation to a later time, potentially allowing a greater increase in inhibitory current, with the overall effect of generating a lower $V(t)$ rather than a higher one. Similarly, in decreasing τ_{ir} one would expect to decrease the overall inhibitory current, since smaller τ_{ir} correlates with smaller maximum inhibitory current. But decreasing τ_{ir} generates a steeper slope in $g_i(t)$, giving rise to a deeper initial inhibitory trough. So the effect of changing variables can be counter-intuitive; it was this fact which led to the graphical interpretation of I_i and I_e outlined in the previous chapter.

A second program was built to perform an iterative search of the parameter space outlined in the previous section using the values/ranges indicated in Table 4-1. The code was designed to allow for any range of values and step sizes to be explored, but lacked the graphical niceties of the first program. Compiled in C++, it was essentially a C program built for speed alone. On each iteration, the code would calculate the variance, s^2, between the experimental data and the model. Whenever the variance exceeded a value greater than the best variance obtained up to that point, the program would abort the current parameter set and jump to the next iteration. This statistic, essentially a sample variance without suitable weighting according to the variance σ_i at each point i, (over j total samples) was intended only to give a rough and ready measure of the difference between the experimental data and the model. Given that the actual voltage does not vary by more than a few millivolts around -65 mV, this was not an unreasonable assumption, one that helped speed the computations somewhat. Assuming that the variance σ_i is roughly constant for each data point i, then the value of s^2 should be roughly equal to the reduced Chi-squared for the complete data set.

Both programs were based on original Fortran code supplied by Andre Longtin, and were tested to ensure the accuracy of the results. For example, the values of $V(t)$ at each t may be calculated exactly when $g_L=0$ and $g_i(t)=0$ in equation 3.1d, and these values compared with the program output. While the code was not validated against any specific, well-described experimental standard, the relative simplicity of the equations involved, the provenance of the code, and the rigour with which it was tested give us a high degree of confidence in the validity of our simulations.

At the time of writing, the second of the two programs described above has executed through the equivalent of approximately four trillion complete iterations, exploring various configurations of parameter space in the search for a best fit parameter set. If anything, the program has reinforced the fact, as stated in Sections 3-5 and 3-6, that vastly different sets of data may be used to generate near-identical output, with variances differing by only a very small amount.

This brute force approach, in which an 8-, 9- and sometimes 10- dimensional parameter space is searched exhaustively, has its own particular set of drawbacks. One unfortunate consequence is that one never knows by just how small an amount an ideal solution may have been missed; if the mesh size is too coarse, it is very easy to miss an ideal solution. As mentioned earlier, the model is extraordinarily sensitive to small changes in some of the parameters, and this made it particularly difficult to establish how small an increment to use for any one parameter.

Curiously, the graphical methods outlined in Chapter 3 often proved to be the most effective way to resolve problems. The actual values of the best parameter set were obtained using both the 'brute-force' computer approach in conjunction with the more-intuitive graphical approach. Some sample fittings are shown below in Section 4-7.

4.6 Reduction of Parameters

As mentioned at the start of the Section 4.4, we can effectively remove one parameter from the above list by assuming a membrane capacitance effectively equal to 1, dropping the units. Since C acts as a simple scaling factor in the equation, the validity of the model will not be affected significantly. At any rate, C=1.0 *uF* may be reliably assumed based on experimental evidence.

Two other possibilities exist for making substitutions which reduce the parameter space, thus potentially simplifying equation 4-1 and thereby decreasing the number of iterations required. First, as outlined in Appendix A, it is possible to effectively remove one of the time constants, τ_e, by making the non-dimensional substitution

$$T_e \equiv {}^{t}/_{\tau_e} \qquad (4\text{-}22)$$

In this case, the peak value of the excitatory alpha function conductance becomes the standard by which all other times are measured.

Second, if we assume that $v(t)=V_i-V(t)$, equation 4-1 can be rewritten as:

$$-\frac{dv}{dt} = A_e t' e^{-\alpha_e t}\,(V'_e + v(t')) + A_i(e^{-\alpha_{id}(t'-\Delta t)} - e^{-\alpha_{ir}(t'-\Delta t)})v(t')) + g_L(V'_R + v(t')) \quad (4\text{-}21)$$

where $V'_e=V_e-V_i, V'_R=V_R-V_i$, *and* $t'=t-t_o$. But since V_i is already assumed to be close to zero, this has little practical effect on the equation except to invert $V(t)$; IPSPs look like inverted EPSPs, and vice versa. Under different circumstances (in which, say, $V_e=-20\ mV$), this would have the effect of effectively reducing one parameter. But here, because $V_e\approx 0\ mV$, this substitution contributes nothing to the reduction of parameters and was not actually employed, although the other two substitutions, for C and τ_e, were.

Beyond these three possible substitutions, there appear to be no other shortcuts available to ease the computational burden.

4.7 The Best-Fit Parameter Set

Using the brute-force method just outlined, a number of parameter sets were obtained which approximate the average single-call response to varying degrees. The results shown in Figure 4-5 show one such possible output; the values are listed in Table 4-2. Here, the red line denotes the experimental data and blue denotes the model. The fit is reasonably good (variance=0.0086) but this is due to small modifications in both the model and the software. First, a rather irregular sample, referred to as 1-d in Figure 3-7, was excluded from the single-call data set used to construct the average single call response. As a result, the second EPSP is less pronounced. Second, the interval around the EPSP was blocked out and the best-fit search performed without that data included.

The second EPSP has proven to be problematic to generate with a single-parameter

excitatory alpha function. The reason is almost certainly due to the effect referred to in Section 3.4, in which the inhibitory current tracks the excitatory current. Therefore, a second series of trials was performed using a second two-parameter alpha function employed to model the excitatory conductance. The 'best-fit' result is shown below in Figure 4-6. The results show the same broad features found in the single-call data set: an initial EPSP, rapid hyperpolarization, followed by the gradual return to V_R—but no second EPSP.

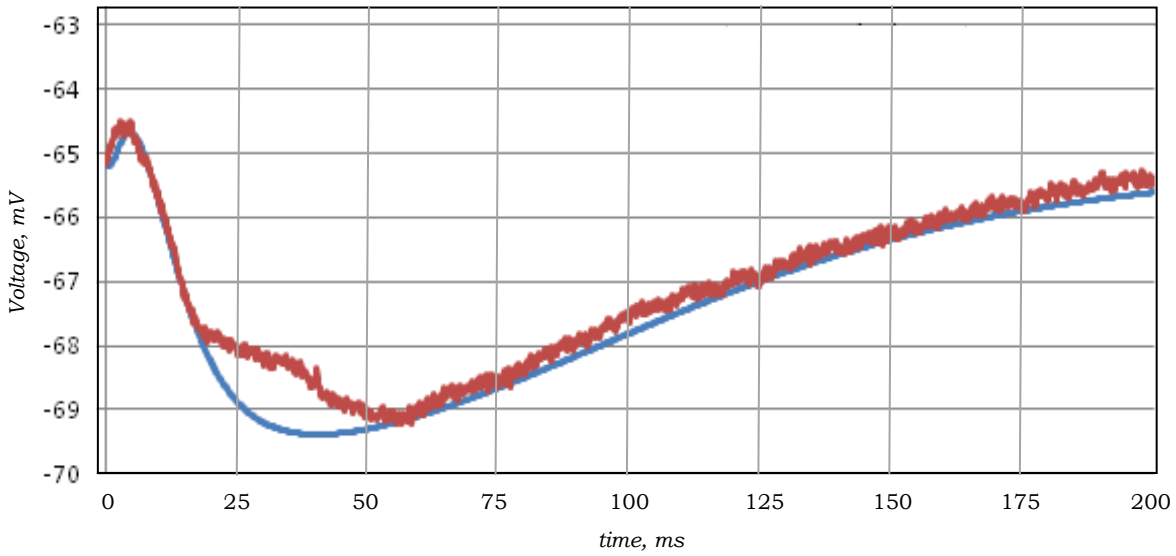

Figure 4-5: The best-fit parameter set, using the one-call data, a one-parameter alpha function for excitation, but with call 1-d removed from the data set used to construct the averaged single-call response. s^2=0.0086; this value excludes a block 60 ms around the second EPSP, which could not be modeled accurately with only a single-parameter excitatory alpha function. Parameters are listed in the first column of Table 4-2.

Table 4-2: Summary of Best-Fit Parameter Set Values

Variable	***Presumed Value***	***'Best Fit' Observed***	
		2-parameter inhibitory a-function and 1-parameter excitatory a-function	*2-parameter inhibitory a-function and 2-parameter excitatory a-function*
V_R	-65 *mV*	-65 *mV*	-65 *mV*
V_e	~0 *mV*	0 *mV*	0 *mV*
V_i	-78 *mV*	-80 *mV*	-80 *mV*

C	1 uF	1 uF	1 uF
g_L	~0.026 $\mu F \bullet ms^{-1}$	0.023 $\mu F \bullet ms^{-1}$	0.023 $\mu F \bullet ms^{-1}$
A_e	~0.0013 $\mu F \bullet ms^{-1}$	0.640 $\mu F \bullet ms^{-1}$	0.005 $\mu F \bullet ms^{-1}$
A_i	~0.0035 $\mu F \bullet ms^{-1}$	0.015 $\mu F \bullet ms^{-1}$	0.028 $\mu F \bullet ms^{-1}$
Δt	< 5 ms	2.2 ms	8 ms
τ_e (α_e)	20 ms < τ_e < 40 ms	18 ms	24 ms
τ_{ir} (α_{ir})	2 ms < τ_{ir} < 25 ms	14 ms	8 ms
τ_{id} (α_{id})	$\tau_{id} > \tau_{ir}$	22 ms	21 ms
Var, s^2		0.0086	0.036
N, # of data points		1400	2000

While the two-parameter excitatory alpha function *is* capable of producing a second EPSP (see Figure 4-7), the problems involved with fitting both the extra excitation *and* the other features are significant. Figure 4-7 gives some idea of what the model is capable of doing. Note that the value of some of the parameters varies quite widely within the small set shown, even though they all map the data to the same degree. *For the remainder of this thesis, a one-parameter excitatory alpha function and a two-parameter inhibitory alpha function are used.*

As stated previously, the model is extremely sensitive to small changes in some parameters; discovering exactly which ranges to sweep and the granularity of the step size has proved elusive. Frequently, the same (approximate) features can be generated by a large number of parameter sets. For example, Figure 4-8 shows the effect of changing a single parameter, τ_{ir}, while holding all the other values constant. The effect of making even small changes to this parameter is clearly significant. Given the number of parameters, the sensitivity of the model, and range of values which must be searched, the

total number of iterations needed to make a thorough search of parameter space may be on the order of ~5 x 10^{16}.

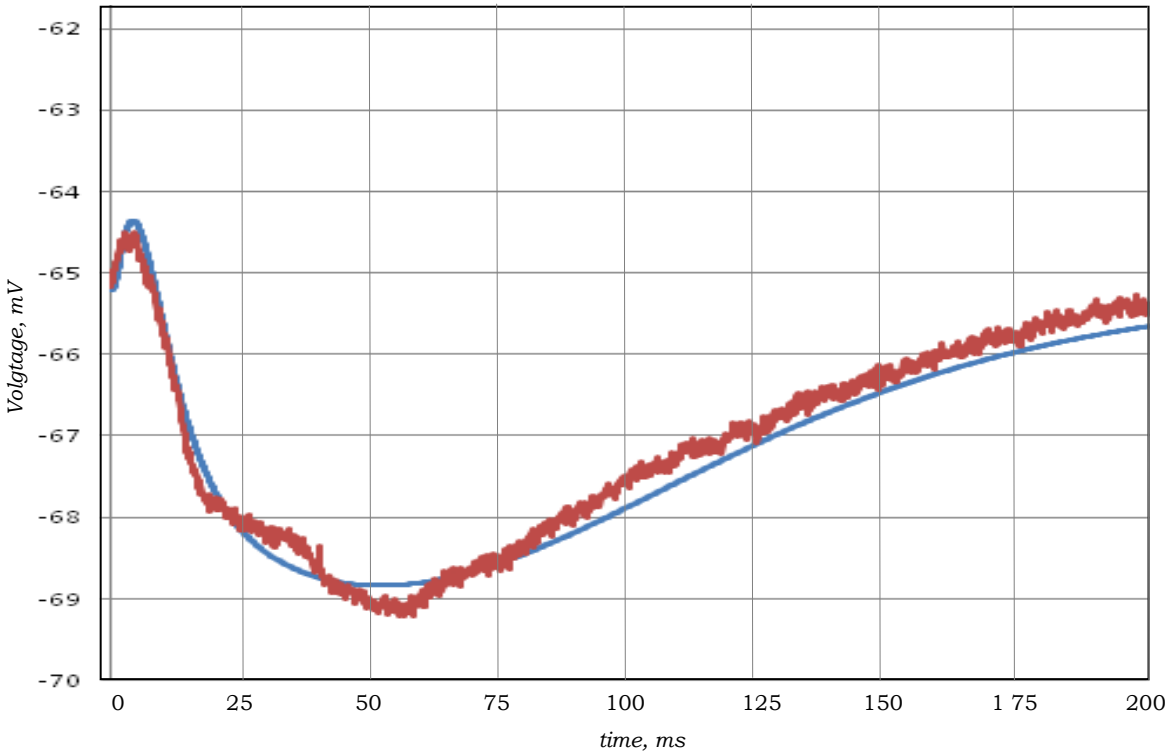

Figure 4-6: The model (in blue) and the experimental data (in red), using a two-parameter alpha functions for both inhibition and excitation. The variance is higher (s^2=0.036), and the parameter set, seen in the second column of Table 4-2, is very different from that used to generate Figure 4-5, which was generated using the parameters in the first column.

4.7 Summary

The single-call response has (potentially) a simple explanation, one in which the interplay between excitatory and inhibitory currents combine to create the complex behaviour seen in Figure 2-7. Unfortunately, while a definitive parameter set, one supported by solid experimental results, could not be obtained for this thesis, the broad qualitative results hold. At best, the results presented show that the model gives a possible explanation for the single-call data, but an accurate parameter set is not possible at this time. If any of the parameters varies from call to call, the resulting time course can vary considerably; this explains to a certain extent the range of waveforms seen in the data.

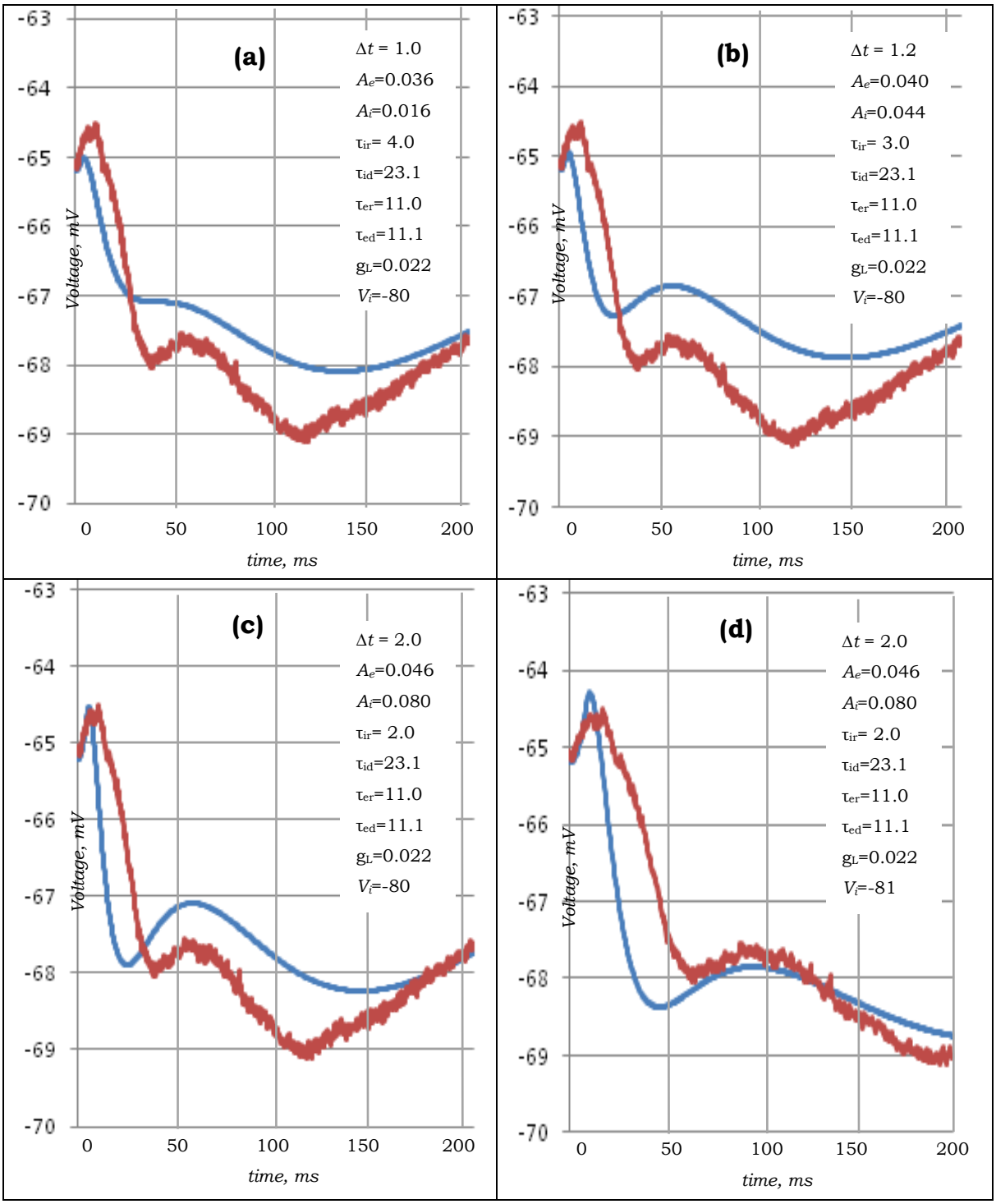

Figure 4-7: The effect of small changes to various parameters on the output produced by the model (in blue) compared with the single-call data (in red). (Note that the data referred to as 1-d in Figure 3-7 *has* been included in the calculation of the average single-call response.) (a) and (b) differ somewhat in the values of Δt, A_e, A_i, and τ_{ir} used, but the two plots are fairly similar; (c) and (d) differ only in the value of V_i used—(d) is 1 mV lower—but the effect is dramatic.

Having established a possible mechanism for the response of call-counting neurons to a single call, can we now generalize this behaviour to multiple calls? The final chapter introduces additional parameters into equation 4.20e to account for the apparent increase in excitatory current required for the response seen in Figure 2-7.

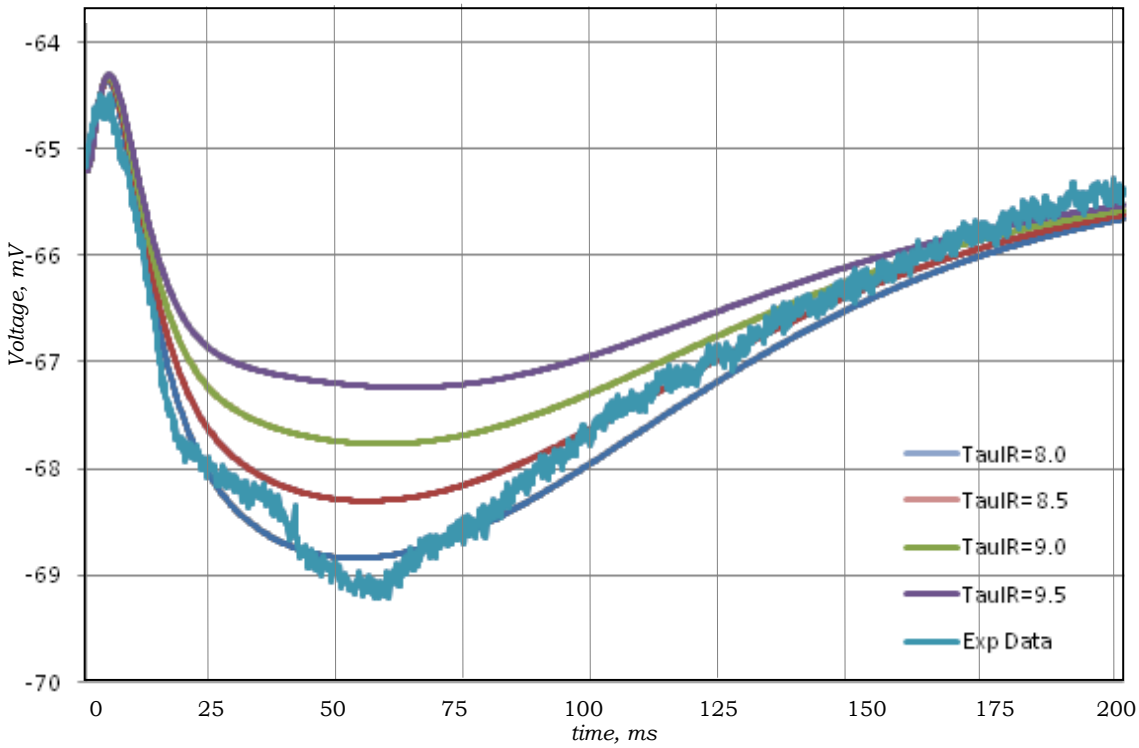

Figure 4-8: Effect of changing the value of τ_{ir} on the output of the model, along with the averaged single call response data (in blue). The other parameters used are: $\Delta t=1.5$ *ms*; $A_e=0.005$; $A_i=0.028$; $\tau_{id}=24$; $\tau_{er}=8$; $\tau_{ed}=21$; $g_L=0.023$; $V_i=-80$.

Chapter 5: Response of the Model to Additional Calls

5.1 Introduction

Thus far, this thesis has dealt entirely with the pooled single-call data in data set A as a means of devising a model to explain the results reported in *Edwards et al.* The advantage to dealing with the single-call response is its simplicity: there are no network effects to deal with, and the cumulative effects of synaptic *plasticity* that result from multiple calls (the subject of this chapter) don't factor into the analysis; we need only deal with the pure response of a neuron to a single impulse. In this chapter we augment the existing model with a feature intended to provide the rising excitatory current needed to overcome inhibition and depolarize the neuron sufficiently enough to reach a spiking threshold.

This will of course be a rather hypothetical endeavour, given that the single-call response data provides little concrete evidence on which to extrapolate an experimentally-verifiable multiple-call model. Nonetheless there are hints that the three features of call-counting neurons noted in Chapter 2—i.e. frequency sensitivity, counting, and resetting on missed calls—can all be reproduced using the simple model first introduced qualitatively in Chapter 3, and elaborated upon in Chapter 4. The problem, as before, lies in finding one set of parameters that adequately reproduce all of these features. But before proceeding, it is necessary to first add one final postulate—and three more parameters—to the model in order to explain the response of call-counting neurons to multiple calls.

5.2 Plasticity

Thus far we have treated synapses as non-linear elements whose conductances behave identically with each call according to a simple alpha-function type response. While this is generally true and forms the basis for much (useful) modern neuroscience, it ignores the behaviour of individual synapses with regard to the strength, duration and variability of their response, as mentioned in Section 4.3. Moreover, there is yet another dimension

to this issue which appears whenever synapses are triggered in rapid succession, a feature known as plasticity. The term refers to changes in the synaptic strength which may endure for a short duration, on the order of milliseconds, or of a much longer duration, as for example is believed to happen when memories are formed. Essentially, plasticity is the synapse's way of modifying its behaviour according to events in its history, and these changes may be fleeting, long-lived, or permanent.

The fleeting variety is due to *short term potentiation*, or *STP*, and it varies widely throughout the brains of organisms. Generally speaking, it has two forms, according to its effects on synaptic strength. When synaptic strength (and therefore conductance) increases in response to repeated spiking from the pre-synaptic neuron, the process is known as facilitation (or alternately, potentiation); when it decreases with frequency, depression is said to have occurred [45][46]. It is hypothetically possible for any synapse, whether excitatory and inhibitory, to either increase or decrease its synaptic current with repeated stimulation. So an increase in depolarization seen after a series of identical stimuli could be due to either the facilitation of excitatory currents *or* to the depression of inhibitory currents (or both).

As mentioned above, plasticity may be either slow or fast; a short-term excitatory synapse triggered at high frequency may generate the same voltage in a few milliseconds as a slow excitatory synapse triggered at low frequency over hundreds of milliseconds.

To summarize then, synaptic currents vary in three important and mutually exclusive ways: in the polarity of their currents (excitatory or inhibitory); in their plasticity (facilitation or depression); and in the duration of their effect (slow or fast).

As with conductances, plasticity has been studied in living organisms and can be reasonably well modeled mathematically [47][48]. Again however, there is a high degree of variability between synapses, and even the best mathematical model will provide only a rough approximation to reality. (For example, two recent papers suggest that, based on experimental evidence, synapses are only successful at producing post-synaptic responses from presynaptic spikes 10%-30% of the time [49][50]). Facilitation (F) and depression (D) are assumed to have an exponential time course following a spike, a dependence which is updated on each incoming spike. This relationship may be described mathematically as:

$$\frac{dF(t)}{dt} = \frac{F_o - F(t)}{\tau_F} \quad \text{where} \quad F(t) \rightarrow F(t) + \Delta F \quad \text{when } t=t_N \tag{5.1a}$$

for facilitation, and

$$\frac{dD(t)}{dt} = \frac{1 - D(t)}{\tau_D} \quad \text{where} \quad D(t) \rightarrow D(t) + \Delta D \quad \text{when } t=t_N \tag{5.1b}$$

for depression, where t_N is the time of the incoming N^{th} spike transmitted via the putative afferent due to incoming calls, τ is a time constant that describes how quickly the variable drops off after each call, and ΔF and ΔD are the sizes of the incremental increases imparted to each variable on each pulse/call [51][52].

Biophysically, *D(t)* and *F(t)* reflect the build up of residual calcium in the pre-synaptic terminals. D_o and F_o are the steady state values of *D(t)* and *F(t)* in the absence of calls. For facilitation, incoming calls build up the number of Ca^{2+} ions in the presynaptic terminal, triggering the release of larger amounts of neurotransmitter into the synaptic cleft, thereby increasing the conductivity of the synapse; for depression, the effect is reversed, with repeated calls decreasing the available Ca^{2+} and thus the synaptic conductivity. In this model, time constants τ_F and τ_d reflect the speed of build-up (for facilitation) or depletion (for depression), while the Δ values reflect the actual size of neurotransmitter release on each pulse [53].

In both the exemplary data shown in *Edwards et al.* as well as in data set A, an initial trough of inhibition is followed by a rising swell of excitation as the call count increases; the point at which *V(t)* rises above the resting potential V_R appears to occur around the third input call. This suggests that either facilitation of excitation or depression of inhibition plays a role in the gradual depolarization of the membrane, leading eventually to spiking.

A theoretical model by Buonomano [54] combining facilitation of excitation *and* depression of inhibition has been proposed to explain frequency-sensitive call-counting. This was a hypothetical exercise only, not unlike the models proposed in Chapter 3; no attempt was made to simulate the broad features seen in the Rose data. So Buonomano's model is not supported by the experimental evidence published in *Edwards et al.*: depression of inhibition, if it exists, plays a minor role in the eventual depolarization of

these neurons. Three lines of evidence largely rule out the possibility of depression of inhibition as an explanation for gradual depolarization:

(1) In *Edwards et al.*, attempts were made to tease apart the effects of inhibition and excitation through the use of both current clamps and the injection of Cs^+ into call-counting neurons, as reported in Section 2.2. No fewer than three tests were performed to determine the effect of changes in inhibition that resulted from repeated calls, and the results were clear. Using the method of Priebe and Ferster [33] to determine conductances, *Edwards et al.* concludes that "[t]hese data…establish that the depolarizations in response to successive stimulus pulses actually reflect changes in excitation to the cell, as opposed to changes in inhibition." A virtually identical statement is made further on based upon a test in which recordings are made in negative current clamp mode. Farther on still, after examining the relative sizes of IPSPs following calls, *Edwards et al.* again concludes that "[t]hese data suggest that little, if any, depression of inhibition occurred in response to a series of optimal intervals (i.e. optimum PRR)" [55]. So the experimental results would appear to be unambiguous in this matter: depression of inhibition plays little or no role in the behaviour of call-counting neurons.

(2) The neuron initially hyperpolarizes before depolarizing back to V_R; if the inhibition were depressed on successive calls, then the IPSP that results from the second call should be relatively less than the hyperpolarization effect due to the first call. But this does not occur: Figure 2-7 shows an initial IPSP of ~-4 *mV* due to the first call, while the '2-1' data in Figure 3-1 shows that the second call produces a relative increase of ~-6 *mV*. If depression of inhibition is present, then compared with the relative rise of excitation it is, at best, a minor effect.

(3) In general, neurotransmitters may signal inhibition or excitation, may act rapidly or slowly, and may facilitate or depress with repetition. But not all possible combinations are observed in nature. A synapse capable of depressing its inhibition, while not impossible, has not been observed at this time, and it is unlikely that an as-yet-undiscovered neurotransmitter/synapse is at work here [56].

We may conclude then, that facilitation of excitation should provide a reasonable explanation for the increases in excitatory current seen in both data set A and *Edwards*

et al. After introducing a new variable, F, into the model outlined in Section 4.2 to account for this fact, our equations now become:

$$C\frac{dV}{dt} = A_e F(t-t_o)e^{-\alpha_e(t-t_o)}(V_e - V(t-t_o)) + A_i(e^{-\alpha_{id}(t-t_o-\Delta t)} - e^{-\alpha_{ir}(t-t_o-\Delta t)})(V_i - V(t-t_o)) + g_L(V_R - V(t-t_o)), \quad (5.2a)$$

where

$$\frac{dF(t-t_N)}{dt} = \frac{F_o - F(t-t_N)}{\tau_F} \text{ where } F(t-t_i) \to F(t-t_N) + \Delta F \text{ when } t=t_N, \quad (5.2b)$$

where t_N is the time of each pulse. So A_e in equation 5.2 can now be "potentiated" by incoming spikes due to the factor F, which progressively increases on each spike.

The discrete analogs of these equations are (as outlined in Appendix A):

$$h_e(t+dt) = h_e(t) - dt\left[\left(\frac{g_{e(t)}}{{\tau_e}^2}\right) + 2h_e(t)/\tau_e\right] + \delta(t)\cdot F(t)/{\tau_e}^2 \quad (5.3a)$$

$$g_e(t+dt) = g_e(t) + dt\cdot h_e \quad (5.3b)$$

$$h_i(t+dt) = h_i(t)(1-\frac{dt}{\tau_{ir}}) + \delta(t-\Delta t) \quad (5.3c)$$

$$g_i(t+dt) = g_i(t)\left(1-\frac{dt}{\tau_{id}}\right) + dt\cdot h_i \quad (5.3d)$$

$$V(t+dt) = V(t) + dt[(g_L(V_L - V) + A_e g_e(t)(V_e - V) + A_i g_i(t)(V_i - V)] \quad (5.3e)$$

$$F(t+dt) = F(t) + dt\cdot\frac{(F_o - F(t))}{\tau_e} \quad (5.3f)$$

where, as before, dt is the time step size, $\delta(t)$ is one or zero depending on whether a spike occurs in a particular time step or not—the integral of a Dirac delta function—and Δt is

the delay time between the onset of the excitatory current and a belated inhibitory current.

Unlike conductances, which change continuously with time and must therefore be updated on each iteration, a facilitation variable need only be calculated when a pulse actually occurs. Equation 5.1a may be calculated directly [57] as:

$$F(t_{N+1}) = F_o + (\Delta_F + F(t_N) - F_o)e^{-\Delta t/\tau_F}, \tag{5.4}$$

where t_N is the time of the N^{th} pulse (due to the N^{th} call), $F(t_{N+1})$ is the state of facilitation just prior to the next call, Δ_F is the size of the increment imparted to F on each call, Δt is the interval between calls, and τ_F is the time constant that describes how quickly facilitation drops back to its baseline F_o after each call. Whether one chooses to use equation 5.4 or equation 5.3f is a matter of preference. When pulses are closely packed together, the exponential in 5.4 makes its repeated use more costly.

Note that facilitation introduces three new parameters into the model. First, we must determine an initial value F_o. In the single-call response model, F_o was usually set to 1, since for a single call, the amplitude, A_e, of the alpha function is sufficient to entirely describe the conductance behaviour of the excitatory current. When this conductance changes with each call, it becomes necessary to fit this parameter with more accuracy. The actual rate at which $F(t_N)$ increments for each t_i is determined by Δ_F, and this too must be varied so that it best fits the available data. Finally, τ_F is (yet another) exponentially sensitive variable which measures how quickly the facilitation falls after each pulse.

As with most of the parameters in Chapter 4, none of the facilitation parameters is directly accessible to experimental determination from the data available. The value of Δ_F may be approximated, given a large enough collection of samples and a range of calls, by considering changes to the slope of $V(t)$ immediately following a pulse. Since facilitation increases the conductance on each pulse, increasing larger rates of $dV(t)/dt$ must be due to the increment added to the facilitation parameter each time. Values of F_o will typically be around 1 or slightly less, and this serves as a reasonable starting point for a search through parameter space. And as with τ_{ir}, τ_{id}, *and* τ_e, the value of τ_F can only be approximated from general considerations of what constitutes a reasonable value; a range

of between a few milliseconds and not more than a few dozen milliseconds serves as a reasonable start in any search through parameter space.

This assumes that one has a solid set of single-call response parameters on which to build. Given the ambiguity of the values seen in Chapter 4, the best we can hope to achieve is to capture the three general features of call-counting neurons using reasonable parameters roughly in accord with those listed in Table 4-2. But, as in Chapter 4, a definitive parameter set will remain elusive.

5.3 Response of the Model to Multiple Calls

Figure 5-1 shows the output from a simulation using facilitated excitation. In the top of the figure are the incoming calls, represented by vertical lines indicating the spikes from the putative afferents to the model neuron—a pictorial representation of the value of $\delta(t)$ used in equations 5-3. Also shown are the excitatory and inhibitory conductances, along with facilitation, to be discussed shortly. As seen in the bottom of the figure, following the onset of spiking (at 59 Hz in this case), an initial (and very small) EPSP is followed by a trough of inhibition for approximately two incoming spikes before facilitation causes the excitatory current to once again dominate, leading to spiking above a set voltage threshold. Note that, since Hodgkin-Huxley type Na^+ and K^+ gated channels are not included in the model, spikes have been generated artificially in each of the figures below, and are indicated with a short vertical line. In a real neuron, spiking is followed by a quick reset to a lower voltage, and this too has been simulated with a 'forced' reset to the resting voltage immediately following each spike. The remaining spikes are a natural consequence of the high excitatory current that remains even after the first spike has been reached, shown by the green line in the top of the figure.

The values of Δ_F (5.6) and τ_F (13.6) are very large compared with those used in similar work (for example, Lewis and Maler report a Δ_F=0.23 and τ_F=0.079 in the cerebellar granular cells of weakly electric fish [58]). This may be the result of unknown network effects in the afferents to call-counting neurons. For example, small levels of facilitation may be pooled in increasingly larger population of neurons recruited on each successive call, so that even while each afferent contributes only a small increase of Δ_F, the cumulative effect grows larger as the population of participating neurons grows. '*Recruitment*', as it is known, may thus explain this seemingly large value.

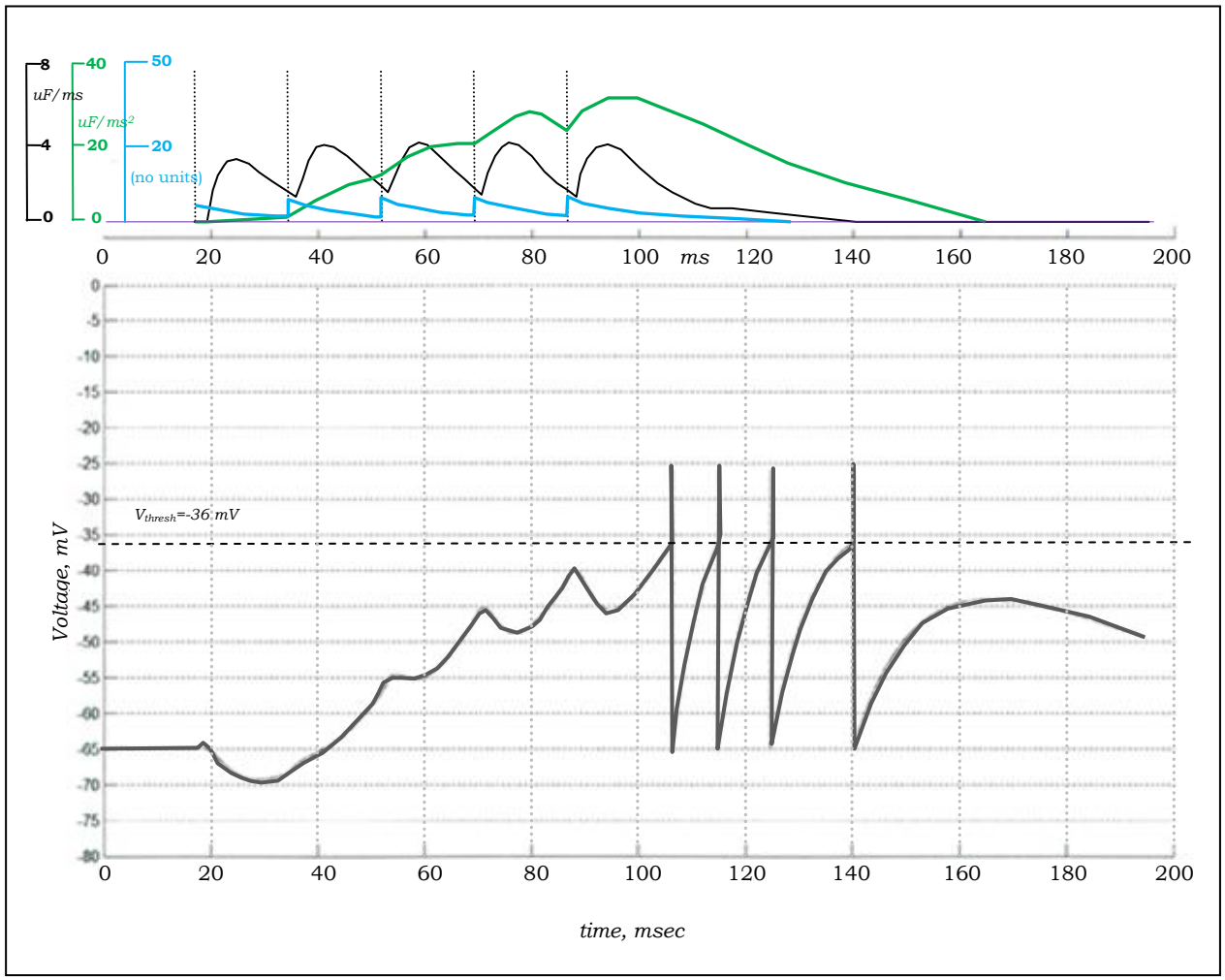

Figure 5-1: A five-counter generated by facilitating the excitation. The bottom graph shows the actual output predicted by the model; the top graph shows the inhibitory conductance (in black), the excitatory conductance (in green) and the facilitation parameter (in blue) used in generating *V(t)* for the model. A_e= *0.95*; A_i= *1.53*; τ_e=*19*; τ_F=*13.6*; F_o=*0.5*; Δ_F =*5.6*; τ_{ir}=*4*; τ_{id}=*20;* call frequency= 59 Hz; The threshold for spiking is taken as V_{thresh} = *-36 mV*.

Alternately, the large Δ_F may simply be a consequence of the values used for A_e (=*0.95*) and A_i (=*1.53*). As τ_F increases, equation 5.4 becomes increasingly linearized, and on each pulse the facilitation increases by Δ_F, without the usual exponential decay between pulses: the facilitation effectively becomes $F(t) = F_o+\Delta_F \cdot N\Delta t$ on the Nth pulse. At this point it doesn't really matter whether we start with a larger A_e and smaller values of F_o and Δ_F, or smaller A_e and larger F_o and Δ_F, the effect is the same. So it may be that the larger values of Δ_F and τ_F used in Figure 5-1 simply compensate for the value of A_e initially chosen. (The value of F_o used here, 0.5, is at least approximately equal to the F_o obtained by Lewis and Maler, who found F_o=*0.1* [59]).

Of particular note, the three overlapping plots in the top diagram indicate just how subtle the effects of increased facilitation can be. The incremental change in $F(t)$ at each spike is very small, but the cumulative effect on excitatory conductance (and current) is sufficiently large to overwhelm the inhibitory conductance. Note that in each of Figures 5-1, 5-2 and 5-3, the green and black lines represent conductances, not currents, and are intended to convey relative changes in conductance values. Also, recall from Chapter 3 that since $I_x=-g_x(V_x-V(t))$, the further $V(t)$ is from V_x, the greater the effect the battery term $(V_x-V(t))$ has on the currents. Hence in Figures 5-2 and 5-3, while the inhibitory conductance (in black) in the interval following the fourth pulse is represented as being smaller than the excitatory conductance (in green), in fact the inhibitory current is temporarily stronger because $|V_i-V|$ is greater (and concomitantly, $|V_e-V|$ is smaller), and so the model hyperpolarizes as a result.

The output shown in Figure 5-1 is an exemplar. As before, finding the right combination of values for each parameter—our parameter space has effectively grown to fifteen variables (including input frequency) of which only a few are known with any accuracy or can be removed through non-dimensionalization—involves a combination of deduction (as evidenced in previous chapters), along with intuition and some luck. Our exploration of parameter space once again suggests that multiple satisfactory parameter sets exist.

5.4 Response of the Model to Missed Calls

Another feature of the call-counting neurons presented in *Edwards et al.* was their response to missed calls, the "resetting" feature noted in Chapter 2. When a series of regular pulses at optimum PRR was interrupted just short of its final call prior to spiking, the neuron affected a temporary reset of its voltage; once calls were resumed following this brief reset period, the voltage continued to depolarize up to a spiking potential. Here too the model shows some degree of success. In Figure 5-2 input calls at a PRR of ~80 Hz were interrupted at the fifth call; the model clearly shows a brief 'resetting' interval followed (in the latter case) by spiking on the sixth call after the reset interval.

Figure 5-3 shows another example of resetting, this time at a PRR of 40 Hz, but with different parameters, shown below in Table 5-1. Again, the neuron is nominally a five-counter, but a missed fifth call generates an effective resetting interval of 50 *ms*, triggering a broad *hyperpolarization* on the resumption of calls—a curious feature also

seen in Figure 2-6 (top right). The model eventually generates spiking on the sixth call (not shown) following the resumption of input spikes.

Table 5-1. Summary of Values Used in Figures 5-1, 5-2 and 5-3.

Variable	***Presumed Value (from Chap. 4)***	**Figure 5-1**	**Figure 5-2**	**Figure 5-3**
V_i	-78 mV	-75 mV	-75 mV	-75 mV
g_L	~0.026 $\mu F/ms$	0.030	0.030	0.030
A_e	~0.0013 $\mu F/ms^2$	0.95	0.72	0.51
A_i	~0.0035 $\mu F/ms$	1.53	1.44	1.46
Δt	< 5 ms	2	2	2
τ_e (α_e)	20 ms< τ_e <40 ms	19	51	51
τ_{ir} (α_{ir})	2 < τ_{ir} < 25 ms	4	5	7
τ_{id} (α_{id})	τ_{id} > τ_{ir}	20	35	65
F_o	N/A	0.50	0.50	0.53
Δ_F	N/A	5.6	22.3	8.96
τ_F	N/A	13.6	10	33

The ability to demonstrate resetting was somewhat unexpected; the model was not explicitly designed to explain this feature, and in fact it was initially thought that we would be unlikely to capture it. But the two figures clearly show that a drop in the facilitation variable during the reset period is enough to temporarily cause a brief period of hyperpolarization—a feature seen in Figure 2-6. With an ideal set of parameters—

these two cases are again exemplars—the reset feature seen in Edwards et al. can, somewhat surprisingly, be replicated by the model.

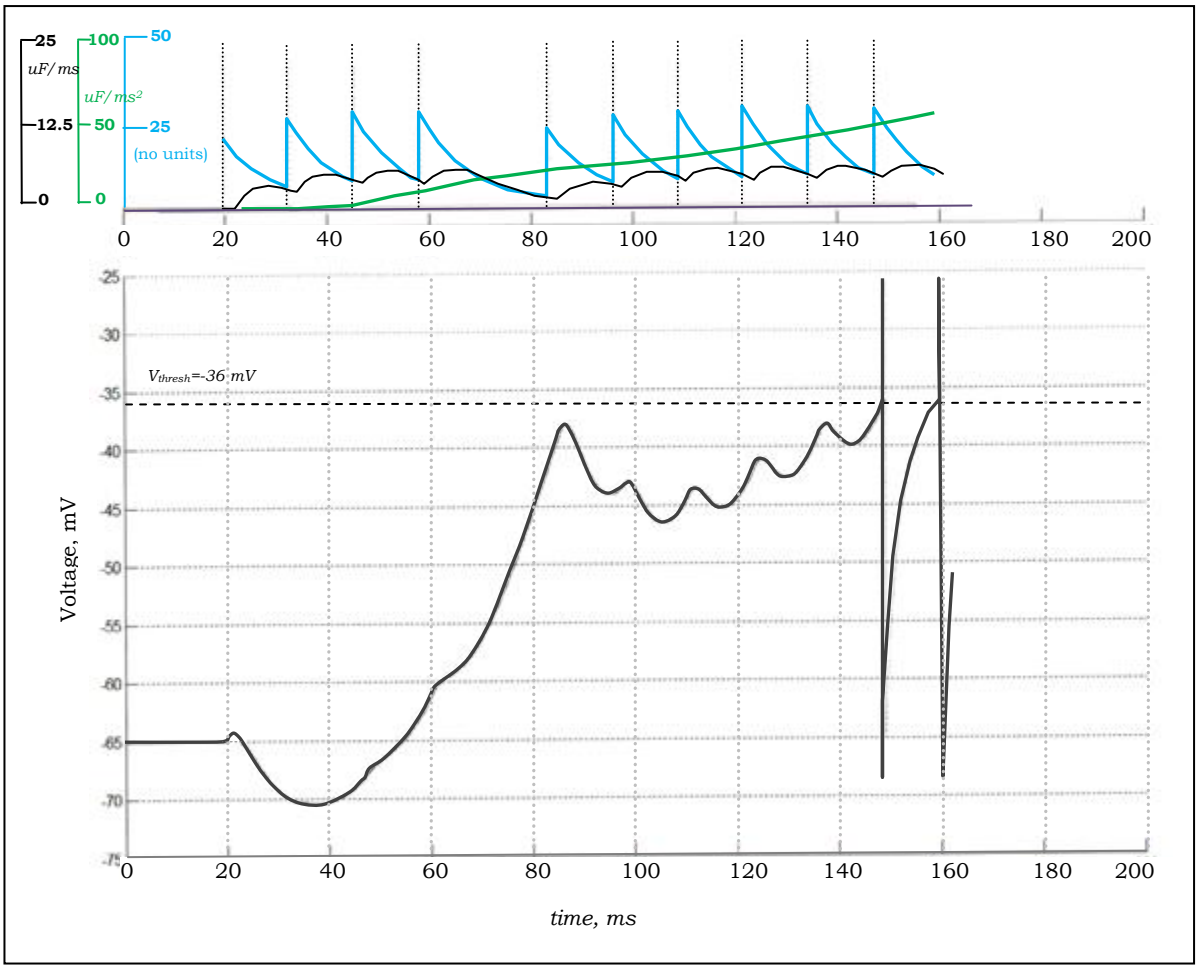

Figure 5-2: The effect of missed pulses/calls on the voltage response of a call-counting neuron with a call frequency of 79 Hz. As before, the bottom graph shows the actual output predicted by the model; the top graph shows the inhibitory conductance (in black), the excitatory conductance (in green) and the facilitation parameter (in blue) used in generating *V(t)* for the model. (The actual size of the outputs are unrelated to the scale at left; they are shown only to give a graphical idea of the change in each parameter, not the actual magnitude.) A_e= *0.72*; A_i= *1.44*; τ_e=*51*; τ_F=*10*; F_o=*0.5*; Δ_F =22.3; τ_{ir}=5; τ_{id}=*35;* call frequency= 79 Hz.

Once again, it was not possible to find a consistent set of parameters, and the values used in the creation of Figures 5-2 and 5-3 are very different than those used in the generation of Figure 5-1 above, as indicated in Table 5-1. Values not listed in this table are as follows: V_R = *-65 mV*; V_e = *0 mV*; and *C= 1 uF*.

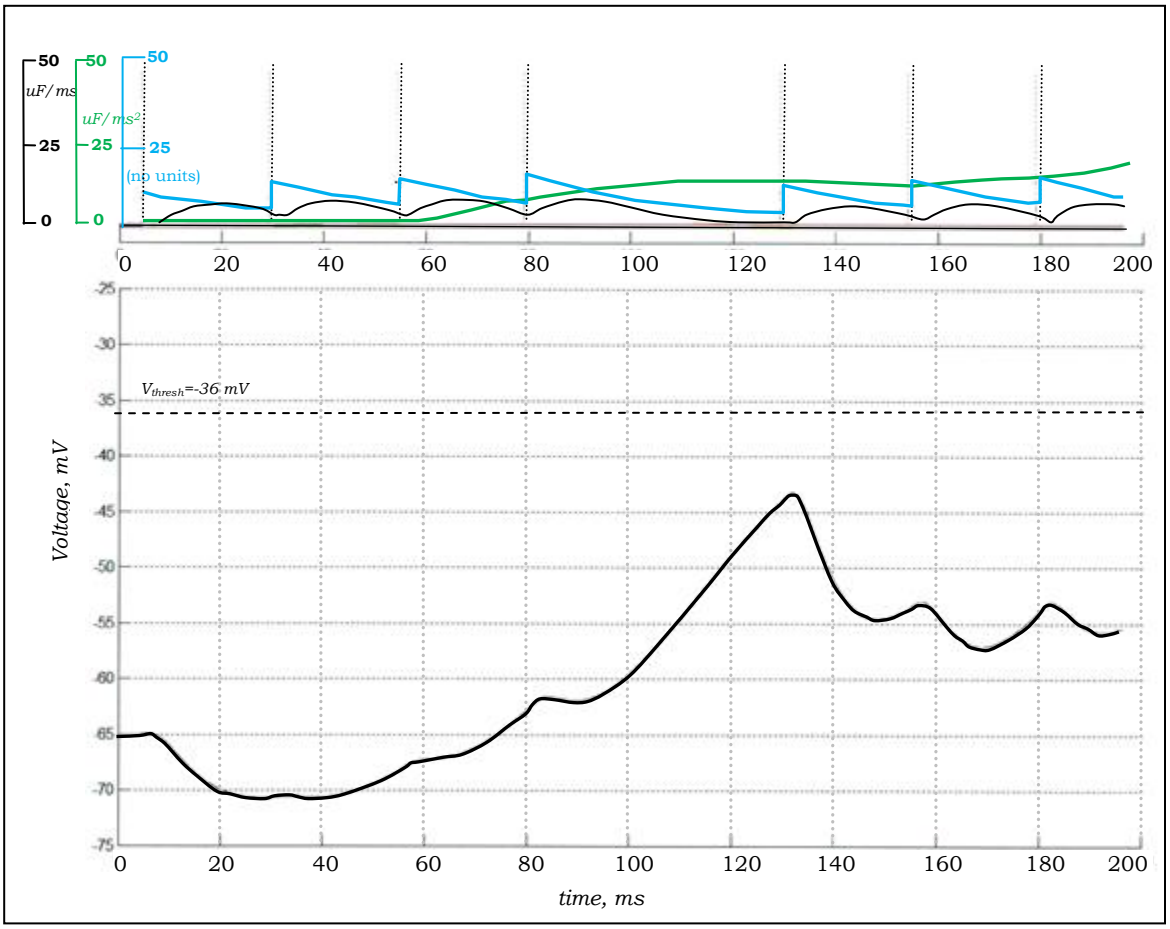

Figure 5-3: The effect of missed pulses/calls on the voltage response of a call-counting neuron, this time with a call frequency of 40 Hz. As before, the bottom graph shows the actual output predicted by the model; the top graph shows the inhibitory conductance (in black), the excitatory conductance (in green) and the facilitation parameter (in blue) used in generating *V(t)* for the model. The output spikes on the sixth call following the resumption of input calls/spikes (not shown). A_e= *0.51*; A_i= *1.46*; τ_e=*51*; τ_F=*33*; F_o=*0.53*; Δ_F =8.96; τ_{ir}=*7*; τ_{id}=*65;* call frequency= 40 Hz.

As in Chapter 4, A_e and A_i are the values most at odds with the values estimated from the available data (reproduced here in the second column). Curiously, the ratio of A_e/A_i stays roughly the same (typically between 1/3 and 1/2) even while the actual values of these two parameters differ over three orders of magnitude. This suggests that, even though we can't obtain accurate values for A_e and A_i (due to the unknown value of Δt perhaps) the ratio of $A_e/A_i \approx 0.42 \pm 0.08$ is in the correct range (although the values used in the two 'best-fit' scenarios in Table 4.2 give widely different values.)

5.5 Frequency Dependence

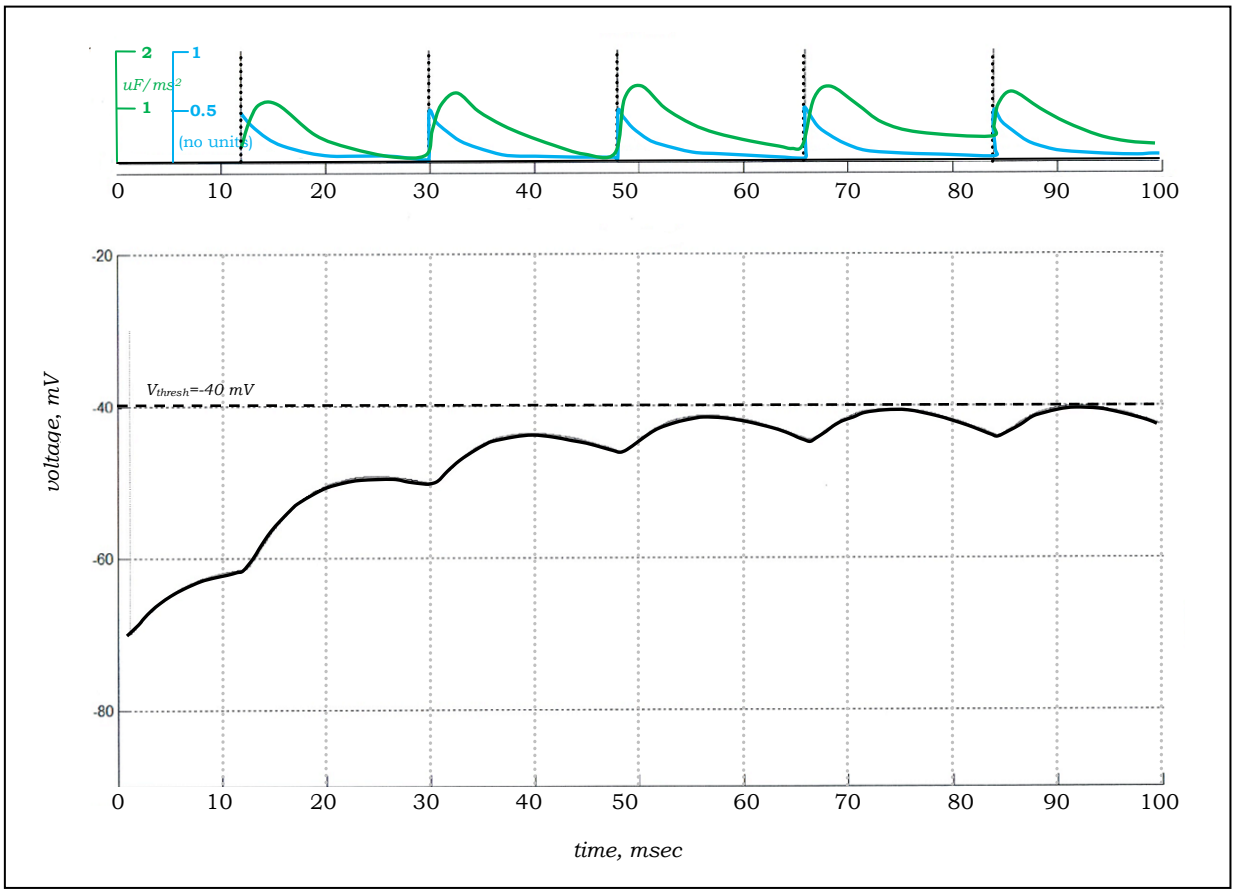

Figure 5-4: The response to multiple calls using a barely-subthreshold parameter set. Any change in a parameter that increases excitation will trigger spiking; otherwise, the voltage will remain subthreshold forever. $\tau_e = 7$; $A_e=3.4$; $\tau_F=2.94$; $\Delta_F= 2.13$; $F_o = 0.02$; $V_i=-75$; $V_e=0$; $g_L=0.030$; $V_{thresh}=-40$; call frequency = 56 Hz.

One of the three cardinal features of Gary Rose's call-counting neurons is their dependence on call frequency, or PRR, as shown in Figures 2-2 and 2-5. For almost any set of parameters in which excitation ultimately predominates—whether via large A_e, small A_i, large Δ_F or F_o, or large τ_{ir}—there will always be a PRR capable of generating spiking. Figure 5-4 shows a typical situation based on a rather simplified version of the model, in which inhibition and propagation delay have been eliminated, and only facilitated excitation drives the model. A set of parameters has been constructed which allows *V(t)* to *almost* reach the threshold (set at -40 *mV* here) required for spiking. Any small change—a slight increase in frequency, an increase in any of the facilitation parameters, a reduction in the presumed threshold by half a millivolt—will tip the balance towards spiking. As this parameter is increased, the call-count will tend to

decrease; a five-counter with low A_e will progressively become a four-counter, then a three-counter, etc. as A_e is increased.

Situations like the one shown in Figure 5-4 are the rule rather than the exception for any parameter set in which excitation ultimately dominates over inhibition. So a plot of *Spikes out vs. PRR* will invariably show a step function, rather than a standard sigmoidal gain response curve similar to that of Figure 2-5. The present model is entirely deterministic, and it will generate spikes or not, but it will never sometimes spike for a fixed parameter set in which excitation prevails over inhibition, and sometimes not. To obtain such a plot, one need only incorporate noise into the current model. But lacking a definite parameter set in which to ground the model—much less having some idea of how much noise to include and which parameters (aside from propagation jitter) to apply it to—such an exercise means little at this stage and will not be explored further.

Curiously then, the one feature which is most easily demonstrated by the model is also the one about which almost nothing definite can be said, since almost any set of parameters in which excitation predominates can be made to spike by changing the conditions just slightly.

5.6 The N-(N-1) Data Revisited

One possibility exists for determining accurate values of the three facilitation parameters Δ_F, F_o, and τ_F, and it recalls the arguments made in Section 3-2 regarding the N-(N-1) data. Given that the conductivity of the $N+1^{th}$ pulse in a series of regularly-spaced pulses can be written in terms of N^{th} pulse (see Appendix, Section A-4), it should be possible, in principle, to write the voltages over the time course of the N^{th} and $N+1^{th}$ pulses, and take the difference between the two signals. If the assumptions made earlier in this chapter are correct, then the increasing excitation seen after multiple calls is due entirely to the three facilitation parameters, and so perhaps the N-(N-1) data in Figure 3-1 could be put to actual use.

For example, the voltage after N+1 calls, according to equation 4.1 (with facilitation added) is just:

$$C\frac{dV_{N+1}}{dt} = g_{e,N+1}(t, F_{N+1})(V_e - V_{N+1}(t)) + g_{i,N+1}(t - \Delta t)(V_i - V_{N+1}(t)) + g_L(V_R - V_{N+1}(t)), \quad (5.5a)$$

and after the Nth call

$$C\frac{dV_N}{dt} = g_{e,N}(t, F_N)(V_e - V_N(t)) + g_{i,N}(t - \Delta t)(V_i - V_N(t)) + g_L(V_R - V_N(t)). \quad (5.5b)$$

Subtracting the two equations yields

$$C\frac{d\Delta V_N}{dt} = \Delta g_{e,N}(t, F_N)V_e + \Delta g_{i,N}(t - \Delta t)V_i - g_L(\Delta V_N(t)) - g_{i,N+1}(t - \Delta t)V_{N+1} + g_{i,N}(t - \Delta t)V_N - g_{e,N+1}(t, F_{N+1})V_{N+1} + g_{e,N}(t, F_N)V_N, \quad (5.6)$$

where $\Delta V_N = V_{N+1} - V_N$, $\Delta g_{i,N}(t-\Delta t) = g_{i,N+1}(t-\Delta t) - g_{i,N}(t-\Delta t)$, and $\Delta g_{e,N}(t,F_N) = g_{e,N+1}(t,F_{N+1}) - g_{e,N}(t, F_N)$.

Since the facilitation on the Nth pulse can be expressed exactly using equation 5.4, and the conductances $g_{x,N+1}(t)$ expressed as a function of $g_{x,N}(t)$ using equations A-41 and A-42, it should in principle be possible to write equation 5.6 in the form

$$C\frac{d\Delta V_N}{dt} = p(\Delta V_N, t) + q(t) + k, \quad (5.7)$$

where p and q are generic functions to be determined, and k is some constant. The three plots of $\Delta V(t)$ versus t that comprise the N-(N-1) data seen in Figure 3-1 might therefore be put to use in determining approximate values for our three facilitation parameters.

Notwithstanding the lack of solid values for the dozen or so other parameters already discussed, this method is problematic. To begin with, the forms of the equations are (apparently) intractably dense. For example, using $\beta_n = (1 - e^{-n\alpha\Delta t})^{-1}$ and $\varphi_n = \beta_1 e^{-\alpha\Delta t} -$

$n\beta_n e^{-n\alpha\Delta t}$ from Appendix A (equations A-41 and A-43 respectively), the term for the difference of the single-parameter alpha function, $\Delta g_{e,n}(t)$ (without facilitation added) is:

$$\Delta g_{e,n}(t) = A_e \beta_n^{-1} e^{-\alpha t}\{t\beta_n^{-1} + n\Delta t \beta_n e^{-n\alpha\Delta t}\}. \tag{5.8}$$

But with facilitation included, this comparatively straightforward equation becomes:

$$\begin{aligned}\Delta g_{e,N}(t, F_N) = \; & A_e \beta_1 e^{-\alpha t}\Bigg\{t\Big[(F_o + (\Delta F - F_o)e^{-\Delta t/\tau_F})\beta_{N+1}^{-1} \\ & + F_N\left(\beta_{N+1}^{-1} e^{-\Delta t/\tau_F} - \beta_N^{-1}\right)\Big] \\ & + \Delta t\left[F_N\left(\beta_{N+1}^{-1} e^{-\frac{\Delta t}{\tau_F}}\varphi_{N+1} - \beta_N^{-1}\varphi_N\right) + (F_o \right. \\ & \left. + (\Delta F - F_o))\beta_{N+1}^{-1}\varphi_{N+1}\right]\Bigg\}\end{aligned} \tag{5.9}$$

where $\varphi_N = \beta_1 e^{-\alpha\Delta t} - N\beta_N e^{-N\alpha\Delta t}$ according to equation A-43. We see that equation 5-7 could be very complicated indeed. Furthermore, it would appear that, at best, the parameters derived from the N-(N-1) data, based on the slopes and intercepts of logarithmic functions similar to equations 4.11, 4.14 and 4.16, will be critically dependent on a very large number of parameters which collectively would make any solution a crude approximation at best. The possibility of using the N-(N-1) data to extract approximate values of Δ_F, F_o, and τ_F in this way has, perhaps, some merit, but owing to the apparent complexities involved in its actual use, was not actively pursued.

5.7 Summary

Facilitation and depression reflect actual changes in the conductance of synapses based on their history. A series of increasing EPSPs may result from either facilitation of excitation or depression of inhibition. Certain lines of evidence—most particularly the experimental evidence reported in *Edwards et al.*—strongly argues against the latter possibility. Unfortunately, facilitation introduces three new parameters into the model, none of which can be accurately extracted from the experimental data. While the

possibility of exploiting the N-(N-1) data to determine these values offers some hope, it is first necessary to determine reliable values of the other parameters first, as was attempted in Chapter 4. When the model introduced in Chapters 3 and 4 is augmented with facilitation, many of the salient features described in the *Edwards et al.* data can be reproduced, and this lends some credibility to the model despite the lack of one single, complete set of parameters that consistently demonstrate all the features seen in call-counting neurons.

Our exploration of parameter space clearly suggests that multiple satisfactory parameter sets exist; the problem that remains is largely one of narrowing this set down to a manageable few.

Conclusions

The vocalizations of animals and insects play an important role in their survival and reproduction. Evolutionary pressure has no doubt worked to ensure the efficacy of communications between organisms through the creation of elaborate neural processes; a call from a neighbour means nothing if it does not elicit a proper species-specific response. The enumeration of stimuli in the environment, along with frequency selectivity and the response to missed calls, undoubtedly constitutes a large portion of the computational burden involved in processing these signals—just as it does in the receivers of modern telecommunications equipment. This thesis has attempted to investigate the neurological foundations of this field, and to shed some light on its mechanisms.

Chapters 1 and 2 provided a snapshot of the basic tenets of the field of *neuroethology*, and included both the experimental evidence available from Gary Rose's anurans as well as the neuroelectrodynamic processes underpinning the behaviour of all neurons. Despite the seeming complexity of the recorded data, *Edwards et al.* make it abundantly clear that the interplay between excitation and inhibition is largely responsible for creating the output seen in Figure 2-7, and this has been experimentally verified to a reasonable degree using the various tests available.

Independent of these specific tests, there are empirical grounds on which to base a model, and these were presented in Chapter 3. The impetus for this model is the N-(N-1) data which, regardless of the problems inherent in its derivation—the small data set size, the noise present in the data, and the potential for inducing artifacts by simply taking an average of a half dozen time courses—the results indicate that, underlying the manifest complexity and variety of the single-call response data, a simple model might offer a reasonably complete explanation, a model involving, yet again, only excitation and inhibition. This model, while based entirely on mathematical arguments derived from the data and the biophysics of neurons, is thus broadly consistent with the conclusions of *Edwards et al.* Given the limited size of the data set, this in itself represents a small step forward, since nothing in *Edwards et al.* suggests an actual mechanism like the one described in this thesis, much less one which makes an attempt at describing *all* of the salient features observed.

In spite of the apparent potential of the model, problems with its verification arise almost immediately. The Rose data, while relatively 'clean' considering the circumstances of its acquisition, has noise enough to be problematic, typically on the order of a half millivolt or so. In considering the single-call data, it's worth recalling that we are looking at information that varies by not more than six millivolts over a few dozen milliseconds, and so this noise is not insignificant. Also, there is some drift present in the recorded resting potential, V_R, on the order of $1\ mV$ over the course of the one-minute long data collection process, and this needs to be compensated for by manually shifting the data into alignment. The sampling rate is 10 kHz, and under most circumstances this might be adequate. But where we are attempting to measure effects which may be only a few milliseconds in duration (i.e, τ_e or τ_{in}), this means, practically speaking, that there may only be 30-70 data points on which to make a determination. And while the propagation delay between a call and its initial effect is unknown, we can still only estimate its onset to within ±1 *ms*. Finally, not only is the data set rather limited, but it sometimes possesses a second, still-inexplicable EPSP, one which has eluded accurate reproduction despite a detailed search through a (typically) 8- or 9- dimensional parameter space over hundreds of hours of processing time. The fact that the second EPSP does not appear in any of the data in *Edwards et al.* further complicates matters. It has at times seemed as if we are attempting to explain a phenomenon via two disparate, mutually-exclusive sets of data each showing different features of the same neuron, but never revealing the same features all at once.

Furthermore, noise needs to be incorporated into the model, thus making equation 4.1 a stochastic differential equation where one input (inhibition) is delayed with respect to another (excitation). Aside from adding some jitter to the propagation delay parameter Δt, it is not immediately clear what other parameters should have noise added to them. The inclusion of noise would hopefully bear out some of the assumptions made regarding signal variability in Section 3.5. In particular, it should help produce a smooth output in the graph of the spiking probability versus PRR, similar to Figure 2-5, rather than the 'all-or-nothing' spiking response that currently exists in the model.

Even if these problems were overcome by the availability of a much larger number of relatively noise-free data sets—which would presumably show the effect of different PRRs and mixed calls—a more challenging predicament still looms: the very nature of the model itself bedevils attempts at its verification. The intertwined dependence of the parameters, and in particular the relationship between the propagation delay and the amplitudes of the two alpha functions (A_e, A_i), make finding definite values far more

difficult than they should be without the presence of propagation delay—and A_e and A_i should be the *easy* ones. Moreover, the exponential dependence of the alpha functions—there are four exponents built into equations 5.2(a-f)—plays havoc with any attempt to experimentally determine accurate values of τ_e, τ_{ir}, τ_{id}, and τ_F. So in a practical sense, A_e and A_i are too unwieldy too be of much service, since there's always a Δt to compensate for any pair of values. At the same time, τ_e, τ_{ir}, and τ_{id} are sensitive too even small changes, making it difficult to pin down actual values. If one imagines an 8- or 9-dimensional space in which A_e and A_i control a slowly undulating hypersurface with near-identical minima, into which are embedded a very large number of deep pocks controlled by τ_e, τ_{ir}, and τ_{id}, then one has an idea of the difficulties involved in finding a global minima, a feat greatly exacerbated by the inability to narrow down the region of this space appropriate for investigation.

Despite the lack of a single, dependable parameter set, certain parametric values can be determined with some reliability, or at very least, are restricted to some verifiable range. The capacitance, C and the two battery terms V_e and V_i, are well established, and the values of V_R and g_L can be accurately measured. Unfortunately, other parameters such as A_e, A_i and Δt appear to be connected in ways which defy easy determination. And parameters such as τ_{ir}, τ_{id}, and τ_e appear to require considerably more sophisticated methods than are presently available; at the very least, they will require much larger data sets than have been made available for this thesis.

The effects of facilitation, which were added in Chapter 5, lend credibility to the central position of this thesis that other network effects are perhaps *not* required to explain the published results of *Edwards et al.*, and that the interplay between inhibition and facilitated excitation, alone, should suffice. However, the high values of Δ_F required in section 5.4 compared to those, e.g. seen in other modeling studies of STP [59] suggest that perhaps recruitment plays a role, reflecting increased input from an increasingly larger pool of neurons as the call-count increases—a hypothesis supported by Gary Rose [60].

Can the model be simplified? Possibly, provided one is prepared to dispose of decades of research into the electrophysiology of neurons. But the evidence presented in Chapters 3, 4 and 5 suggests that the three key features of counting neurons cannot be described with fewer parameters, and any attempt to do so will be detrimental to the efficacy of the model.

To truly verify this model, it would first be necessary to perform a series of experiments designed to eliminate certain parameters from consideration, thus narrowing the local parameter space to a tractable number. This would require a much closer working relationship with Gary Rose and his team than has been possible thus far.

The model, if correct, might prove a useful adjunct in helping to determine how best to proceed with this process—the suggestions made in Section 5-6 for teasing out the facilitation parameters offer one such possibility. Indeed, the model suggests other ways in which this might be achieved.

(1) By using a voltage clamp set to $V=V_i$ and measuring the current changes following each call, it should be possible to eliminate entirely the effects of the inhibitory current I_i. The current measured in voltage clamp mode would just be a constant leak current, $I_L=g_L(V_L-V_i)$ plus the varying excitatory current, $I_e = A_e \cdot e^{-t/\tau_e} \cdot (V_e-V_i)$. Since V_e and V_i can be determined reasonably accurately, and I_e can be measured directly, the time of the peak of the current should correspond to τ_e, and the value A_e then determined from $A_e = e \cdot I_e/(V_e-V_i)$ at time $t=\tau_e$.

(2) Excitatory antagonists could be used to block the excitatory current contribution, while the inhibitory current was measured in the absence of excitatory effects. A current clamp could be set to counter the presumed value of the leak current for each voltage, leaving only $dV/dt=A_i \cdot [exp(-t/\tau_{ir})-exp(-t/\tau_{id})] \cdot (Vi-V(t))$. This has an exact analytical solution from which values of A_i, τ_{ir} and τ_{id} might be extracted.

Other possibilities, involving combinations of current clamps, voltage-clamps and pharmacological antagonists could no doubt also be employed to help elucidate the various parameters which have largely eluded analysis in this thesis.

Additionally, it might be worth investigating counting in other species to see if, perhaps, the experimental difficulties that make signal acquisition so difficult in anurans might be alleviated in, say, bats. If the model is valid, then it might be worth attempting to locate counting neurons in the *inferior colliculus* of the rodent brain.

Despite its limitations, the model represents a step forward in our understanding of the phenomenon of call-counting in anurans, and therefore, potentially in more-highly evolved species as well. These achievements deserve to be emphasized:

(1) To our knowledge, this is the first attempt to construct a model of call-counting based on cutting-edge neuroelectrophysiological data, i.e. from the bottom-up rather than the top-down.

(2) While other plausible models are possible (and several, not mentioned in this document, were considered), the analysis presented in this thesis naturally points to a simply model involving *only* inhibition and facilitated excitation, a fact entirely consistent with the experimental evidence presented in *Edwards et al.*

(3) The model is capable of explaining each of the three main features seen in the Rose neurons—including, somewhat surprisingly, resetting—without the need to incorporate additional mechanisms in a jury-rigged fashion. (The size of the facilitation parameter is, however, somewhat suspicious. It may be that recruitment of additional neurons is required on each successive call in order to generate the facilitation value needed for excitation to overcome inhibition).

(4) The model suggests a further means for testing its validity, and even, perhaps for determining a single, consistent parameter set, or at least narrowing the range of possibilities considerably. At present, experimental limitations prevent progress in this area. It is conceivable, however, that in the not too distant future these difficulties will be overcome, at which point this model can be set on a firmer experimental footing.

On this final point, *if* it were possible to make an accurate determination of these parameters for each call-counting neuron, this would potentially open the door to a wide variety of other experiments. The following list indicates three somewhat speculative possibilities for future exploration, assuming that the model presented is correct:

- Anuran call rates are temperature dependent (the PRR drops with temperature) and so, presumably, are the neurons that receive calls in the *torus semicircularis*. It would be interesting to see if the model can shed some light on this mechanism by changing the temperature of frogs while measuring their call response (i.e. is facilitation temperature dependent?)

- The two anuran species studied by Gary Rose and his colleagues respond to fairly high PRR frequencies; other species have much lower call rates. It is then reasonable to ask whether or not the model just presented can be modified to

include low call rates on the order of 1 or 2 calls per second? Furthermore, can these low-call-count neurons be found in other species of frog, and therefore, does the model hold for anurans in general?

- Not all frogs emit calls, and it would be interesting to understand the genetic differences between calling and non-calling species to see which set of genes is responsible for the formation of the neurons that lead to call-counting. If these genetics were determined, this might allow for the creation of genetically deafened 'knockout' frogs lacking excitatory or inhibitory inputs to call-counting neurons, which might then permit an exact determination of certain parameters, independent of conflicting signals. The problem of teasing out excitation independent of inhibition, described in section 2.2, would be eliminated.

In conclusion, we find good, if not decisive evidence to support the hypothesis that relatively complex output like that seen in Figure 2-7 can be explained in simple terms of excitation and inhibition. The desired features seen in the observed data can be reproduced—just not with a unique parameter set. On balance, the evidence in favour of the model is not insubstantial, and the exercise involved in pursuing it, despite the difficulties, is nonetheless worthwhile. The model suggests that counting and interval-selectivity, and species-specific responses in general, far from being the product of sophisticated networks of neurons (like those of Dehaene and Changeux, and Abarbanel and Talathi) may be readily explained in a simple model involving a single neuron and two putative, opposing inputs. But it would appear that, for the moment, the fine interplay between excitation and inhibition required by the model is perhaps *too* fine to be verified experimentally. It may be that new techniques, both experimental and theoretical, will need to be brought to bear before these difficulties can be adequately resolved.

Appendix A: Alpha Functions

A.1 One- and Two-Parameter Alpha Functions

Alpha functions arise naturally in situations where a quantity, such as charge, accumulates rapidly over a short period of time while simultaneously leaking off in proportion to the amount of charge present e.g. in the voltage output of a scintillation counter when the scintillator decay time is much larger than the anode time constant [61]. Very generally, if some product, *f*—neurotransmitter in this case—is produced linearly with time at some rate λ, then we have

$$f = \lambda t, \tag{A-1}$$

which implies that

$$\frac{df}{dt} = \lambda = \frac{f}{t}. \tag{A-2}$$

But if the rate of production of neurotransmitter is limited by the actual amount present, then λ is not constant, but varies with time. The rate of change of *f* will then be generally described by

$$\frac{df}{dt} = \frac{f}{t} - \alpha f \tag{A-3}$$

where α determines the sensitivity of the production mechanism to the quantity of product present; larger α has a more pronounced effect on inhibiting production.

The solution to A-3 has the form of an alpha function, since,

$$\frac{df}{dt} = f\left(\frac{1}{t} - \alpha\right) \tag{A-4}$$

$$\Rightarrow \int \frac{df}{f} = \int \left(\frac{1}{t} - \alpha\right) dt \tag{A-5}$$

$$\Rightarrow \ln(f) = \ln(t) - \alpha t + \kappa \quad \text{(A-5)}$$

$$\Rightarrow f(t) = A_x t e^{-\alpha t}. \quad \text{(A-6)}$$

where t is the time since the onset of production, and A_x $(=e^{\kappa})$ and a are constants which characterize the overall behaviour of the function, as shown below in Figure A-1. Two common variations are frequently employed. First, setting $a=\tau^{-1}$ emphasizes the decay time constant, giving the function $A_x t e^{-t/\tau}$. A second, less-commonly employed convention sees the function written as $A_x(t/\tau)e^{-t/\tau}$, which emphasizes the importance of the ratio t/τ.

Differentiating equation A-6 yields

$$f'(t) = A_x e^{-\alpha t}(1 - \alpha t). \quad \text{(A-7)}$$

The two constants A_x and a thus determine the slope of the function at $t=0$ and the time at which the function reaches a maximum, respectively, as illustrated in Figure A-1 below. The maximum value reached by the alpha function in equation A-1, at $t=\tau= a^{-1}$, is $A_x\tau/e$.

The value of τ (or α) describes the overall shape of the function, and in many cases this single parameter may be insufficient to describe a complex conductance adequately. In such cases it is useful to use a two-parameter alpha function, which has the form

$$f_2(t) = A_2(e^{-t/\tau_d} - e^{-t/\tau_r}) \quad \text{(A-8)}$$

and so

$$f_2'(t) = -A_2\left(\frac{e^{-t/\tau_d}}{\tau_d} - \frac{e^{-t/\tau_r}}{\tau_r}\right) \quad \text{(A-9)}$$

or

$$f_2'(t) = -A_2(\alpha_d e^{-\alpha_d t} - \alpha_r e^{-\alpha_r t}). \quad \text{(A-10)}$$

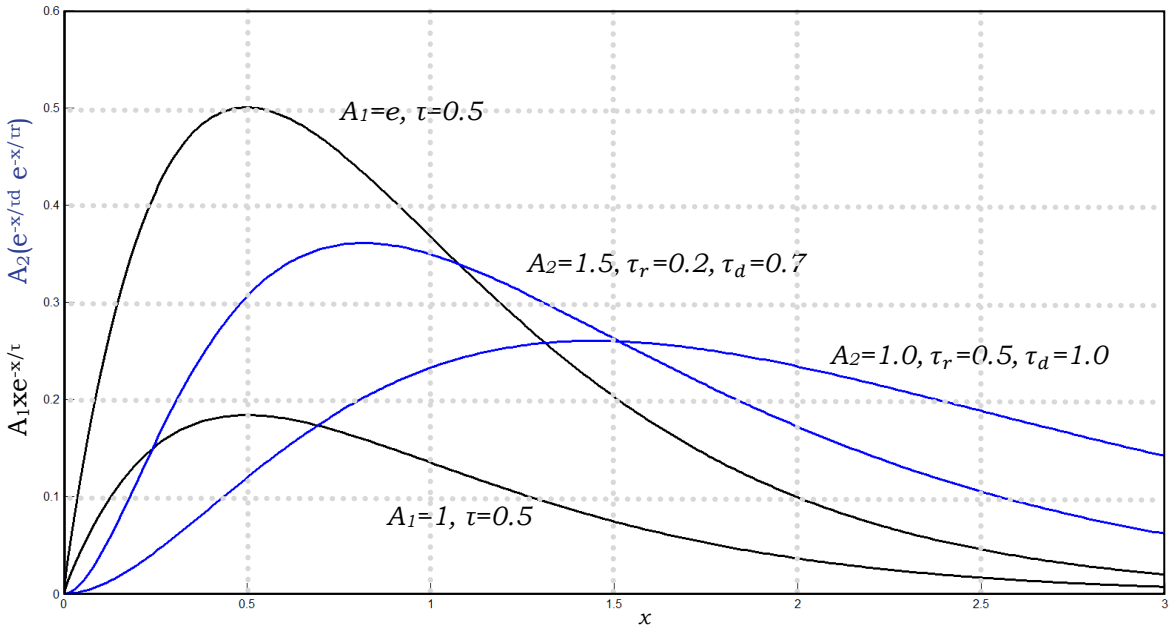

Figure A-1. Sample one- (in black) and two- (in blue) parameter alpha-functions, generated using the values indicated.

The maximum value of this function occurs at

$$t_{max} = \left(\frac{1}{\alpha_r - \alpha_d}\right) ln\ (\frac{\alpha_r}{\alpha_d}) \tag{A-11}$$

and has a value of

$$f(t_{max}) = A_2 \left[\frac{\alpha_r}{\alpha_d}\right]^{-\alpha_d/(\alpha_r - \alpha_d)} (1 - \frac{\alpha_d}{\alpha_r}). \tag{A-12}$$

Equation A-8 can be written as

$$\begin{aligned} f_2(t) &= A_2(e^{-\alpha_d t} - e^{-\alpha_r t}) \\ &= A_2 e^{-\alpha_r t}(e^{\Delta\alpha t} - 1), \end{aligned} \tag{A-13}$$

where $\Delta\alpha = \alpha_r - \alpha_d$. Since $e^{\Delta\alpha t} = 1 + \Delta\alpha t + \frac{(\Delta\alpha t)^2}{2!} + \cdots$ this becomes

$$f_2(t) = A_2 e^{-\alpha_r t}(\Delta\alpha t + \frac{(\Delta\alpha t)^2}{2!} + \cdots). \tag{A-14}$$

In the limit where $\alpha_r \to \alpha_d \to \alpha$, the higher order terms vanish and equation A-14 becomes

$$f_2(t) \approx A_2 \Delta\alpha t e^{-\alpha t} \to A_1 t e^{-\alpha t} = f_1(t). \quad \text{(A-15)}$$

Thus in the limit as $\tau_r \to \tau_d$, a two-parameter alpha function becomes a one-parameter alpha function, with the amplitude A_2 increasing such that

$$A_2 \approx A_1 \left[\frac{\tau_d \tau_r}{\tau_d - \tau_r}\right]. \quad \text{(A-16)}$$

A.2 Alpha Functions via the Euler Method

Section 4.5 introduced the discrete analogs of one- and two-parameter alpha functions. Equations 4-20(a-d) were derived as follows. For a one-parameter alpha function of the form

$$g(t) = A_1 t e^{-t/\tau}, \quad \text{(A-17)}$$

the Euler method would imply an iterative equation in the form:

$$g(t + \Delta t) = g(t) + \Delta t \left[g(t) \cdot (1/t - 1/\tau) \right]. \quad \text{(A-18)}$$

This is obtained by taking the derivative of A-17 and then substituting $g(t)/t$ for $A_1 e^{-t/\tau}$ in the result. But this is problematic for certain values of t, and particularly when $t \simeq 0$. A superior method involves introducing a second variable, $h(t)$, which effectively converts the above equation in one variable ($g(t)$) into an equation in two variables [62]. Setting $h(t)$ equal to the derivative of $g(t)$ in equation A-17 above, we have

$$\frac{dg(t)}{dt} = h(t), \quad \text{(A-19)}$$

where

$$h(t) = [A_1 e^{-\alpha t}(1 - \alpha t)] = A_1 e^{-\alpha t} - \alpha g(t), \tag{A-20}$$

or, putting this expression in terms of $A_1 e^{-\alpha t}$,

$$A_1 e^{-\alpha t} = h(t) + \alpha g(t). \tag{A-21}$$

Taking the derivative of equation A-20, we get

$$\begin{aligned} \frac{dh}{dt} &= \alpha^2 (A_1 t e^{-\alpha t}) - 2\alpha (A_1 e^{-\alpha t}) \\ &= \alpha^2 g(t) - 2\alpha [h(t) + \alpha g(t)] \\ &= -\alpha^2 g(t) - 2\alpha h(t). \end{aligned} \tag{A-22}$$

Using equations A-19 and A-22, the Euler method to generate alpha functions is:

$$g(t + \Delta t) = g(t) + \Delta t \cdot h(t) \tag{A-23a}$$

$$h(t + \Delta t) = h(t) - \Delta t [\alpha^2 g(t) + 2\alpha h(t)]. \tag{A-23b}$$

Similarly, for the two-parameter alpha function described by equation A-13, we have

$$\frac{dg}{dt} = -A_2 (\alpha_d e^{-\alpha_d t} - \alpha_r e^{-\alpha_r t}). \tag{A-24}$$

Or, putting *g(t)* in terms of $A_2 e^{-\alpha_d t}$ and substituting in equation A-13,

$$\begin{aligned} \frac{dg}{dt} &= -\alpha_d (A_2 e^{-\alpha_d t}) + A_2 \alpha_r e^{-\alpha_r t} \\ &= -\alpha_d (g + A_2 e^{-\alpha_r t}) + A_2 \alpha_r e^{-\alpha_r t} \\ &= -\alpha_d g + A_2 e^{-\alpha_r t} (\alpha_r - \alpha_d) \\ &= -\alpha_d g + h(t), \end{aligned} \tag{A-25}$$

where this time we have set

$$h(t) = A_2 e^{-\alpha_r t}(\alpha_r - \alpha_d). \tag{A-26}$$

Taking the derivative of *h(t)* gives

$$\frac{dh}{dt} = -\alpha_r A_2 e^{-\alpha_r t}(\alpha_r - \alpha_d) = -\alpha_r h(t). \tag{A-27}$$

So, using A-25 and A-27, the two iterative equations will be

$$g(t + dt) = g(t) + dt[-\alpha_d g + h(t)] \tag{A-28a}$$

and

$$h(t + dt) = h(t) - dt \cdot \alpha_r h(t). \tag{A-28b}$$

A.3 The Non-Dimensionalization of Time in the One-parameter Alpha Function

Non-dimensionalization allows us to remove a parameter from an equation by effectively 'bundling' it with other values to which it is related, thus reducing the computational load that would otherwise be required to loop through the additional iterations required by the extra parameter. This was addressed briefly in Section 4.6. For the iterative version of the one-parameter alpha function shown in equations A-23a and A-23b above, we can remove τ_e from the equation by creating the non-dimensional time parameter

$$T = t/\tau_e \tag{A-29}$$

and therefore

$$dt = \tau_e dT. \tag{A-30}$$

We also change *h(t)* so that

$$h(t) = H(t)/\tau_e \tag{A-31}$$

and so

$$dH(t) = \tau_e dh(t). \tag{A-32}$$

Equation A-19 becomes

$$\frac{dg(t)}{dt} = \frac{H(t)}{\tau_e}, \tag{A-33}$$

or

$$\frac{dg(t)}{dT} = H(t). \tag{A-34}$$

Now,

$$\frac{dh(t)}{dt} = \frac{1}{{\tau_e}^2}\frac{dH(t)}{dT}. \tag{A-35}$$

And so from equation A-22 we get

$$\frac{1}{{\tau_e}^2}\frac{dH(t)}{dT} = -\frac{g(t)}{{\tau_e}^2} - 2\frac{1}{\tau_e}\cdot\frac{H(t)}{\tau_e}. \tag{A-36}$$

Cancelling off ${\tau_e}^2$ and substituting T in place of t gives the two equations:

$$\frac{dH(T)}{dT} = -g(T) - 2H(T) \tag{A-37a}$$

and

$$\frac{dg(T)}{dT} = H(T). \tag{A-37b}$$

So replacing time t with dimensionless time T effectively removes τ_e from the equations, effectively eliminating one parameter from our parameter space [63][64].

A4. The Sum of N Alpha Functions with Equal Offset

When a synapse is triggered at regular intervals, the conductivity on the Nth pulse is just equal to the sum of N alpha functions. If there is a relationship between the value of $g_{N+1}(t)$ and $g_N(t)$, then this might be exploited, as is suggested in Section 5.6, to allow for the parameters of $g_N(t)$ to be determined from the N-(N-1) data.

The sum of N one-parameter alpha functions, triggered at regular intervals Δt (for $N \geq 1$) can be determined as follows. Assume t is a variable that varies over a limited time interval between $0<t<\Delta t$, resetting to zero as each new call arrives. To convert between the total time T and this 'piecewise' time t, use $t \rightarrow T\text{-}N\Delta t$.

On the first pulse we have

$$g_1(t) = Ate^{-\alpha t},$$

which is essentially just equation A-6. Following the second pulse this expression becomes

$$g_2(t) = A\Big[\underbrace{te^{-\alpha t}}_{\text{the 2nd alpha function}} + \underbrace{(t+\Delta t)e^{-\alpha(t+\Delta t)}}_{\text{the tail end of the first alpha function}}\Big].$$

Following the third pulse this becomes

$$g_3(t) = A\Big[\underbrace{te^{-\alpha t}}_{\substack{\text{the 3rd} \\ \text{alpha function}}} + \underbrace{(t+\Delta t)e^{-\alpha(t+\Delta t)}}_{\substack{\text{contribution of the 2nd} \\ \text{alpha function}}} + \underbrace{(t+2\Delta t)e^{-\alpha(t+2\Delta t)}}_{\substack{\text{contribution of the 1st} \\ \text{alpha function}}}\Big].$$

The value of the alpha function, $g_N(t)$ on the N^{th} pulse is given by

$$g_N(t) = A\Big[te^{-\alpha t} + (t+\Delta t)e^{-\alpha(t+\Delta t)} + \cdots + (t+(N-1)\Delta t)e^{-\alpha(t+(N-1)\Delta t)}\Big], \quad \text{(A-38)}$$

Factoring out $e^{-\alpha t}$ gives

$$g_{\text{N}}(t) = Ae^{-\alpha t}\left[t + (t+\Delta t)e^{-\alpha(\Delta t)} + \cdots + (t + (N-1N)\Delta t)e^{-\alpha((N-1)\Delta t)}\right]. \tag{A-39}$$

The sum in the square brackets is an arithmetic geometric-series, and so for the N^{th} call we can write:

$$g_N(t) = Ae^{-\alpha t}\left[t \cdot \frac{1-e^{-\alpha N\Delta t}}{1-e^{-\alpha\Delta t}} + \Delta t e^{-\alpha\Delta t}\left\{\frac{1-Ne^{-\alpha(N-1)\Delta t}+(N-1)e^{-\alpha N\Delta t}}{(1-e^{-\alpha\Delta t})^2}\right\}\right]. \tag{A-40}$$

For convenience, set

$$\beta_n=(1-e^{-N\alpha\Delta t})^{-1}. \tag{A-41}$$

(Hyperbolic trigonometric functions can be used as well, but there is no appreciable advantage in doing so.)

We can rewrite equation A-40 as

$$\begin{aligned} g_N(t) &= Ae^{-\alpha t}\left[t \cdot {\beta_N}^{-1}\beta_1\right. \\ &\qquad \left. + \Delta t e^{-\alpha\Delta t}{\beta_1}^2\left\{1 - Ne^{-\alpha(N-1)\Delta t} + (N-1)e^{-\alpha N\Delta t}\right\}\right] \\ &= Ae^{-\alpha t}\left[t \cdot {\beta_N}^{-1}\beta_1 + \Delta t e^{-\alpha\Delta t}{\beta_1}^2\left\{{\beta_N}^{-1} + Ne^{-\alpha N\Delta t}(1-e^{\alpha t})\right\}\right] \\ &= A{\beta_N}^{-1}\beta_1\left[t + \Delta t\left\{\beta_1 e^{-\alpha\Delta t} - N\beta_n e^{-N\alpha\Delta t}\right\}\right]e^{-\alpha t}\ . \end{aligned} \tag{A-42}$$

By setting

$$\varphi_N = \beta_1 e^{-\alpha\Delta t} - N\beta_n e^{-N\alpha\Delta t}\ , \tag{A-43}$$

$$t'_N = t + \Delta t\varphi_N, \tag{A-44}$$

and

$$A' = Ae^{\alpha\Delta t\varphi_N}{\beta_N}^{-1}\beta_1, \tag{A-45}$$

we finally arrive at

$$g_N(t'_N) = A' t'_N e^{-\alpha t'_N}. \quad \text{(A-46)}$$

So the sum of N alpha functions is itself a time-shifted, amplified alpha function. The peak of this pulse-dependent alpha function both increases, and shifts left relative to its predecessor, with each call or pulse.

Finally, note that for $N = 1 \rightarrow \varphi_N = 0 \rightarrow t' = t \rightarrow A' = A,$ and equation A-46 reduces to the one-parameter alpha function in equation A-6, as we would expect after a single call.

An expression for the sum of N alpha functions separated by random intervals Δt_i, where Δt_i is distributed according to a Poisson process, may be found Lindner *et al.* [65]

A5. The Continuity of $g_n(t)$ and $g_n'(t)$ For a Single-Parameter Alpha Function

Note from the definition of β_N above we have

$$\beta_N = 1 + \beta_N e^{-N\alpha\Delta t}, \quad \text{(A-47)}$$

or, upon rearranging,

$$e^{-N\alpha\Delta t} = 1 - \beta_N^{-1}, \quad \text{(A-48)}$$

This relationship will be put into service on the next page. Another useful identity based on this definition is:

$$\beta_{N+1}^{-1} = \beta_N^{-1} e^{-\alpha\Delta t} + \beta_1^{-1} \quad \text{(A-49)}$$

We can then show that

$$\begin{aligned}
\beta_{N+1}^{-1}\varphi_{N+1} &= \beta_{N+1}^{-1}\left(\beta_1 e^{-\alpha\Delta t} - (N+1)\beta_{N+1}e^{-(N+1)\alpha\Delta t}\right) \\
&= \beta_{N+1}^{-1}\beta_1 e^{-\alpha\Delta t} - (N+1)e^{-(N+1)\alpha\Delta t} \\
&= e^{-\alpha\Delta t}\left[\left(\beta_N^{-1}e^{-\alpha\Delta t} + \beta_1^{-1}\right)\beta_1 - (N+1)(1-\beta_N^{-1})\right] \\
&= e^{-\alpha\Delta t}\beta_N^{-1}\left[\beta_1 e^{-\alpha\Delta t} - N\beta_N + (N+1)\right] \\
&= e^{-\alpha\Delta t}\beta_N^{-1}\left[\beta_1 e^{-\alpha\Delta t} - N(\beta_N - 1) + 1)\right] \\
&= e^{-\alpha\Delta t}\beta_N^{-1}\left[\beta_1 e^{-\alpha\Delta t} - N\beta_N e^{-\alpha N\Delta t} + 1\right] \\
&= e^{-\alpha\Delta t}\beta_N^{-1}[1+\varphi_N]. \qquad \text{(A-50)}
\end{aligned}$$

Finally, from the general definition of conductance at time t (equation A-46)

$$\begin{aligned}
g_N(\Delta t) &= Ae^{-\alpha\Delta t}{\beta_N}^{-1}\beta_1\left(\Delta t + \varphi_N\Delta t\right) \\
&= A\left(e^{-\alpha\Delta t}{\beta_N}^{-1}\right)\left(1+\varphi_N\right)\beta_1\Delta t \\
&= A\beta_1\beta_{N+1}^{-1}\varphi_{N+1}\Delta t \\
&= A\beta_1\beta_{N+1}^{-1}\left(0 + \varphi_{N+1}\Delta t\right)e^0 \\
&= g_{N+1}(0). \qquad \text{(A-51)}
\end{aligned}$$

So $g_N(t)$ is piecewise continuous. However, since

$$g'_N(t) = Ae^{-\alpha t}{\beta_N}^{-1}\beta_1\left(1 - \alpha\Delta t\varphi_N + \alpha t\right), \qquad \text{(A-52)}$$

then

$$\begin{aligned}
g'_{N+1}(0) &= A{\beta_{N+1}}^{-1}\beta_1\left(1 - \alpha\Delta t\varphi_{N+1}\right) \\
&= A\beta_1\left({\beta_{N+1}}^{-1} - {\beta_{N+1}}^{-1}\alpha\Delta t\varphi_{N+1}\right) \\
&= A\beta_1\left(\left({\beta_N}^{-1}e^{-\alpha\Delta t} + {\beta_1}^{-1}\right) - e^{-\alpha\Delta t}{\beta_N}^{-1}\left(1+\varphi_{N+1}\right)\alpha\Delta t\right) \\
&= A\beta_1{\beta_N}^{-1}e^{-\alpha\Delta t}\left({\beta_1}^{-1}\beta_N e^{\alpha\Delta t} + 1 - \left(1+\varphi_N\right)\alpha\Delta t\right) \\
&= A + A\beta_1{\beta_N}^{-1}e^{-\alpha\Delta t}\left(1 - \left(1+\varphi_N\right)\alpha\Delta t\right).
\end{aligned}$$

The latter half of this equation is just the expression for $g'_N(\Delta t)$. So

$$g'_{N+1}(0) = A + g'_N(\Delta t). \tag{A-53}$$

The slope of *g(t)* immediately after a pulse is equal to the slope just before the pulse plus the size of the amplitude variable A. So $g'_N(t)$ is discontinuous, the magnitude of the discontinuity being equal to the amplitude term, A. In the event that facilitation *F(t)* occurs, this term effectively becomes *A·F(t).* This fact might be put to practical use in determining A if the other factors present could be controlled.

References

[1] Edwards JE., Alder TB., and Rose GJ. Auditory midbrain neurons that count. *Nature Neuroscience*. 5(10), 2002. pg. 934.

[2] Edwards CJ, Leary CJ, and Rose GJ. Counting on inhibition and rate-dependent excitation in the auditory system. *Journal of Neuroscience* 27(49), 2007. pg. 13384.

[3] Kroodsma DE. The diversity and plasticity of birdsong. In Marler P., Slabbekoorn H. (eds), *Nature's Music: The Science of Birdsong*. Elsevier Academic Press, New York, N.Y., 2004. pg 108.

[4] Searcy WA. And Yasukawa K. Song and female choice. In Kroordsma DE. and Miller EH. (eds.) *Ecology and Evolution of Acoustic Communication in Birds*. Comstock Publishing, Ithica, N.Y., 1996. pg. 454.

[5] McComb K., Parker C., and Pusey A. Roaring and numerical assessment in contests between groups of female lions, *Panthera leo*. *Animal Behaviour (47)*, 1994. pg. 379.

[6] Corcoran A., *et al*. Tiger moth jams bat sonar. *Science* 325, 2009. pg. 325.

[7] Schindl R. and Weghuber J., Electrophysiological techniques for mitochondrial channels. In Kaneez FS. (ed.) *Patch Clamp Technique*, Intech, Rijeka, Croatia, 2012. pg. 163.

[8] Rumbaugh DM., Savage-Rumbaugh S., and Hegel MT. Summation in the chimpanzee (*Pan troglodytes*). *Journal of Experimental Psychology: Animal Behaviour Processes*, 13(2) , 1987. pg. 107.

[9] Davis H. and Bradford SA. Counting behavior in rats in a simulated natural environment. *Ethology*. 73(4),1986. pg. 265.

[10] Gross HJ., Pahl M., Si A., Zhu H., Tautz J. and Zhang S. Number-based visual generalisation in the honeybee. PLoS ONE 4(1):e4263. Available at http://www.plosone.org/article/info%3Adoi%2F10.1371%2 Fjournal.pone.0004263

[11] Church RM. and Meck WH. The numerical attribute of stimuli. In Roitblat HL., Bever TG., and Terrace HS (Eds), *Animal Cognition*. Laurence Erlbaum Associates, Hillsdale, N.J., 1984. pg. 527.

[12] Dehaene S., Piazza M., Pinel P., and Cohen L. Three parietal circuits for number processing. *Cognitive Neuropsychology*. 20, 2003. pg. 487.

[13] Davis H. and Pérusse R. Numerical competence in animals: definitional issues, current evidence, and a new research agenda. *Behavioral and Brain Sciences* 11, 1988. pg. 561.

[14] Stevens SS. Mathematics, Measurement, and Psychophysics. Originally published in *Handbook of Experimental Psychology*. ed. Stevens. John Wiley, New York, N.Y., 2002. pg. 13.

[15] Davis H. Discimination of the number three by a raccoon (Procyon lotor). *Animal Learning and Behavior*. 12, 1984. pg. 409.

[16] Pepperberg IM. Evidence for conceptual quantitative abilities in the African Grey Parrot: labeling of cardinal sets. *Ethology* 75, 1987. pg. 37.

[17] Murofushi K. Numerical matching behavior by a chimpanzee (*Pan troglodytes*): Subitizing and analog magnitude estimation. *Japanese Psychological Research* 39(3), 1997. pg. 140.

[18] Referred to without a specific citation in Dehaene, *The Number Sense*. Oxford University Press, Oxford U.K., 1997. pg. 23.

[19] Dehaene S. and Changeux JP. Development of elementary numerical abilities: A Neuronal Model. *Journal of Cognitive NeuroScience* 5, 1993. pg. 390.

[20] Abarbanel HDI. and Talathi SS. Neural circuitry for recognizing interspike interval sequences. *Physics Review Letters* 96, 2006. pg. 148104.

[21] Talathi SS., Abarbanel HDI., and Ditto WL. Temporal spike pattern learning. *Physical Review E*. 78, 2008. pg. 31918.

[22] Cassaday JH and Covey E. Frequency tuning properties of neurons in the inferior colliculus of an FM bat. *Journal of Comparative Neurology* 319(1), 1992. pg. 34.

[23] Casseday JH., Ehrlich D., and Covey E. Neural tuning for sound duration: role of inhibitory mechanism in the inferior colliculus. *Science* 264(5160), 1994. pg. 847.

[24] Mora EC. And Kossl M. Ambiguities in sound-duration selectivity by neurons in the inferior colliculus of the bat *Molossus molossus* from Cuba. *Journal of Neurophysiology* 91(5), 2004. pg. 2215.

[25] Gutig R. and Sompolinsky H. The tempotron: a neuron that learns spike timing-based decisions. *Nature Neuroscience* 9(3), 2006. pg. 420.

[26] Minsky ML. and Papert SA. *Perceptrons* (MIT Press, Cambridge Mass., 1969).

[27] Hodgkin A. and Huxley A. A quantitative description of membrane current and its application to conduction and excitation in nerve. *Journal of Physiology* 117, 1952. pg. 500.

[28] Matthews, GG. *Cellular Physiology of Nerve and Muscle, 2nd ed*. Blackwell, Oxford, U.K., 1991. pg. 50.

[29] Gerhardt, HC. *The Evolution of the Amphibian Auditory System.* (eds. B. Fritzsch, *et al.*) Wiley, New York, N.Y., 1988. pg. 455.

[30] Alder TB, Rose GJ. Integration and recovery processes contribute to the temporal selectivity of neurons in the midbrain of the northern leopard frog, *Rana pipiens. Journal of Comparative Physiology A: Neuroethology, Sensory, Neural, and Behavioral Physiology* 186, 2000. pg. 923.

[31] Rose GI, Fortune ES. New techniques for making whole-cell recordings from CNS neurons *in vivio. Neuroscience Research* 26, 1966. pg. 89.

[32] Leary CJ., Edwards CJ., and Rose GJ. Midbrain auditory neurons integrate excitation and inhibition to generate duration selectivity: An *in vivo* whole-call patch study in anurans. *The Journal of Neuroscience*, 28(21), 2008. pg. 5481.

[33] Priebe NJ., Fester D. Direction selectivity of excitation and inhibition in simple cells of the cat primary visual cortex. *Neuron* 45, 2005. pg.133.

[34] Rall W. Distinguishing theoretical synaptic potentials computed from different soma-dendritic distributions of synaptic inputs. *Journal of Neurophysiology* 30, 1967. pg. 1138.

[35] Roth A., van Rossum MCW. *Computational Modeling Methods for Neuroscientists.* (*ed.* De Schutter, E.) MIT Press, Cambridge, Mass, 2010. pg 142.

[36] Johnston D., Wu SM. *Foundations of Cellular Neurophysiology*. MIT Press, Cambridge, Mass, 1995. pg. 100.

[37] Gerstner W. and Kistler W. *Spiking Neural Networks: Single Neurons, Populations, and Plasticity*. Cambridge University Press, Cambridge UK, 2005. pg. 101.

[38] Roth A. and van Rossum MCW., ibid, pg. 143.

[39] Johnston D., Wu SM., ibid, pg. 398.

[40] Katz B. *Nerve, Muscle, and Synapse.* McGraw-Hill, New York, N.Y., 1966. pg. 91.

[41] Spiegel MR. *Schaum's Outline Series Mathematical Handbook of Formulas and Tables*. Schaum's, Toronto, Canada, 1968. pg. 104.

[42] Johnston D., Wu SM., ibid, pg. 39.

[43] Roth A. and van Rossum MCW, ibid, pg. 234.

[44] Personal communication from Andre Longtin, in conversation with Dr. Gary Rose.

[45] Johnston D. and Wu SM., ibid, pg. 309.

[46] Dayan P. and Abbott LF. *Theorectical Neuroscience: Computational and Mathematical Modeling of Neural Systems.* MIT, Cambridge, Mass, 2001. pg. 184.

[47] Abbott LF. and Regehr WG. Synaptic Computation. *Nature*, 431(7010), 2004. pg. 796.

[48] Koch C. *Biophysics of Computation: Information Processing in Single Neurons.* Oxford University Press, Oxford, U.K., 1999. pp 308-329.

[49] Hessler NA, Shirke AM, and Malinow R. The probability of neurotransmitter release at a mammalian central synapse. *Nature*, 366(6455), 1993. pg. 569 (1993).

[50] Markram H., Lubke J., Frotscher M. and Sakmann B. Redistribution of synaptic efficacy between neocortical pyramidal neurons. *Nature*, 382(6594), 1996. pg. 807.

[51] Lewis J. Modeling synapses and plasticity. In *3rd Computational neuroscience Summer School Notes, uOttawa Centre for Neural Dynamics*, June 7-19, 2009, pp. 228-229.

[52] Lindner B, Gangloff D., Longtin A. and Lewis JE. Broadband Coding with Dynamic Synapses. *Journal of Neuroscience*, 29(7), 2009. pg. 2086.

[53] Johnston D., Wu SM., ibid, pp. 309-315.

[54] Buonomano DV. Decoding temporal information: a model based on short-term synaptic plasticity. *Journal of Neuroscience* 20(3), 2000. pg. 1129.

[55] *Edwards et al* (2007), ibid. The quotes are from pages 13386 and 13387.

[56] Personal communication from Andre Longtin, in conversation with Dr. John Lewis.

[57] Lewis J., ibid, pg. 229

[58] Lewis J. and Maler L. Synaptic Dynamics on Different Time Scales in a Parallel Fiber Feedback Pathway of the Weakly Electric Fish. *Journal of Neurophysiology,* 91(2), 2004. pg. 1064.

[59] Lewis J. and Maler L., ibid, pg. 1066.

[60] Personal communication from Andre Longtin, in conversation with Dr. Gary Rose.

[61] Knoll GF. *Radiation Detection and Measurement,* 3rd ed. John Wiley, Hoboken, NJ, 2000. pg. 295.

[62]Roth A. and van Rossum MCW, ibid, pg. 143.

[63] Strogatz SH. *Nonlinear Dynamics and Chaos*. Westview Press, Cambridge, Mass., 2000. pg 64.

[64] Lin, CC, Segel LA. *Mathematics Applied to Deterministic Problems in the Natural Sciences*. Macmillan Publishing, New York, N.Y., 1974. pg. 185.

[65] Lindner B, Gangloff D., Longtin A. and Lewis JE., ibid, pg. 2086.